

TRPML1 PROMOTES PROTEIN HOMEOSTASIS IN MELANOMA CELLS BY
NEGATIVELY REGULATING MAPK AND MTORC1 SIGNALING

APPROVED BY SUPERVISORY COMMITTEE

Sean J. Morrison, Ph.D.

Ralph J. Deberardinis, M.D., Ph.D.

Joshua T. Mendell, M.D., Ph.D.

Steven Vernino, M.D., Ph.D.

DEDICATION

In loving memory of my Nai Nai, who inspired me to pursue a career in cancer research.

I would like to thank my mentor, Sean Morrison, for his guidance and determination to help me succeed. I would also like to thank my wonderful colleagues—especially the melanoma group and my fellow CRI graduate students—for their help, suggestions, and friendship.

Most importantly, I would like to thank my family members for their unwavering love and support. I would like to thank my parents for giving me countless opportunities to learn and grow, for teaching me the value of hard work, and for pushing me to chase my dreams. I would also like to thank my sister, Alice, for being my forever role model.

Finally, I would like to thank my husband, Donald, for always encouraging me, challenging me, comforting me, and making me laugh when I needed it most.

TRPML1 PROMOTES PROTEIN HOMEOSTASIS IN MELANOMA CELLS BY
NEGATIVELY REGULATING MAPK AND MTORC1 SIGNALING

by

STACY YUAN KASITINON

DISSERTATION / THESIS

Presented to the Faculty of the Graduate School of Biomedical Sciences

The University of Texas Southwestern Medical Center at Dallas

In Partial Fulfillment of the Requirements

For the Degree of

DOCTOR OF PHILOSOPHY

The University of Texas Southwestern Medical Center at Dallas

Dallas, Texas

August, 2019

© Copyright

by

Stacy Yuan Kasitinon, 2019

All Rights Reserved

TRPML1 PROMOTES PROTEIN HOMEOSTASIS IN MELANOMA CELLS BY
NEGATIVELY REGULATING MAPK AND MTORC1 SIGNALING

STACY YUAN KASITINON, Ph.D.

The University of Texas Southwestern Medical Center at Dallas, 2019

SEAN J. MORRISON, Ph.D.

A major goal of studying melanoma is to identify therapeutic vulnerabilities that can be exploited to improve patient treatment. Melanoma cells are particularly sensitive to perturbations in ion homeostasis, especially when ion gradients are perturbed in combination with MAP kinase inhibition. I hypothesized that melanoma cells preferentially require certain ion channels and transporters for growth and survival. I thus screened ion channels and transporters throughout the genome to identify those required by human melanoma cells but not by normal human melanocytes. I discovered

that *Mucolipin-1 (MCOLN1)*, which encodes the lysosomal cation channel TRPML1, is preferentially required for the survival and proliferation of melanoma cells. Loss of *MCOLN1/TRPML1* function impaired the growth of patient-derived melanomas in culture and in xenografts but did not affect the growth of human melanocytes. TRPML1 expression was elevated in melanoma cells relative to melanocytes and was required in melanoma cells to negatively regulate MAPK pathway and mTORC1 signaling. TRPML1-deficient melanoma cells exhibited decreased survival, proliferation, tumor growth, and macropinocytosis as well as serine depletion and proteotoxic stress. All of these phenotypes were partially or completely rescued by mTORC1 inhibition. Melanoma cells thus increase TRPML1 expression relative to melanocytes to attenuate MAPK and mTORC1 signaling. This helps melanoma cells prevent overactivation of these oncogenic signaling pathways, sustain macropinocytosis and avoid proteotoxic stress. Further investigation of the role of TRPML1 in melanoma may ultimately guide future patient therapies and contribute to our understanding of ion channels and transporters in cancer.

TABLE OF CONTENTS

Prior Publications	ix
List of Figures	xi
List of Appendices.....	xiii
Chapter One: The physiological roles of ion channels and transporters.....	1
1.1 Introduction	1
1.2 Transport of molecules across membranes.....	3
1.3 Regulation of pH.....	5
1.4 Regulation of cellular volume.....	7
1.5 Control of hormone and fluid secretion.....	8
1.6 Sensation of external stimuli.....	10
1.7 Regulation of cellular proliferation	11
1.8 Coordination of cellular migration	13
1.9 Modulation of intracellular signaling.....	14
Chapter Two: Ion channels and transporters in the context of cancer.....	20
2.1 Introduction	20
2.2 Ion channels and transporters are overexpressed in cancer.....	20
2.3 Somatic mutations in cancer.....	22
2.4 The therapeutic potential of ion channel and transporter inhibition	26
Chapter Three: TRPML1 promotes protein homeostasis in melanoma cells by negatively regulating MAPK and mTORC1 signaling.....	30
3.1 Introduction.....	30

3.2 Results	35
3.3 Materials and methods	71
3.4 Acknowledgments.....	86
Chapter Four: Discussion and future directions	88
4.1 Targeting ion channels and transporters in cancer.....	88
4.2 The role of TRPML1 in melanoma	89
4.3 The combination of TRPML1 inhibition with other therapies	92
4.4 mTOR inhibition in cancer	94
4.5 Implications for patients with mucopolipidosis type IV.....	95
4.6 Final remarks	96
Appendices	97
References	121

PRIOR PUBLICATIONS

Kasitinon, S. Y., Eskiocak, U., Martin, M., Bezwada D., Khivansara, V., Tasdogan, A., Zhao, Z., Mathews, T., Aurora, A., and Morrison, S. J. (2019) TRPML1 promotes protein homeostasis in melanoma cells by negatively regulating MAPK and mTORC1 signaling. *In progress.*

Tasdogan, A., Faubert, B., Ramesh, V., Ubellacker, J. M., Solmonson, A., Murphy, M. M., Gu, W., Martin, M., **Kasitinon, S. Y.**, Mathews, T., Vandergriff, T., Zhao, Z., Schadendorf, D., DeBerardinis, R. J., and Morrison, S. J. (2019) Metabolic heterogeneity among melanoma cells confers differences in metastatic potential. *In progress.*

Mohan, A. S., Dean, K. M., Isogai, T., **Kasitinon, S. Y.**, Murali, V. S., Roudot, P., Groisman, A., Reed, D. K., Welf, E. S., Han, S. J., Noh, J., and Danuser, G. (2019) Enhanced dendritic actin network formation in extended lamellipodia drives proliferation in growth-challenged Rac1^{P29S} melanoma cells. *Developmental Cell* 49, 440-460.

Frankel, A. E., Eskiocak, U., Gill, J. G., **Yuan, S.**, Ramesh, V., Froehlich, T. W., Ahn, C., and Morrison, S. J. (2017) Digoxin plus trametinib therapy achieves disease control in BRAF wild-type metastatic melanoma patients. *Neoplasia* 19, 255-260.

Eskiocak, U., Ramesh, V., Gill, J. G., Zhao, A., **Yuan, S. W.**, Wang, M., Vandergriff, T., Shackleton, M., Quintana, E., Johnson, T. M., DeBerardinis, R. J., and Morrison, S. J. (2016). Synergistic effects of ion transporter and MAPK kinase pathway inhibitors in melanoma. *Nat Commun* 7, 12336.

LIST OF FIGURES

<i>Figure 1.1: Different classes of ion channels and transporters</i>	2
<i>Figure 1.2: Endocytosis of activated receptor tyrosine kinases</i>	18
<i>Figure 3.1: An in vivo screen identified MCOLN1 as being preferentially required by melanoma cells</i>	36
<i>Figure 3.2: Ion channels and transporters that appeared to be required by melanoma cells based on the shRNA screen</i>	38
<i>Figure 3.3: Loss of MCOLN1/TRPML1 impaired melanoma cell survival in vitro and in vivo</i>	42
<i>Figure 3.4: Generation of MCOLN1-deficient melanoma cells using CRISPR</i>	44
<i>Figure 3.5: Gating strategy used to identify melanoma cells by flow cytometry</i>	47
<i>Figure 3.6: MCOLN1 expression and melanoma patient survival</i>	48
<i>Figure 3.7: MCOLN1/TRPML1 deficiency activated MAPK and mTORC1</i>	49
<i>Figure 3.8: MET accumulates in endosomes in MCOLN1-deficient cells</i>	53
<i>Figure 3.9: ERBB3 accumulates in endosomes in MCOLN1-deficient cells</i>	55
<i>Figure 3.10: mTORC1 inhibition rescued the growth of MCOLN1-deficient cells</i> ..	57
<i>Figure 3.11: MCOLN1/TRPML1 deficiency increased protein synthesis as a result of mTORC1 activation</i>	60
<i>Figure 3.12: Puromycin treatment blocked the increase in protein synthesis and cell death in MCOLN1-deficient cells</i>	61
<i>Figure 3.13: MCOLN1/TRPML1 deficiency increased proteotoxic stress and induced an unfolded protein response as a result of mTORC1 activation</i>	63

Figure 3.14: Treatment with proteasome activator reduced protein aggregation in MCOLN1-deficient cells..... 65

Figure 3.15: Significantly higher levels of macropinocytosis in melanoma cells as compared to normal melanocytes 67

Figure 3.16: MCOLN1/TRPML1 deficiency impairs macropinocytosis and depletes serine 68

Figure 3.17: Metabolomics of parental versus MCOLN1-deficient cells 70

Figure 4.1: Model of TRPML1 function in melanoma cells..... 91

LIST OF APPENDICES

<i>Appendix A: Log₂-transformed tumor shRNA enrichment values in the primary shRNA screen</i>	97
<i>Appendix B: Log₂-transformed tumor shRNA enrichment values in the secondary shRNA screen</i>	117
<i>Appendix C: Significantly changed metabolites in metabolomics of parental versus MCOLN1-deficient tumors with and without rapamycin treatment</i>	119

CHAPTER ONE

The physiological roles of ion channels and transporters

1.1 Introduction

Ion channels and transporters are membrane-spanning proteins that facilitate the movement of charged ions across lipid bilayers. These proteins modulate local ion concentrations, electrochemical gradients, and membrane potential across both the plasma membrane and intracellular membranes. In doing so, they regulate diverse biological processes, including neural excitation, muscle contraction, hormone secretion, sensory transduction, pH balance, volume regulation, cellular proliferation, and cellular migration (Clapham, 2003; Gadsby, 2009; Kew and Davies, 2010; Purves, 2004).

Proteins that transport ions across membranes can be broadly divided into two general classes: ion channels and ion transporters (pumps) (**Figure 1.1**) (Gadsby, 2009; Purves, 2004). Ion channels form selective pores through the hydrophobic lipid layers of membranes and allow passive diffusion of ions down their electrochemical gradients. Ion transporters, however, are distinct from ion channels in that they can move ions across membranes against their electrochemical gradients, consuming energy in the process. Primary ion transporters, or ATPases, hydrolyze ATP to transport ions against their gradients whereas secondary ion transporters—sometimes also called co-transporters—use the energy stored in the electrochemical gradients of other ions to drive the uphill transport of their substrates (Gadsby, 2009). In general, transporters

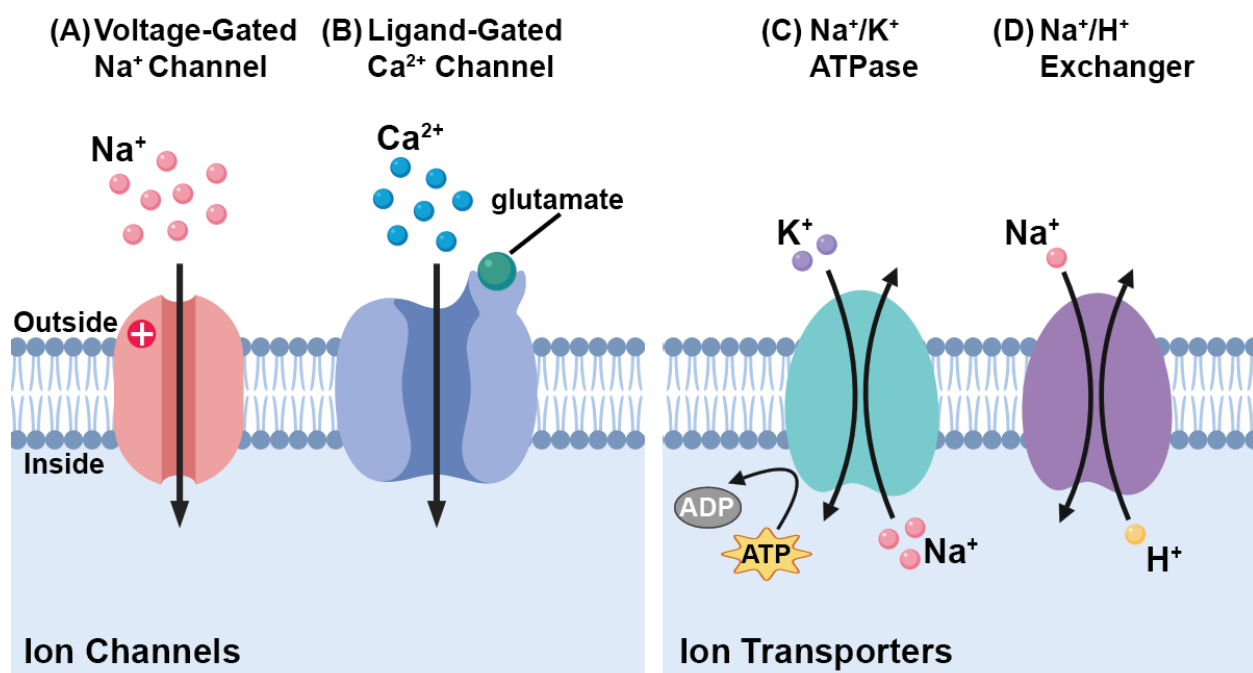


Figure 1.1. Schematic demonstrating several different classes of ion channels and transporters. **A**, Voltage-gated Na⁺ channels are activated by depolarization of the plasma membrane. They allow the influx of Na⁺ down its concentration gradient. **B**, A ligand-gated ion channel, the *N*-methyl-D-aspartate (NMDA) receptor, is activated upon the binding of glutamate, allowing Ca²⁺ influx down its concentration gradient. **C**, The Na⁺/K⁺-ATPase, which maintains resting membrane potential and ion gradients, hydrolyzes ATP to pump three Na⁺ ions out of the cell and two K⁺ ions into the cell. **D**, Na⁺/H⁺ exchangers (NHEs) use the inward Na⁺ gradient to extrude H⁺ ions.

work hard to build charge and concentration gradients across membranes while ion channels instantaneously release this stored energy to alter membrane potential or cellular signaling.

1.2 Transport of molecules across membranes

Because lipid membranes are hydrophobic, they are mostly impermeable to polar or charged molecules such as ions, sugars, nucleotides, amino acids, and many other metabolites (Alberts, 2002). Thus, specific channels and transporters are required to deliver each of these substrates across membranes. Voltage-gated ion channels are activated by depolarizing changes in membrane potential while ligand-gated ion channels are activated upon binding to their specific ligands (**Figure 1.1**) (Jan and Jan, 1989). Once open, ion channels simply allow the diffusion of selective ions down their electrochemical gradients. For example, during an action potential in a neuron, depolarization of the cell membrane above a certain threshold triggers the opening of voltage-gated Na^+ channels, allowing the massive influx of Na^+ down its gradient and creating an action potential spike. Then, in response to the large Na^+ -driven membrane depolarization, voltage-gated K^+ channels open rapidly, allowing K^+ to leave the cell down its gradient. This K^+ efflux repolarizes the cell and terminates the action potential (Purves, 2004).

To prevent electrochemical gradients from dissipating due to flux through ion channels, ion transporters instead use energy to move displaced ions back across

membranes. The most prominent example of an ion transporter is the Na^+/K^+ -ATPase (ATP1A1), which hydrolyzes ATP to pump two K^+ ions out of the cell and three Na^+ ions into the cell against their concentration gradients (Kaplan, 2002). This activity is required to maintain membrane potential, cell volume, pH, and secondary active transport of other solutes (Eskiocak et al., 2016; Jorgensen et al., 2003).

In secondary active transport, ion transporters use the energy stored in existing electrochemical gradients to move substrates against their gradients. The $\text{Na}^+/\text{Ca}^{2+}$ exchanger (NCX) family of transporters uses the Na^+ gradient established by the Na^+/K^+ -ATPase to extrude Ca^{2+} from cells against its chemical gradient. These transporters serve a housekeeping role in many cells by helping to maintain a low intracellular Ca^{2+} concentration (Blaustein and Lederer, 1999; Liao et al., 2012). Ion transporters can also transport polar or charged metabolites across membranes (Schultz and Curran, 1970). In the cells lining the small intestine and proximal tubules of the kidneys, the family of Na^+ -dependent glucose cotransporters uses the downhill Na^+ gradient to transport glucose across the apical cell membrane against its gradient so that glucose can be absorbed by the body (Crane, 1960; Wright et al., 2011). By transporting ions and other solutes across membranes, ion transporters deliver these molecules to the correct cellular compartments, where they can then be metabolized or used for downstream signaling.

1.3 Regulation of pH

Intracellular pH needs to be tightly regulated to ensure optimal enzymatic activity and general biological function (Boron, 1986; Roos and Boron, 1981). Many important processes are regulated by intracellular pH. For example, the rate-limiting enzyme of glycolysis, phosphofructokinase, is sensitive to changes in pH and adjusts cellular metabolism accordingly. Phosphofructokinase is stimulated by increased pH in response to insulin signaling so that the rate of glycolysis can increase in the presence of high blood glucose (Fidelman et al., 1982; Ui, 1966). Protein and nucleic acid synthesis rates are also highly affected by pH, as efficient synthesis cannot occur if cells are too acidic (Kurkdjian and Guern, 1989; Pouyssegur et al., 1985). Furthermore, carefully controlled pH oscillations are known to be important in governing cell proliferation (Casey et al., 2010; Madhus, 1988). In order to achieve stringent control of intracellular pH, several different ion transporters must work together to regulate both cytosolic and intraorganellar pH (Boron, 1986; Casey et al., 2010).

The cytosol has a natural tendency to acidify due to the production of organic acids from metabolic reactions and the uptake of H^+ and efflux of HCO_3^- ions driven by the membrane potential (Casey et al., 2010). To prevent the accumulation of H^+ ions inside the cell, proton exchangers must extrude H^+ from the cytosol. H^+ -ATPases expressed on the plasma membrane have the ability to pump H^+ ions out of the cell. However, their primary role is not to regulate intracellular pH, but to secrete acid from specialized cells like osteoclasts or gastric parietal cells (Blair et al., 1989; Sachs et al., 1995; Teitelbaum, 2000). In cells that produce a substantial amount of lactate,

monocarboxylate transporters (MCTs) that facilitate the outward co-transport of organic acids like lactate with protons play a role in regulating intracellular pH (Casey et al., 2010; Halestrap and Meredith, 2004). The transporters that play the largest roles in regulating pH include the Na^+/H^+ exchangers (NHEs) and the $\text{Na}^+/\text{HCO}_3^-$ transporters. NHEs use the inward electrochemical Na^+ gradient established by the Na^+/K^+ -ATPase to export H^+ from the cytosol. $\text{Na}^+/\text{HCO}_3^-$ transporters bring both Na^+ and HCO_3^- into the cell, which helps to buffer excess H^+ ions in the cytosol (Casey et al., 2010). These transporters are not only sensitive to intracellular pH, but they can also adjust their activity precisely and rapidly (Aronson, 1985; Gross and Hopfer, 1999; Soleimani et al., 1991).

Sometimes cells instead experience intracellular alkalinization, so they have also developed ways to import H^+ ions when needed. The $\text{Cl}^-/\text{HCO}_3^-$ anion exchangers driven by the inward Cl^- gradient allow HCO_3^- to exit the cytoplasm, effectively reducing intracellular pH (Casey et al., 2010; Cordat and Casey, 2009). In addition, MCTs are bidirectional transporters, and some cells instead use MCT1 to import lactate, leading the importation of protons and the lowering of intracellular pH (Feron, 2009; Halestrap, 2013). Overall, the ability of ion transporters to both alkalinize and acidify the cytosol enables fine control of intracellular pH and thus fine control of important cellular processes.

1.4 Regulation of cellular volume

The membranes of mammalian cells are highly permeable, and water movement across these membranes is largely dictated by osmotic pressure gradients determined by the intracellular and extracellular concentrations of ions and solutes (Lang et al., 1998a). Cell volume regulation is important for maintaining intracellular osmolality, cell shape, cell migration (Lang et al., 1998b), cell growth and cell death (Wehner et al., 2003), and metabolism (Haussinger, 1996; Lang et al., 1989; Wehner et al., 2003). To avoid drastic variations in cell volume, cells use several volume regulatory mechanisms, including the rapid and efficient transport of ions across cell membranes (Lang et al., 1998a; Verbalis and Gullans, 1991).

On one hand, during cell swelling, cells must extrude ions to draw water out and reduce cell volume. Most often, K^+ channels (Deutsch and Chen, 1993; Felipe et al., 1993), nonselective anion channels, and transporters that transport Cl^- (Grunder et al., 1992; Perry and O'Neill, 1993; Thiemann et al., 1992), HCO_3^- (Volkl and Lang, 1988), and organic anions (Kirk et al., 1992) are activated to allow the efflux of ions (Weiss and Lang, 1992). Loss of intracellular ions is followed by the loss of water, and cell volume decreases back to normal.

On the other hand, cells accumulate ions to increase cell volume in response to cell shrinkage. The major ion transport systems that compensate for cell shrinkage are the $Na^+/K^+/Cl^-$ cotransporter (NKCC) (Dunham et al., 1990; Geck and Pfeiffer, 1985) and the Na^+/H^+ exchanger (NHE) (Grinstein et al., 1983). To increase cell volume, the $Na^+/K^+/Cl^-$ cotransporter brings two positively charged ions, Na^+ and K^+ , into cells

alongside two negatively charged Cl^- ions, followed by water. More commonly, cellular shrinkage activates the Na^+/H^+ exchanger, causing the uptake of Na^+ ions in exchange for the extrusion of H^+ ions and multiple downstream effects (Demaurex and Grinstein, 1994). The cellular loss of H^+ ions actually results in net osmotic gain because it is not only compensated by the dissociation of intracellular buffers but also because cytoplasmic HCO_3^- increases as intracellular pH rises. This rise in HCO_3^- then drives the inward flow of Cl^- in exchange for intracellular HCO_3^- through anion antiporters. Together, the Na^+/H^+ and $\text{Cl}^-/\text{HCO}_3^-$ exchangers promote the uptake of NaCl coupled to osmotic water uptake, facilitating cell volume increase (Demaurex and Grinstein, 1994). In some types of cells, the electrolyte accumulation required for volume regulation is accomplished through activation of Na^+ channels (Wehner et al., 1995) or nonselective cation channels (Chan and Nelson, 1992; Volk et al., 1995). Depolarization through flux of positive ions through these channels then promotes Cl^- entry into the cell, bringing in additional ions. Different types of cells may use different ion channels and transporters to compensate for changes in cellular volume, but it is clear that these membrane proteins are essential for effective cell volume regulation.

1.5 Control of hormone and fluid secretion

Ion channels have also been reported to regulate secretion in epithelial and endocrine cells (Catterall et al., 2005; Kew and Davies, 2010). One of the best characterized channels that regulates lung and gut epithelial fluid secretion is the cystic fibrosis transmembrane regulator (CFTR) Cl^- channel. Loss-of-function mutations in

CFTR that affect Cl^- channel function cause cystic fibrosis (Kerem et al., 1989; White et al., 1990), which is characterized by thickened mucus in the lungs that causes frequent and serious respiratory infections as well as pancreatic insufficiency that leads to diabetes and malnutrition (O'Sullivan and Freedman, 2009). CFTR is expressed in the sweat glands, pancreas, pulmonary ionocytes, and gut epithelial cells (Plasschaert et al., 2018). It releases Cl^- ions from cells, which normally prevents sodium resorption by epithelial Na^+ channels and encourages the outward osmotic movement of water. Defective ion transport through CFTR results in dehydration of the epithelial extracellular environment, leading to thickened mucus that can foster respiratory infections in the lung and obstruct the secretion of digestive enzymes from the exocrine pancreas (Matsui et al., 1998; O'Sullivan and Freedman, 2009).

Other ion channels, such as Ca^{2+} and K^+ channels, are required for the secretion of hormones from pancreatic β -cells and adrenal cells (Ashcroft and Rorsman, 1989; Petersen and Findlay, 1987). In general, insulin secretion from β -cells and epinephrine and aldosterone secretion from the adrenal gland are stimulated by increases in intracellular Ca^{2+} that promote the exocytosis and release of hormones (Douglas and Rubin, 1961; Wollheim and Sharp, 1981). Multiple different ion channels are involved in glucose-induced insulin secretion from β -cells (Ashcroft and Rorsman, 1989; Henquin and Meissner, 1984). First, glucose enters β -cells through a glucose transporter, and ATP is produced as glucose is metabolized by the cell. ATP then binds ATP-sensitive K^+ channels, inducing channel closure, reducing K^+ outflux, and depolarizing the cell (Ashcroft et al., 1984; Ashcroft and Rorsman, 1989; Cook and Hales, 1984; Rorsman

and Trube, 1985). This depolarization activates voltage-gated L-type Ca^{2+} channels, allowing the rapid influx of Ca^{2+} ions that triggers the exocytosis of insulin-containing vesicles (Findlay et al., 1989; Schulla et al., 2003; Wollheim and Sharp, 1981). Then, both delayed rectifying and Ca^{2+} -dependent K^+ channels work together to repolarize the cells (Smits, 1996). Adrenal glands use a similar mechanism that is also dependent on Ca^{2+} influx through activated voltage-gated Ca^{2+} channels for stimulating exocytosis and hormone release (Douglas and Rubin, 1961; Spat and Hunyady, 2004).

1.6 Sensation of external stimuli

Some ion channels have the ability to mediate a variety of sensations—including temperature, pain, taste, and pressure—at both the cellular and organismal levels. The transient receptor potential (TRP) channels are a small group of nonselective cation channels that convert external stimuli into cellular messages. TRP channels were first discovered in *Drosophila* with *trp* mutations, which demonstrated small, transient changes in membrane potential in response to continuous light stimuli (Minke, 1977). These channels are ubiquitously expressed and can be active at resting membrane potentials, making them suitable to sense small changes in external stimuli and amplify these signals via Ca^{2+} permeation and membrane depolarization. TRP channels can be activated by multiple kinds of stimuli. Some are activated by G protein-coupled receptors (GPCRs) and receptor tyrosine kinases that in turn activate phospholipase C (PLC) (Clapham, 2003). Others are activated via direct binding with ligands such as capsaicin, menthol, saccharin, lipid metabolites, nucleotides, or inorganic ions like Ca^{2+}

and Mg^{2+} (Caterina et al., 1997; Peier et al., 2002; Zhang et al., 2003). Still others can be directly activated by changes in ambient temperatures and mechanical stretch (Clapham, 2003; Ramsey et al., 2006). TRP channels likely propagate their signals through a variety of Ca^{2+} signaling mechanisms, but there is still much to learn about their mechanisms of activation and signal transduction.

1.7 Regulation of cellular proliferation

There is evidence that membrane potential can regulate cell mitotic activity and cell cycle progression in both normal and cancer cells (Cone, 1971; Sundelacruz et al., 2009). Multiple studies have found that proliferating cells tend to be more depolarized than nonproliferating cells (Bates, 2015; Cone, 1971; Cone and Cone, 1976).

Manipulation of the membrane potential also affects progression through the cell cycle. Hyperpolarizing endothelial cells by applying electric fields arrests their cell division (Wang et al., 2003) while depolarizing neurons or mouse macrophages promotes progression through the cell cycle (Cone and Cone, 1976; Kong et al., 1991). These data suggest that membrane potential plays an active role in regulating cell cycle progression in different types of cells.

The changes in membrane potential during the cell cycle likely result from the coordinated actions of K^+ and Cl^- channels (Chilton et al., 2005; Lang et al., 2007; Wang, 2004; Wonderlin and Strobl, 1996). There are many different classes of K^+ channels, and many can be activated at resting membrane potential (Chilton et al., 2005; DeCoursey et al., 1984; Wang, 2004). Opening K^+ channels allows the efflux of

K⁺ ions, causing hyperpolarization of cells, while closing K⁺ channels can lead to depolarization. On the contrary, opening Cl⁻ channels allows Cl⁻ exit and depolarization while closing Cl⁻ channels promotes repolarization. Simultaneous activation of both K⁺ and Cl⁻ channels causes the loss of KCl and water from the cell, leading to cell shrinkage (Lang et al., 1998a), which has also been shown to stimulate cell proliferation. Therefore, K⁺ and Cl⁻ currents contribute directly to proliferation by regulating membrane potential and indirectly by regulating cell volume.

Although it is unclear which exact channels are activated to adjust membrane potential during different phases of the cell cycle, multiple studies demonstrate that certain K⁺ and Cl⁻ channels are required for cellular proliferation. Inhibition of the K_v1.3 delayed-rectifier K⁺ channel blocks proliferation of oligodendrocyte progenitor cells by arresting cells in the G₁ phase (Chittajallu et al., 2002; Ghiani et al., 1999). Nonspecific K⁺ channel blockers tetraethylammonium (TEA) and 4-aminopyridine (4-AP) cause proliferating astrocytes and Schwann cells to arrest in the G₀/G₁ phase of the cell cycle, suggesting that K⁺ channel activity is required for the G₁ to S phase transition (MacFarlane and Sontheimer, 2000; Pappas and Ritchie, 1998). In addition, loss of CLC-3 channel function impairs the proliferation of cultured rat aortic vascular smooth muscle cells (Tang et al., 2008; Wang et al., 2002). Together, these studies demonstrate that the activities of both K⁺ and Cl⁻ channels are required for proliferation in normal mammalian cells.

In addition to changes in membrane potential and volume, changes in intracellular Ca²⁺ levels also regulate cellular proliferation (Berridge, 1995; Berridge et

al., 1998; Berridge et al., 2000). A period of repetitive Ca^{2+} spikes is an important growth signal for some normal and cancer cells, and cell proliferation can be reduced by interfering with Ca^{2+} signaling (Berridge et al., 1998; Dartsch et al., 1995). Ca^{2+} is also required for the proliferation of immune cells in response to foreign antigens (Lewis and Cahalan, 1995). When antigens bind to surface receptors in both B and T lymphocytes, inositol-1,4,5-triphosphate is produced, stimulating Ca^{2+} release from internal stores (Berridge et al., 1998). Ca^{2+} then activates transcription factors such as NFAT, turning on genes important for proliferation and for the immune response (Muller and Rao, 2010). Therefore, Ca^{2+} release is broadly important for cell proliferation.

Ion channels and transporters regulate proliferation by controlling membrane potential, cell volume, and K^+ , Cl^- , and Ca^{2+} fluxes. Their effects on cell proliferation are multifaceted, and they must be tightly regulated to maintain normal proliferative balance.

1.8 Coordination of cellular migration

During development, ion channel activity can affect cellular migration in the nervous system (Bates, 2015). For instance, a subunit of the voltage-gated Na^+ channel is required for the migration of cerebellar granule neurons to the intergeniculate leaflet and for the migration of dentate granule neurons in the hippocampus (Brackenbury et al., 2013). Activation of a Ca^{2+} -activated K^+ channel induces neuronal precursor cells to migrate properly to the olfactory bulb (Turner and Sontheimer, 2014). Ca^{2+} channels control Ca^{2+} oscillations that are involved in the migration of nerve growth cones (Gomez et al., 1995). Furthermore, N-Type Ca^{2+} channel function is necessary for the

migration of postmitotic granule cells in mouse cerebellar slice cultures (Komuro and Rakic, 1992). However, ion channel and transporter activity can also control cellular migration in adult cells.

Like cell proliferation, the migration of all cells depends on several interrelated factors that are modulated by ion channels and transporters: membrane potential, cell volume, and intracellular Ca^{2+} (Schwab et al., 2012). Changing membrane potential can control migration by modifying the cytoskeleton, as depolarization of endothelial cells can determine the actin polymerization/depolymerization ratio (Callies et al., 2011). Localized changes in cell volume have also been visualized in migrating cells and are thought to play an active role in directing migration (Schneider et al., 2000; Watkins and Sontheimer, 2011). In these cells, migration is accompanied by an increase in volume at each cell's leading edge and a concomitant decrease in volume at its trailing edge (McFerrin and Sontheimer, 2006; Schwab et al., 2012). In migrating cells, intracellular Ca^{2+} plays a role in directionality, cytoskeleton redistribution, traction force generation, and focal adhesion formation (Brundage et al., 1991; Clapham, 2007; Lee et al., 1999; Wei et al., 2009). Thus, the channels and transporters that regulate membrane potential, volume, and Ca^{2+} flux together regulate cellular migration.

1.9 Modulation of intracellular signaling

Ion channels are most extensively studied in the context of excitable cells like neurons and muscle cells, which use the coordinated activation of multiple types of channels to propagate action potentials or excitation-contraction signals. However,

nonexcitable cells also use ion channels and transporters—especially those that allow the flux of Ca^{2+} ions—for intracellular signaling.

Ca^{2+} is often thought of as the universal signaling molecule. Cells invest a lot of energy in ATPases and ion exchangers to maintain a 20,000-fold concentration gradient between their intracellular ($\sim 100\text{nM}$) and extracellular ($\sim 2\text{mM}$) Ca^{2+} concentrations (Clapham, 2007). Ca^{2+} is also highly regulated within cellular compartments so that cells can precisely regulate signaling pathways in response to various stimuli (Monteith et al., 2007). Ca^{2+} can exert its actions by binding proteins and altering their shapes and functions (Carafoli et al., 2001). For example, when Ca^{2+} binds to calmodulin, it changes the protein's conformation, allowing it to act on other proteins by dimerizing them, relieving autoinhibition, or remodeling active sites (Hoeftlich and Ikura, 2002). This amplification mechanism allows even small bursts of intracellular Ca^{2+} to have huge effects on hundreds of proteins (Clapham, 2007).

Signaling Ca^{2+} can be derived from internal stores or from the extracellular environment. Ca^{2+} channels on the plasma membrane can facilitate the rapid influx of Ca^{2+} from the extracellular environment and can trigger dramatic changes within cells. These channels respond to various stimuli such as membrane depolarization, stretch, ligand binding, and the depletion of intracellular stores (Berridge et al., 2003). For instance, in nerve terminals, the activation of voltage-gated Ca^{2+} channels following depolarization mediates an increase in intracellular Ca^{2+} that triggers the exocytosis of neurotransmitter-containing vesicles (Clapham, 2007; Jahn and Scheller, 2006). The neurotransmitters then travel across the synapse to propagate the action potential to

additional neurons (Sudhof, 2004). Conversely, Ca^{2+} channels on the endoplasmic reticulum (ER) or sarcoplasmic reticulum (SR) membranes release Ca^{2+} from internal stores in response to Ca^{2+} itself or intracellular messengers like inositol-1,4,5-triphosphate (Berridge et al., 2003). The Ca^{2+} released from internal stores can then trigger muscle contraction, downstream signaling pathways, or apoptosis (Clapham, 2007). These examples demonstrate that Ca^{2+} channels that regulate Ca^{2+} flux from both extracellular and intracellular sources contribute to downstream signaling.

Turning off the Ca^{2+} signal also requires the action of ion transporters that remove Ca^{2+} from the cytoplasm. These transporters—which include the plasma membrane Ca^{2+} -ATPase (PMCA), the $\text{Na}^+/\text{Ca}^{2+}$ exchanger (NCX), the sarcoplasmic/endoplasmic reticulum Ca^{2+} -ATPase (SERCA), and the mitochondrial uniporter (MCU)—are important for maintaining Ca^{2+} homeostasis by keeping the intracellular Ca^{2+} concentration low (Berridge et al., 2003). The PMCA and NCX transporters extrude Ca^{2+} ions out of the cytoplasm into the extracellular environment while the SERCA and MCU transporters sequester Ca^{2+} into internal storage compartments. These transporters are equally important as Ca^{2+} channels in maintaining the sensitivity of Ca^{2+} signaling mechanisms.

Ion channels and transporters can also modulate cellular signaling pathways indirectly by altering lysosomal behavior. Mucolipin-1, or TRPML1, is a Ca^{2+} channel that sits on endosomal and lysosomal membranes and regulates their trafficking and fusion (Cheng et al., 2010; Zhang et al., 2018). Activation of this channel by intracellular messengers like phosphatidylinositol 3,5-bisphosphate allows nonspecific cations,

including Ca^{2+} , to flow from the lysosomal lumen to the cytoplasm, where Ca^{2+} can then activate various signaling and trafficking pathways (Cheng et al., 2010; Li et al., 2016b; Zhang et al., 2016). Because TRPML1 not only regulates Ca^{2+} signaling but also endolysosomal trafficking and function, there is a possibility that it plays a role in modulating fundamental cell processes downstream of the PI3K, MAPK, and mTORC1 pathways.

Endosomes and lysosomes have recently emerged as important signaling hubs that can direct cell growth, proliferation, and differentiation (Lawrence and Zoncu, 2019; Perera and Zoncu, 2016; Settembre et al., 2013). Normally, when receptor tyrosine kinases on the cell surface are activated, they are endocytosed into endosomes that are either recycled back to the cell surface or targeted to the lysosome for degradation (**Figure 1.2**) (Cullen and Steinberg, 2018; Katzmann et al., 2002). This process is a way to negatively regulate signaling through surface receptors and requires tight regulation of endosomal and lysosomal trafficking. Therefore, defects in endosome or lysosome trafficking or function—which could be caused by changes in the function of lysosomal cation channels like TRPML1—can alter the activation of signal transduction pathways, including the PI3K and MAPK pathways downstream of surface receptors (Inamura et al., 2018; Kawashima et al., 2009).

Another potential consequence of altering endosome or lysosome trafficking or function is the dysregulation of mTOR, the growth factor- and nutrient-responsive master regulator of cellular growth and metabolism. mTORC1 promotes cellular proliferation by activating anabolic pathways and by inactivating catabolic pathways in

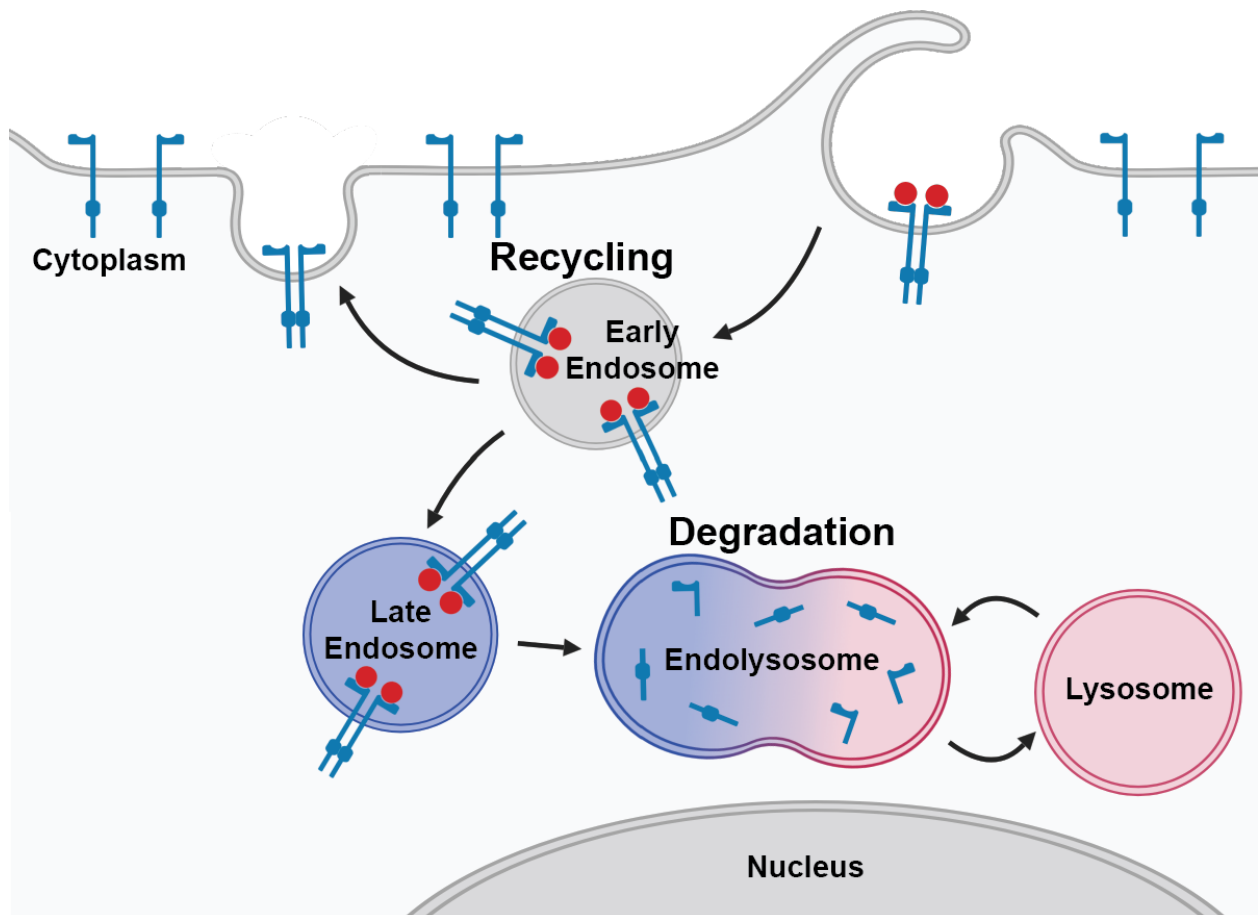


Figure 1.2. Endocytosis of activated receptor tyrosine kinases. The binding of ligands to receptors on the cell surface causes the receptors to dimerize and activate, usually via autophosphorylation. Activated receptors are then endocytosed, trafficked to early endosomes, and either recycled back to the cell surface or targeted to the lysosome for degradation. Activated receptors can continue to signal to downstream effectors in early and late endosomes but are degraded once the late endosomes fuse with lysosomes.

response to nutrient-rich conditions (Saxton and Sabatini, 2017; Valvezan and Manning, 2019). mTORC1 must be recruited to the lysosomal surface by activated Rag GTPases so that it can be fully activated by Rheb (Sancak et al., 2010; Saxton and Sabatini, 2017). If the Rag GTPases are not tethered properly to the lysosomal surface by the pentameric Ragulator complex, mTORC1 becomes insensitive to amino acid activation (Bar-Peled et al., 2012; Sancak et al., 2010). Thus, mTORC1 function may be altered in cells with defective endolysosomal trafficking or function, which are partly regulated by organellar ion channels. This hypothesis is supported by evidence that mTORC1 activity is altered in some cells with lysosomal storage disorders (Bartolomeo et al., 2017).

Ion channels and transporters possess diverse functions that can affect many aspects of cell physiology. Because they affect major cellular processes like proliferation, migration, and signaling, they may be hijacked by cancer cells to promote tumor formation and metastasis. There is accumulating evidence that ion channels and transporters are dysregulated in multiple different cancers and that pharmacologically modifying these channels and transporters may be a viable therapy for these cancers.

CHAPTER TWO

Ion channels and transporters in the context of cancer

2.1 Introduction

Cancer is defined by several key hallmark capabilities: self-sustained proliferative signaling, evasion of growth suppression, resistance to apoptosis, limitless replication, angiogenic capability, invasiveness, metabolic dysregulation, and avoidance of immune-mediated destruction (Hanahan and Weinberg, 2000; Hanahan and Weinberg, 2011).

As normal cells transform into neoplastic cells, they sequentially acquire these characteristics and become more aggressive. As described above, ion channels and transporters regulate basic cellular processes like membrane potential, cell volume, proliferation, migration, and intracellular signaling, all of which are closely associated with one or more hallmarks of cancer (Bates, 2015; Prevarskaya et al., 2010).

Therefore, ion channels and transporters may be involved in promoting tumor initiation, progression, or metastasis.

2.2 Ion channels and transporters are overexpressed in cancer

Mammalian cells highly express the major ion channels and transporters required to maintain baseline membrane potential and intracellular ion homeostasis. Most ion channels and transporters involved in action potential propagation or excitation-contraction coupling are primarily expressed in excitable cells in the brain or muscle, but non-excitable cells like fibroblasts, hepatocytes, endocrine cells, and lymphocytes often

express these membrane proteins at lower levels (Cahalan et al., 1985; Chen et al., 1988; Jan and Jan, 1989; Levitan, 1988; Lewis and Cahalan, 1995; Roger et al., 2015). However, many different cancers exhibit increased expression of certain ion channels or transporters relative to the normal cells from which they derive, and the increased expression of these proteins is thought to be functionally important.

Overexpression of certain ion channels and transporters is associated with the increased growth or aggressiveness of cancer cells. *KCNK9*, which encodes a two-pore domain K⁺ channel, is amplified in 10% of breast cancers and overexpressed in a high frequency of breast, lung, and colon cancers (Mu et al., 2003; Pei et al., 2003).

Overexpression of *KCNK9* is not sufficient to transform mouse embryonic fibroblasts; however, *KCNK9* overexpression in a human mammary epithelial cell line and a *RAS*- and *E1A*-transformed mouse embryo fibroblast cell line enhances subcutaneous tumor formation in nude mice (Mu et al., 2003). Because *KCNK9* functions as an O₂-sensitive K⁺ channel, it is thought to promote cancer cell survival in poorly oxygenated areas of tumors through an unknown mechanism (Hartness et al., 2001). Ectopic expression of another K⁺ channel, the ether à go-go (EAG) channel, was found in breast cancer, cervical cancer, and neuroblastoma cell lines, and overexpression of this channel in Chinese hamster ovary (CHO) cells induces tumor formation in immunocompromised mice (Camacho, 2006; Farias et al., 2004; Pardo et al., 1999; Pardo and Stuhmer, 2014). EAG activation is thought to encourage tumor growth partly by increasing HIF1 α activity and VEGF secretion, thus promoting angiogenesis (Downie et al., 2008). Ca²⁺ channels are also overexpressed in cancer. The TRPV6 and TRPM7 cation channels

are highly expressed in breast and prostate cancer cell lines, and they likely promote the proliferation of cancer cells through the regulation of Ca^{2+} influx (Bolanz et al., 2008; Fixemer et al., 2003; Guilbert et al., 2009). TRPA1, a redox-sensitive cation channel, is functionally overexpressed in breast cancer, lung cancer, kidney cancer, and peripheral nerve sheath tumors and promotes defense against oxidative stress to protect tumor cells from apoptotic death (Takahashi et al., 2018). Finally, overexpression of a Zn^{2+} transporter, ZIP4, promotes the growth of xenografted pancreatic tumors by increasing cellular proliferation (Li et al., 2007).

Ion channel and transporter expression may also affect the metastatic behavior of some cancers. In breast and lung cancer cells, the overexpression of G protein-coupled inward rectifying K^+ channels and certain voltage-gated Na^+ channels correlates with increased metastasis (Campbell et al., 2013; Nelson et al., 2014; Stringer et al., 2001; Yang et al., 2012). Constitutive activity of the Na^+/H^+ exchanger and monocarboxylate transporters—which play active roles in maintaining both intracellular and extracellular pH—acidifies the tumor microenvironment. This acidification allows the degradation and remodeling of the extracellular matrix by acidic proteases, giving tumor cells the ability to better invade and metastasize (Cardone et al., 2005).

Many of the ion channels and transporters that are overexpressed in cancers appear to promote tumor growth by modulating cellular proliferation, pH balance, or cellular migration. However, their exact mechanisms are still not completely understood,

and they seem to each contribute to tumor growth or metastasis by driving different pathways (Prevarskaya et al., 2010).

2.3 Somatic mutations in cancer

In a few cases, somatic mutations in ion channels and transporters have been found to affect the ion-conducting activity of these channels and transporters and contribute directly to tumorigenesis or metastasis. These mutant channels and transporters drive tumor progression by promoting hormone secretion, cancer cell proliferation or pro-growth signaling.

A series of studies found that point mutations in multiple channels and transporters drive the formation of aldosterone-producing adenomas (APAs) (Beuschlein et al., 2013; Choi et al., 2011; Scholl et al., 2013). Aldosterone is a steroid hormone that is normally produced in the adrenal glomerulosa in response to intravascular volume depletion or hyperkalemia (Spat and Hunyady, 2004). Depolarization and the subsequent activation of voltage-gated Ca^{2+} channels in adrenal glomerulosa cells promotes aldosterone secretion and proliferation. Aberrant sustained increases in intracellular Ca^{2+} often lead to uncontrolled cell proliferation and the formation of adrenal adenomas (McEwan et al., 1996; Pawlikowski et al., 2001; Tanabe et al., 1998). Loss-of-function missense mutations in *ATP1A1*, which encodes the major subunit of the Na^+/K^+ -ATPase, lead to cytoplasmic Na^+ retention and depolarization of the cells (Beuschlein et al., 2013). Separately, gain-of-function mutations in a gene encoding an inwardly rectifying K^+ channel, *KCNJ5*, occur near the K^+ channel

selectivity filters, causing the mutant channels to become permeable to Na⁺ ions.

Increased Na⁺ conductance through these mutant channels also causes depolarization of the membrane (Choi et al., 2011; Krapivinsky et al., 1995). Both mutant *ATP1A1* and *KCNJ5* cause aberrant depolarization of the plasma membrane, triggering Ca²⁺ entry through voltage-gated Ca²⁺ channels and subsequent aldosterone production.

Additional loss-of-function mutations in *ATP2B3* and gain-of-function mutations in *CACNA1D* can promote APA formation by directly increasing Ca²⁺ entry. *ATP2B3* encodes a Ca²⁺-ATPase on the plasma membrane that is responsible for extruding Ca²⁺ ions from the cytoplasm, so decreased function of this transporter leads to the buildup of Ca²⁺ ions in the cell (Beuschlein et al., 2013). *CACNA1D* encodes a voltage-gated Ca²⁺ channel located on the plasma membrane, and gain-of-function mutations in *CACNA1D* cause the channel to be activated at less depolarized potentials, thus generally increasing Ca²⁺ influx (Scholl et al., 2013). These data show that multiple different functional mutations in ion channels and transporters can contribute to the formation of APAs by causing sustained increases in intracellular Ca²⁺.

Another channel-encoding gene, *GRIN2A*, is frequently mutated in malignant melanoma (Wei et al., 2011). *GRIN2A* encodes a modulatory subunit of the *N*-methyl-D-aspartate (NMDA) receptor, an ionotropic receptor that permits Ca²⁺ influx upon stimulation by glutamate or glycine (Traynelis et al., 2010). Opening of this channel results in increased intracellular Ca²⁺ levels, leading to the activation of Ca²⁺-dependent signaling pathways that can either promote proliferation or apoptosis depending on the strength and duration of signaling (Traynelis et al., 2010). The wild-type NMDA receptor

can either function as an oncogene or tumor suppressor by tightly regulating Ca^{2+} influx, but its function depends on glutamate concentration in the extracellular environment (D'Mello S et al., 2016). Under low glutamate conditions found in early tumors, activation of the NMDA receptor may facilitate cell survival, proliferation, and migration by increasing intracellular Ca^{2+} (D'Mello S et al., 2016). However, NMDA receptors may function as tumor suppressors under high glutamate conditions. Receptors that are hyperactivated by excess glutamate create a large, prolonged increase of intracellular Ca^{2+} , resulting in the activation of pro-apoptotic signaling pathways and reduced cell proliferation and migration in neurons (Mody and MacDonald, 1995). Some of the *GRIN2A* mutations identified in melanoma activate the channel and promote melanoma cell proliferation and tumor formation. Other point mutations in *GRIN2A* instead have a dominant-negative effect by preventing the NMDA receptor complex from forming properly and thus abolish normal channel function (Prickett et al., 2014). In these cases, by curbing the tumor suppressor activity of NMDA receptors, these *GRIN2A* mutants may also drive melanomagenesis. Additional studies need to be performed to elucidate the functions of each of the *GRIN2A* mutations found in melanoma, but it appears that NMDA receptors can function as both oncogenes and tumor suppressors in melanoma.

Although clear driver mutations are not frequently found in ion channels and transporters, several key examples of both gain-of-function and loss-of-function somatic mutations demonstrate that ion channels and transporters can play pivotal roles in the development or progression of cancer. Additional studies have identified frequent mutations in ion channel or transporter-encoding genes but have not yet investigated

the functional consequences of these mutations (Agrawal et al., 2011; Barbieri et al., 2012; Berger et al., 2012; Krauthammer et al., 2012; Wei et al., 2011). Further work needs to be done to characterize potential driver mutations in these genes.

2.4 The therapeutic potential of ion channel and transporter inhibition

Many studies suggest that aberrant ion channel and transporter function contributes to many different types of cancer. Consequently, ion channels and transporters have been explored as potential therapeutic targets (Fraser and Pardo, 2008; Monteith et al., 2007). Ion channels and transporters are attractive therapeutic targets for cancer because they are often expressed on the cell surface, their pharmacology is relatively well-characterized, and many ion channel and transporter modulators are already used for clinical applications (Fraser and Pardo, 2008; Pedersen and Stock, 2013).

There is growing evidence that inhibition of ion channels and transporters can reduce tumor growth *in vivo*. Systemic administration of a monoclonal antibody against the *KCNK9*-encoded K⁺ channel inhibits the growth of human lung cancer xenografts (Sun et al., 2016). Monoclonal antibody blockade of the EAG K⁺ channel also exerts antitumor activity in a breast cancer xenograft model (Gomez-Varela et al., 2007). Treatment of breast cancer xenograft tumors with AM-0902, an orally-active pharmacological inhibitor of TRPA1, reduces tumor volume without significant side effects (Takahashi et al., 2018). Furthermore, MK-801, an NMDA receptor antagonist, inhibits melanoma xenograft growth by preventing the activation of glutamate-mediated

Ca²⁺ signaling (Song et al., 2012). These are just a few examples of ion channel or transporter antagonists that have successfully inhibited tumor growth *in vivo*, but a number of other studies have shown that blocking specific ion channels or transporters reduces cell proliferation in culture (Prevarskaya et al., 2010).

Antagonists of ion channels or transporters can also inhibit metastasis. Antibodies against the K⁺ channel encoded by *KCNK9* reduce lung metastasis in mice transplanted with a murine breast cancer cell line (Sun et al., 2016). A pharmacological inhibitor of store-operated calcium entry (SOCE) channels greatly reduces the metastasis of 4T1 mouse mammary tumors (Yang et al., 2009). Finally, inhibition of an ectopically expressed Cl⁻ channel, CLC-3, with a synthetic scorpion toxin, TM-601, reduces the invasiveness of glioma cells in cultured brain slices (Sontheimer, 2008; Soroceanu et al., 1999). The inhibitor is thought to work by preventing the Cl⁻ channel-mediated volume changes necessary for glioma cells to squeeze through narrow extracellular brain spaces and invade surrounding tissue (McFerrin and Sontheimer, 2006). One advantage of using this inhibitor is that its Cl⁻ channel target is only expressed on glial tumors but not normal cells such that the drug can specifically target cancer cells (Mamelak and Jacoby, 2007). Due to promising preclinical data, ¹³¹I-conjugated TM-601 was taken into clinical trials for patients with advanced gliomas.

Inhibitors of ion channels and transporters may also be combined with other targeted therapies to achieve antitumoral effects. Our laboratory found that cardiac glycosides, which inhibit the Na⁺/K⁺-ATPase, combine with MAPK inhibitors like trametinib (a MEK inhibitor) or dabrafenib (a BRAF inhibitor) to synergistically reduce

the growth of a subset of patient-derived melanoma xenografts (Eskiocak et al., 2016). Combined inhibition of the ATP1A1 Na⁺/K⁺ transporter and of the MAPK pathway dysregulates intracellular pH, mitochondrial Ca²⁺ levels, and mitochondrial function, leading to melanoma cell death (Eskiocak et al., 2016). Based on these preclinical data, a clinical trial testing digoxin (an ATP1A1 inhibitor) and trametinib in patients with advanced, refractory BRAF wild-type melanoma was initiated at UT Southwestern. In this subset of patients, the drug combination yielded a 20% response rate (Frankel et al., 2017), significantly greater than the expected 10% response rate with trametinib alone (Falchook et al., 2012).

These data suggest that ion channels and transporters are important for tumor development and progression and that inhibitors of these membrane proteins may be viable therapeutic options for cancer patients (Fraser and Pardo, 2008). However, several key caveats need to be considered. Although many pharmacological inhibitors of ion channels and transporters are available for use, selectively targeting ubiquitously expressed channels and transporters in cancer cells is still a challenge (Prevarskaya et al., 2010). To address this issue, therapies that target ion channels and transporters that are more highly expressed in cancer cells should be pursued. There are also many uncharacterized somatic mutations in genes that encode ion channels and transporters that are found in exome or whole genome sequencing studies. Some of those mutations may be activating driver mutations that directly contribute to tumor initiation or progress, and specific inhibitors could be developed against these mutant proteins. Another issue with targeting ion channels and transporters is that many of their pharmacological

modulators are not specific for individual channels but instead target a class of channels or transporters. For instance, most K⁺ channel inhibitors used in the clinic to treat cardiac arrhythmias, diabetes, or multiple sclerosis block more than one type of K⁺ channel (Colatsky et al., 1990). In order to target a specific K⁺ channel subunit, monoclonal antibodies rather than chemical inhibitors may be required (Fraser and Pardo, 2008; Gomez-Varela et al., 2007; Sun et al., 2016). Thus, to successfully target ion channels and transporters in cancer, there is a need to continue studying ion channels and transporters that are overexpressed and mutated in cancers, to elucidate the molecular mechanisms by which they contribute to tumor progression, to identify downstream effector molecules, and to develop new tools to specifically target individual channels and transporters.

CHAPTER THREE

TRPML1 promotes protein homeostasis in melanoma cells by negatively regulating MAPK and mTORC1 signaling

3.1 Introduction

Ion channels and transporters maintain ion gradients that enable the transport of metabolites across membranes and regulate diverse aspects of cellular physiology (Clapham, 2003; Kew and Davies, 2010; Pardo and Stuhmer, 2014; Purves, 2004). Gain-of-function mutations or overexpression of ion channels and transporters can drive cancer cell proliferation or disease progression (Beuschlein et al., 2013; Cardone et al., 2005; Choi et al., 2011; Mu et al., 2003; Pei et al., 2003; Scholl et al., 2013; Takahashi et al., 2018). Cancer cells depend upon ion channels and transporters to regulate many cellular processes including intracellular calcium levels (Choi et al., 2011), pH (Webb et al., 2011), oxidative stress (Takahashi et al., 2018), proliferation (Pardo and Stuhmer, 2014), and cellular migration (Pardo and Stuhmer, 2014). Consequently, ion channels and transporters have been explored as potential therapeutic targets (Fraser and Pardo, 2008; Monteith et al., 2007).

Endosomes and lysosomes are signaling hubs that integrate nutrient stimuli to direct cell growth and metabolism (Perera and Zoncu, 2016; Settembre et al., 2013). After activated receptor tyrosine kinases are endocytosed, they accumulate and signal in endosomes, where adaptor proteins can localize signaling molecules to facilitate increased signaling (Di Fiore and De Camilli, 2001). Defects in endosome or lysosome function can alter the activation of signal transduction pathways, including the PI3K and

MAPK pathways (Inamura et al., 2018; Kawashima et al., 2009). Endosome and lysosome function are regulated by cation channels in their membranes such as TRPML1 (Calcraft et al., 2009; Cang et al., 2013; Venkatachalam et al., 2015). TRPML1, which is encoded by the gene *MCOLN1*, mediates the release of Ca^{2+} and potentially other cations from lysosomes (Dong et al., 2010). It regulates multiple aspects of endolysosomal trafficking, phagocytosis, and the fusion of phagosomes with lysosomes (Dayam et al., 2015; Samie et al., 2013). Loss of *MCOLN1* causes mucopolipidosis type IV, marked by defects in lysosomal storage and autophagy (Chen et al., 1998). The release of Ca^{2+} by TRPML1 also activates calcineurin, which promotes TFEB activation (Medina et al., 2015; Shen et al., 2012). TFEB is a master regulator of lysosome biogenesis (Sardiello et al., 2009; Settembre et al., 2011). TRPML1 activation also activates calmodulin, which promotes mTORC1 activation (Li et al., 2016a). TRPML1 promotes MAPK pathway activation in head and neck cancer cells (Jung et al., 2019) and TORC1 activation in *Drosophila* cells (Wong et al., 2012) while reducing MAPK and PI3K pathway activation in astrocytes (Weinstock et al., 2018). Thus, it seems that the effects of TRPML1 function on signaling pathways is highly dependent on cell type.

mTORC1 promotes cellular proliferation by activating anabolic pathways such as protein synthesis and by inactivating catabolic pathways such as autophagy (Saxton and Sabatini, 2017; Valvezan and Manning, 2019). mTORC1 is hyperactivated in some cells with lysosomal storage disorders (Bartolomeo et al., 2017). mTORC1 promotes the growth and proliferation of cancer cells, though it can inhibit the proliferation of amino

acid-starved cells by suppressing macropinocytosis, the lysosome-mediated catabolism of proteins taken up from outside the cell (Palm et al., 2015). Macropinocytosis is promoted by MAPK pathway activation and can be an important source of amino acids in nutrient-deprived cancer cells (Bar-Sagi and Feramisco, 1986; Commisso et al., 2013; Kamphorst et al., 2015; Palm et al., 2015).

Melanoma cells are particularly sensitive to the dysregulation of calcium homeostasis (Eskiocak et al., 2016). Combined inhibition of the ATP1A1 Na^+/K^+ transporter and of the MAPK pathway dysregulates intracellular pH, mitochondrial Ca^{2+} levels, and mitochondrial function, leading to melanoma cell death (Eskiocak et al., 2016). Furthermore, a clinical trial at UT Southwestern demonstrated that the combination of digoxin, an ATP1A1 inhibitor, and trametinib, a MEK inhibitor, achieved disease control in 65% of patients with advanced, refractory BRAF wild-type melanoma. The drug combination also yielded a 20% response rate (Frankel et al., 2017), significantly greater than the expected 10% response rate with trametinib alone (Falchook et al., 2012).

These data suggest that melanoma cells are sensitive to perturbations in Ca^{2+} homeostasis and raise the possibility that inhibition of other ion channels and transporters would achieve even greater therapeutic responses in melanoma patients. I thus hypothesized that melanoma cells preferentially require certain ion channels and transporters for tumorigenesis and tumor progression. Identification of these ion channels and transporters could not only reveal new vulnerabilities in melanoma cells but also lead to the development of additional therapies.

To test my hypothesis, I sought to conduct an *in vivo* loss-of-function genetic screen against ion channels and transporters to identify those that are required by human melanoma cells but not by normal human melanocytes. *In vivo* loss-of-function screening can be performed using short hairpin RNAs (shRNAs) or CRISPR-Cas9 (Gargiulo et al., 2014; Shalem et al., 2014). shRNAs are RNA molecules that form tight hairpin loops that can be used to stably silence target gene expression in mammalian cells via RNA interference (RNAi) (Brummelkamp et al., 2002; Paddison et al., 2002). CRISPR-Cas9 can be used to introduce targeted loss-of-function mutations in specific genes by inducing DNA double strand breaks at locations in the genome specified by single guide RNAs (sgRNAs) (Cong et al., 2013; Ran et al., 2013). These two genetic approaches are often exploited to conduct large-scale pooled screens (Bric et al., 2009; Gargiulo et al., 2014; Shalem et al., 2014; Wang et al., 2015; Zender et al., 2008). When tumorigenesis screens are performed *in vivo*, shRNA or sgRNA constructs are delivered to cancer cells, and then these cells are injected into mice. Then, using next-generation sequencing (NGS), the relative abundance of each shRNA or sgRNA is compared between the tumor samples and the input samples of cells collected before injection. The shRNAs or sgRNAs that are depleted in tumors as compared to input cells are enriched for target genes that are required by the cancer cells.

A major distinction between shRNAs and CRISPR-Cas9 is that shRNAs tend to reduce gene expression while CRISPR-Cas9 completely eliminates gene expression. Although CRISPR-Cas9 technology can generate more robust phenotypes due to its ability to completely eliminate gene expression and tends to have fewer off-target effects

(Ran et al., 2013), shRNA-mediated screens have a few key advantages. shRNA-mediated knockdown more accurately reflects the pharmacological inhibition of targets that could be achieved in patients, as small molecule inhibitors tend to reduce, but not completely eliminate, the function of gene products. Also, introducing mutations into genes using CRISPR-Cas9 can induce compensatory changes in cancer cells (Peretz et al., 2018). Furthermore, CRISPR-Cas9 can be challenging to execute in primary cells derived from human patients due to the difficulty of clonally expanding primary cells in culture from single cells (Seki and Rutz, 2018; Shifrut et al., 2018). For these reasons, I decided to use an shRNA screen to identify ion channels and transporters that are preferentially required by melanoma cells.

In this study, I conducted an *in vivo* shRNA-mediated screen against all known ion channels and transporters in the human genome. I discovered that TRPML1, a lysosomal cation channel, is necessary for the survival and proliferation of human melanoma cells but not human melanocytes. Loss of TRPML1 in melanoma cells decreased cell growth *in vitro*, decreased tumor growth *in vivo*, increased apoptosis, increased proteotoxic stress, decreased macropinocytosis, and depleted serine levels. Surprisingly, I found that all of these phenotypes were partially or completely rescued by mTORC1 inhibition. Even though melanoma cells rely on increased MAPK and mTORC1 signaling, my data suggest that TRPML1 protects melanoma cells from overactivation of mTORC1, which can be detrimental to cancer cells (Chen et al., 2005). Thus, TRPML1 enhances melanoma cell survival by attenuating MAPK and mTORC1 signaling to sustain protein homeostasis and macropinocytosis.

3.2 Results

To identify ion channels and transporters on which melanoma cells preferentially depend, we performed an *in vivo* drop-out screen of a library of shRNAs in xenografted melanomas. The library contained 2,589 shRNAs against 572 genes that encode ion channels and transporters, with 3 to 7 shRNAs per gene. We infected melanomas from three patients (M214, M481, and M491) with 27 pools of shRNAs (~100 shRNAs/pool), then transplanted the infected cells subcutaneously into NOD-SCID-*Il2rg*^{-/-} (NSG) mice, allowed tumors to form, and sequenced to compare the abundance of shRNAs in the tumors versus input cells (**Figure 3.1A**). In dropout shRNA screens, it is important to represent as many hairpins as possible in each tumor to control for factors such as stochastic drift and heterogeneity in tumorigenic potential (Gargiulo et al., 2014). Because we wanted to inject a maximum of 100,000 melanoma cells into each mouse, we chose to divide the shRNA library into pools of 100 shRNAs per pool so that an average of nearly 1000 cells were infected with each shRNA in each mouse (Gargiulo et al., 2014). Additionally, each pool included two scrambled negative control shRNAs and three positive control shRNAs against a gene known to be required by melanoma cells (*EIF3A*) (Dong and Zhang, 2006). The scrambled negative control shRNAs did not significantly change in abundance in tumors as compared to input cells (**Figures 3.1B-3.1D**) while the positive control shRNAs against *EIF3A* were significantly depleted (**Figures 3.1B-3.1D**). Based on our criteria (**Figure 3.2A**), we identified shRNAs against 40 genes that were significantly depleted in tumors as compared to input cells,

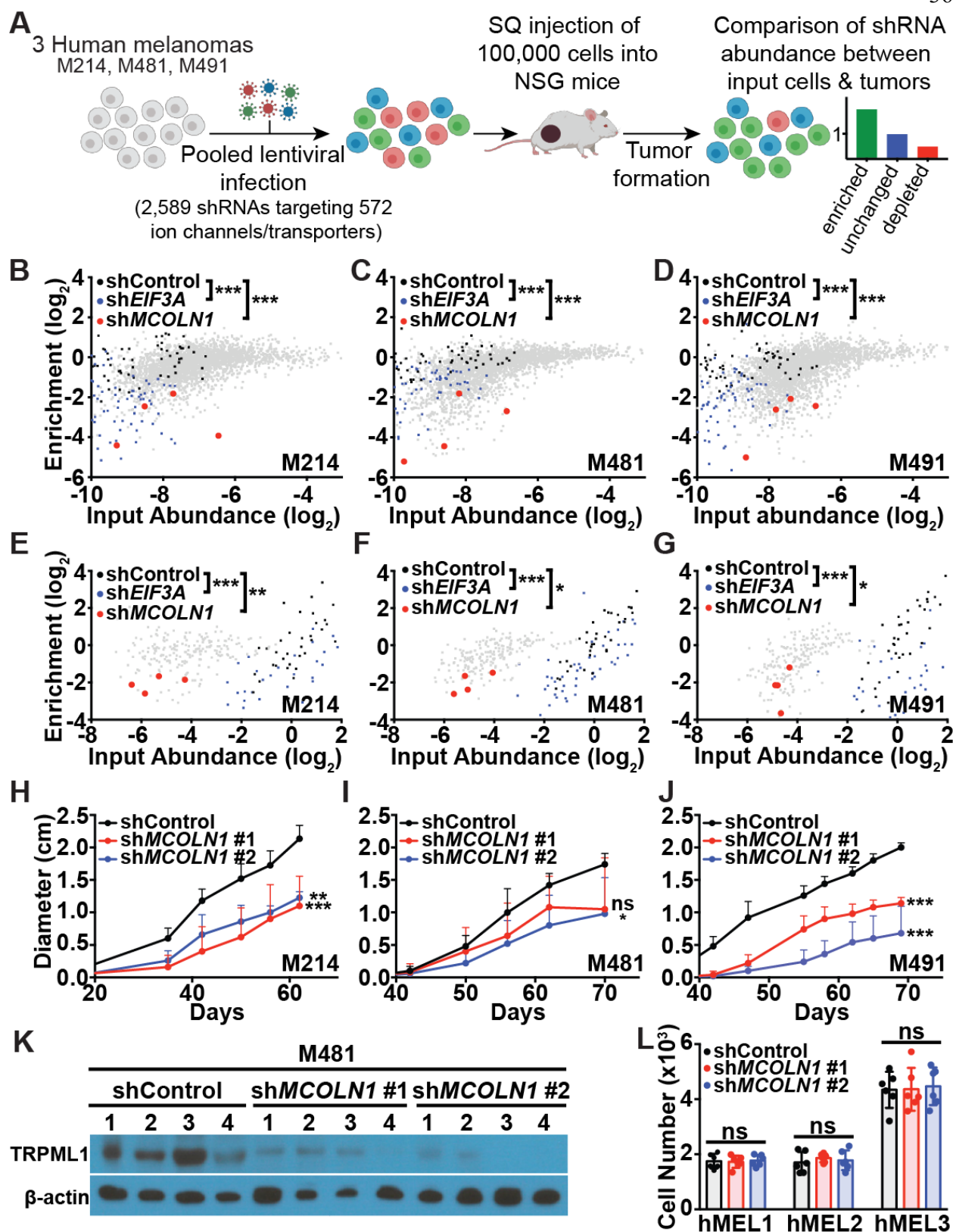


Figure 3.1. An *in vivo* shRNA screen identified *MCOLN1* as being preferentially required by melanoma cells. **A**, Melanoma cells from three patients (M214, M481, and M491) were transduced with 27 pools of shRNAs targeting ion channels and transporters throughout the human genome. 100,000 infected cells were subcutaneously transplanted into each of 4 NSG mice per pool (324 NSG mice total). **B-D**, In the primary screen of 2,589 shRNAs, shRNAs targeting *MCOLN1* (red) were significantly depleted in tumors relative to input cells and in tumors relative to scrambled negative control shRNAs (black) in all three melanomas. Positive control shRNAs against *EIF3A* (blue) were also significantly depleted. **E-G**, In the secondary screen of 210 shRNAs, shRNAs targeting *MCOLN1* (red) were significantly depleted in tumors relative to input cells and in tumors relative to scrambled negative control shRNAs (black) in all three melanomas. Positive control shRNAs against *EIF3A* (blue) were also significantly depleted. **H-J**, Growth of subcutaneous tumors in mice transplanted with three different melanomas expressing scrambled control shRNA (black) or two shRNAs against *MCOLN1* (red and blue). The data represent mean \pm s.d. from one representative experiment (of two performed) with 5 mice per shRNA per melanoma. **K**, Western blot analysis of TRPML1 and β -actin in melanoma cells expressing two shRNAs against *MCOLN1* versus scrambled negative control shRNA. The blot reflects one representative experiment (of two performed) per melanoma. **L**, Growth of primary human melanocytes in culture from three donors (hMEL1, hMEL2, hMEL3) expressing scrambled control shRNA (black) versus two shRNAs against *MCOLN1* (red and blue). The data represent mean \pm s.d. from two independent experiments with 3 replicate cultures per clone per experiment. Statistical significance was assessed using Kruskal-Wallis tests followed by Dunn's multiple comparisons tests (**B-G**), one-way analyses of variance (ANOVA) or Kruskal-Wallis tests followed by Dunnett's or Dunn's multiple comparisons tests, respectively, for the last time points measured (**H-J**), or one way analyses of variance (ANOVA) followed by Dunnett's multiple comparisons test (**L**); ns, not significant; *, $p < 0.05$; **, $p < 0.01$; ***, $p < 0.001$.

A

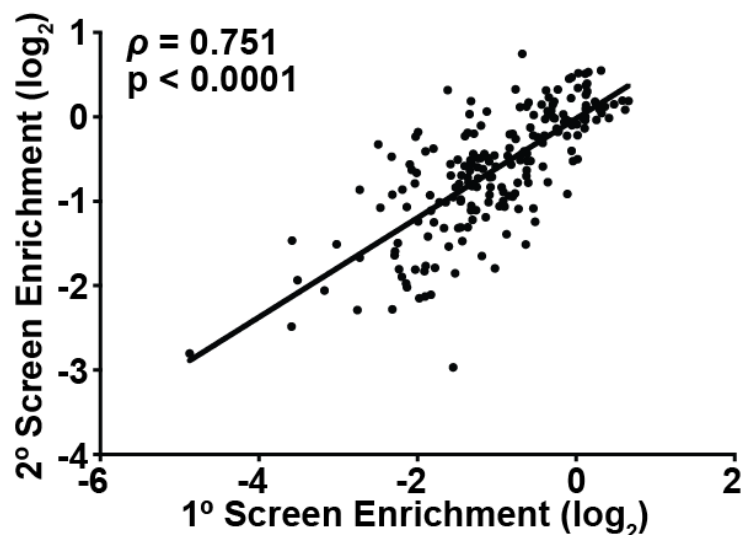
Candidate shRNAs

- must be depleted $\geq 50\%$ in tumors as compared to input cells in at least 2 out of 3 melanomas
- tumor abundance relative to input abundance, $p \leq 0.05$

Candidate genes

- must have ≥ 2 unique shRNAs that meet the candidate shRNA criteria
- must be expressed at the RNA level in all 3 melanomas

C



B

Gene	# Depleted shRNAs
<i>KCNK15</i>	5 out of 6
<i>MCOLN1</i>	4 out of 4
<i>TOMM40</i>	3 out of 5
<i>TRPM2</i>	2 out of 7
<i>TSPO</i>	2 out of 4
<i>FXYD3</i>	3 out of 7
<i>KCNC4</i>	2 out of 5
<i>KCNG1</i>	2 out of 6
<i>KCNH2</i>	2 out of 6
<i>KCNJ12</i>	2 out of 3
<i>KCTD7</i>	2 out of 9
<i>RYR1</i>	2 out of 6
<i>SCN9A</i>	2 out of 7
<i>MLC1</i>	2 out of 6
<i>TPCN2</i>	2 out of 7
<i>P2RX4</i>	3 out of 5
<i>SLC39A3</i>	2 out of 3
<i>SLC39A4</i>	2 out of 3
<i>SLC9A1</i>	2 out of 6
<i>TPCN1</i>	2 out of 9
<i>FXYD1</i>	2 out of 4
<i>FXYD7</i>	2 out of 5
<i>TTYH1</i>	3 out of 4
<i>ATP6V0D1</i>	3 out of 3
<i>ITPR3</i>	3 out of 6
<i>KCNA5</i>	3 out of 8
<i>ATP13A1</i>	2 out of 3
<i>ATP5D</i>	2 out of 3
<i>CACNB1</i>	2 out of 6
<i>CLCN4</i>	2 out of 6
<i>HCN1</i>	2 out of 8
<i>KCNK5</i>	2 out of 5
<i>KCTD12</i>	2 out of 6
<i>KCTD14</i>	2 out of 6
<i>KCTD15</i>	2 out of 5
<i>PKD1</i>	2 out of 3
<i>PKD2</i>	2 out of 6
<i>SLC12A9</i>	2 out of 3
<i>SLC22A5</i>	2 out of 3
<i>SLC41A1</i>	2 out of 3

Figure 3.2. Ion channels and transporters that appeared to be required by melanoma cells based on the shRNA screen. A, Criteria for identifying significantly depleted shRNAs and genes required by melanoma cells in the primary and secondary screens. **B,** Forty genes met these criteria in the primary screen and 15 were validated in the secondary screen (highlighted in blue). The table includes the number of shRNAs against each gene that were significantly depleted in tumors relative to input cells in the primary screen. **C,** Correlation between the enrichment (negative values mean depletion) of each shRNA in the primary and secondary screens. Statistical significance was assessed based on Spearman's correlation coefficient (**C**).

suggesting these gene products were required by melanoma cells (**Figure 3.2B**).

Surprisingly, we did not identify many shRNAs that were enriched in the screen. This suggests that either shRNAs are all slightly toxic to melanoma cells or that ion channels and transporters rarely suppress tumorigenesis by melanoma cells.

We performed a secondary screen using 210 shRNAs against the 40 candidate genes, divided into 18 pools (~12 shRNAs/pool). Again, the scrambled negative control shRNAs did not significantly change in abundance in tumors as compared to input cells (**Figures 3.1E-3.1G**) while the positive control shRNAs against *EIF3A* were significantly depleted (**Figures 3.1E-3.1G**). From this secondary screen, we identified shRNAs against 15 genes that were significantly depleted in the tumors as compared to input cells using the same criteria as in the primary screen (**Figures 3.2A and 3.2B**). We found a significant correlation between the results of the primary and secondary screens (**Figure 3.2C**). Although shRNAs against a potassium channel, *KCNK15*, were the most significantly depleted in the screens, *KCNK15* was expressed only at very low levels in melanoma cells and thus potentially represented a false positive. We therefore focused on the next-best candidate, *MCOLN1*.

All four shRNAs targeting *MCOLN1* were significantly depleted in tumors relative to input cells in the primary (**Figures 3.1B-3.1D**) and secondary (**Figures 3.1E-3.1G**) screens. In screens for essential genes, *MCOLN1* was not required for the survival of CML cells or Burkitt's lymphoma cells (Blomen et al., 2015; Wang et al., 2015), raising the possibility it is preferentially required by melanoma cells. To test this, we infected melanoma cells from three patients with two shRNAs that efficiently knocked down

MCOLN1/TRPML1 (**Figure 3.1K**) or scrambled control shRNA, then injected the cells subcutaneously in NSG mice. Both shRNAs against *MCOLN1* significantly decreased the growth of tumors relative to control shRNA in all three melanomas (**Figures 3.1H-3.1J**). However, neither shRNA against *MCOLN1* significantly affected the growth of melanocytes from three donors (**Figure 3.1L**). *MCOLN1* is thus required by melanoma cells but not normal melanocytes. Consistent with this, *MCOLN1* was more highly expressed by melanoma cells than melanocytes (**Figure 3.3A**).

To independently assess whether *MCOLN1*/TRPML1 is required by melanoma cells, we deleted *MCOLN1* from melanoma cells using CRISPR. We generated three independent clones of *MCOLN1*-deficient melanoma cells from each of a melanoma cell line (A375) and two patient-derived melanomas (M214 and M481; **Figure 3.4A**). In each case, the *MCOLN1*-deficient clones had a 34 base pair deletion in exon 2, causing a frame-shift. Compared to parental cells, the *MCOLN1*-deficient clones had little *MCOLN1* mRNA (**Figures 3.4B-3.4D**) and no detectable TRPML1 protein (**Figures 3.3B-3.3D**).

All of the *MCOLN1*-deficient melanoma cells grew significantly more slowly in culture as compared to parental cells (**Figures 3.3E-3.3G**), exhibiting significantly higher frequencies of activated caspase 3/7⁺ cells (**Figure 3.3H**) and significantly lower frequencies of Ki-67⁺ proliferating cells (**Figure 3.3I**). *MCOLN1* overexpression in the *MCOLN1*-deficient cells rescued the growth of these cells in culture (**Figure 3.4E**), demonstrating that their poor growth reflected a loss of *MCOLN1*/TRPML1 function rather than off-target mutations. After xenografting subcutaneously in NSG mice, all of

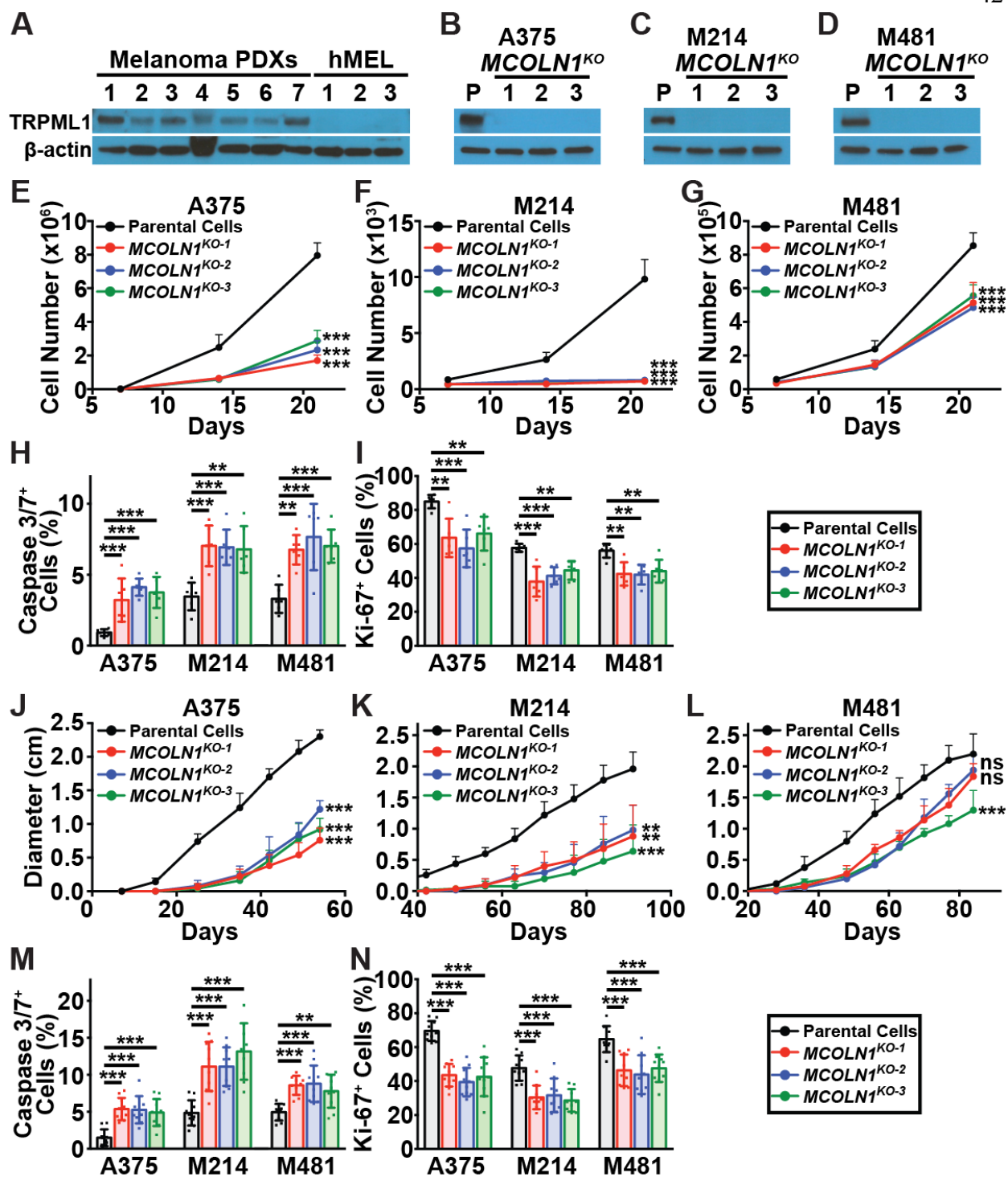


Figure 3.3. Loss of *MCOLN1*/TRPML1 impaired melanoma cell survival *in vitro* and *in vivo*. **A**, Western blot analysis of TRPML1 and β -actin in melanoma cells derived from 7 patients (Melanoma PDXs; M214, M405, M481, M491, UT10, M528, M597) and normal melanocytes derived from 3 donors (hMEL). The blot reflects one representative experiment of two performed. **B-D**, Western blot analysis of TRPML1 and β -actin in parental cells (P) from three melanomas (A375 cell line; M214 and M481 patient-derived melanomas) as well as in 3 clones per melanoma in which *MCOLN1* had been deleted using CRISPR. The blot reflects one representative experiment (of two performed) per melanoma. **E-G**, Growth in culture of parental cells (black) versus *MCOLN1*-deficient clones (red, blue, and green). **H, I**, Frequencies of activated caspase 3/7+ cells (**H**) and Ki-67+ cells (**I**) among cultured parental cells versus *MCOLN1*-deficient clones. Panels **E-I** show mean \pm s.d. from two independent experiments with 3 replicate cultures per clone per experiment. **J-L**, Growth of subcutaneous tumors in mice transplanted with parental cells versus *MCOLN1*-deficient clones. Data show mean \pm s.d. from one representative experiment (of two performed) with 5 mice per clone. **M, N**, Frequencies of activated caspase 3/7+ cells (**M**) and Ki-67+ cells (**N**) in subcutaneous tumors grown from parental cells versus *MCOLN1*-deficient clones. Data represent mean \pm s.d. from two independent experiments with 5 mice per clone per melanoma per experiment. Statistical significance was assessed using one-way ANOVA or Welch's one-way ANOVA followed by Dunnett's or Dunnett's T3 multiple comparisons tests, respectively, for the last time point measured (**E-G, J-L**), or one-way ANOVAs followed by Dunnett's multiple comparisons tests (**H-I, M-N**); ns, not significant; **, $p < 0.01$; ***, $p < 0.001$.

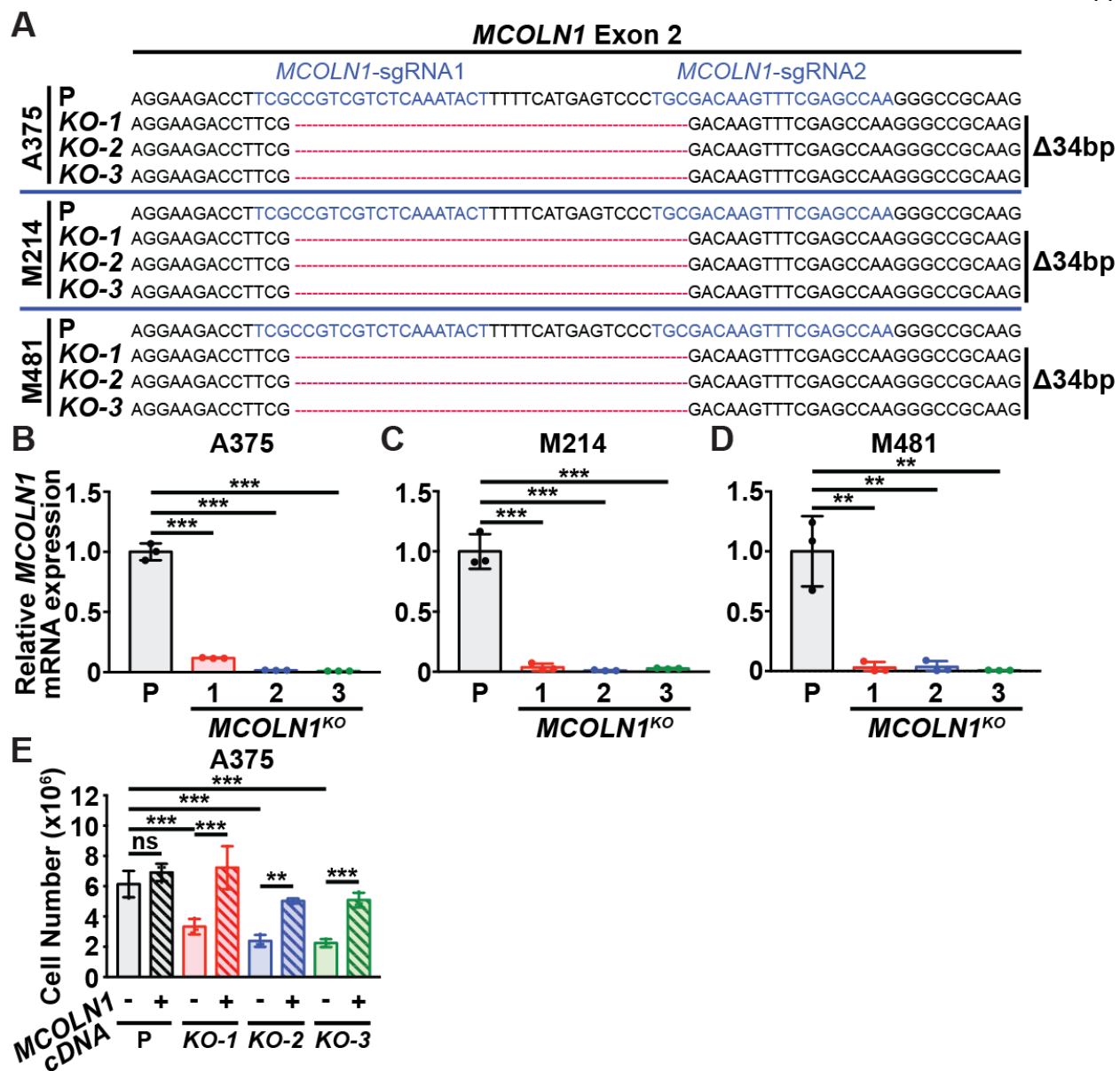


Figure 3.4. Generation of *MCOLN1*-deficient melanoma cells by CRISPR editing. **A**, CRISPR editing of *MCOLN1* in three melanomas (A375, M214, and M481) to generate three clones per melanoma bearing a 34 base pair deletion in exon 2. This created a frameshift near the start codon and therefore was predicted to give a strong loss of function. **B-D**, Reverse Transcription qPCR analysis of *MCOLN1* transcript levels in parental cells (black) versus three *MCOLN1*-deficient clones from each melanoma (red, blue, and green). These data represent mean \pm s.d. from one experiment with 3 replicates per clone. **E**, Growth in culture of A375 parental cells versus *MCOLN1*-deficient clones expressing empty vector or human *MCOLN1* cDNA. *MCOLN1* expression rescued the growth of *MCOLN1*-deficient clones. Data represent mean \pm s.d. from one experiment with 3 replicate cultures per treatment per clone. Statistical significance was assessed using one-way ANOVAs followed by Dunnett's multiple comparisons tests (**B-D**) or a two-way ANOVA followed by Sidak's and Dunnett's multiple comparisons tests (**E**); ns, not significant; **, $p < 0.01$; ***, $p < 0.001$.

the *MCOLN1*-deficient clones formed tumors that grew significantly more slowly as compared to parental cells (**Figures 3.3J-3.3L**). The *MCOLN1*-deficient tumors always contained significantly higher frequencies of activated caspase 3/7⁺ cells (**Figure 3.3M**; see **Figure 3.5** for the gating strategy used to identify melanoma cells by flow cytometry) and significantly lower frequencies of Ki-67⁺ proliferating cells (**Figure 3.3N**) as compared to tumors formed by parental cells. *MCOLN1/TRPML1* thus promoted the survival and proliferation of human melanoma cells *in vitro* and *in vivo*.

These observations may be relevant to patients as melanomas with above average *MCOLN1* expression are associated with significantly worse survival as compared to melanomas with below average *MCOLN1* (**Figure 3.6**).

Given that TRPML1 localizes to endosomal/lysosomal membranes (Venkatachalam et al., 2015), which serve as signaling hubs (Perera and Zoncu, 2016; Settembre et al., 2013), we tested whether loss of *MCOLN1/TRPML1* affected MAPK and PI3K pathway activation. *MCOLN1*-deficient melanoma cells consistently exhibited increased ERK, TSC2, and S6K phosphorylation, and sometimes exhibited increased AKT phosphorylation, as compared to parental melanoma cells (**Figures 3.7A-3.7C**).

We treated *MCOLN1*-deficient and parental melanoma cells with the MEK inhibitor, trametinib. Trametinib blocked the increases in ERK, TSC2, and S6K phosphorylation in *MCOLN1*-deficient clones (**Figures 3.7D-3.7F**), suggesting that the increase in mTORC1 signaling was caused by the phosphorylation and inactivation of TSC2 by the MAPK pathway, as has been observed (Johannessen et al., 2005; Ma et al., 2005; Shaw and Cantley, 2006). However, trametinib did not consistently rescue the

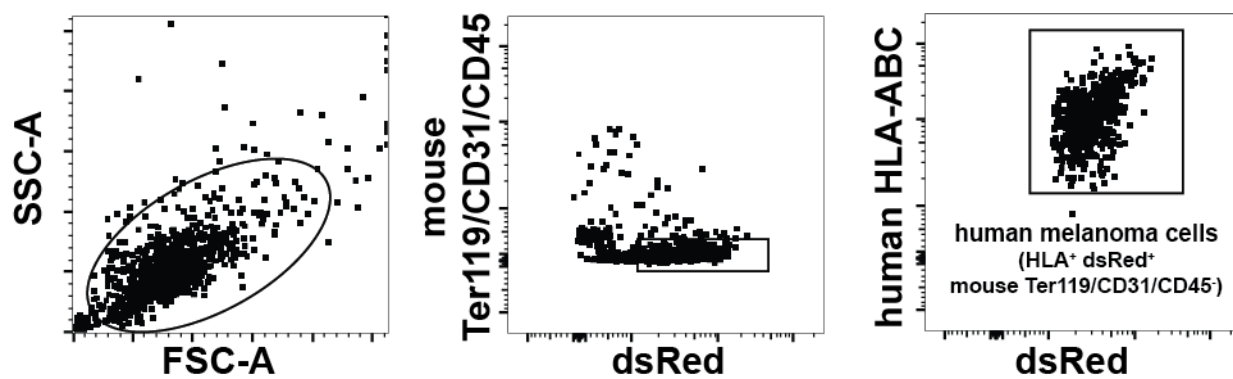


Figure 3.5. Gating strategy used to identify human melanoma cells by flow cytometry. Human melanoma cells were identified and isolated as cells that were positive for DsRed and HLA and negative for mouse CD45, CD31, and Ter119.

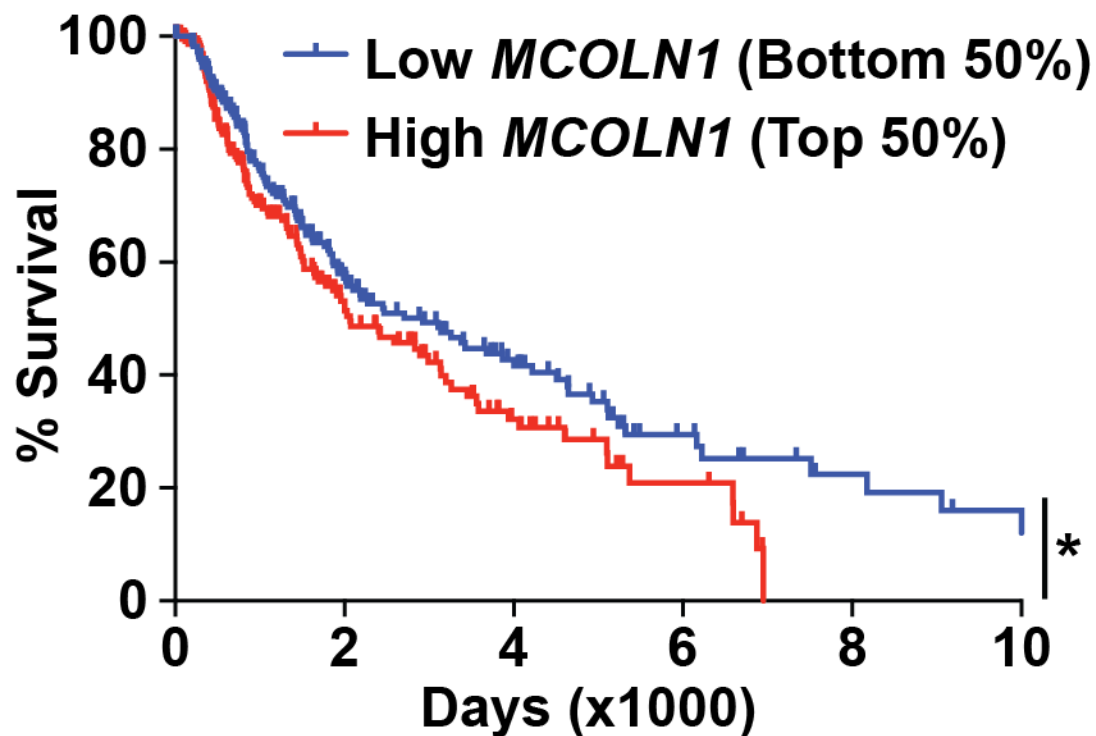


Figure 3.6. *MCOLN1* expression and melanoma patient survival. Kaplan-Meier survival curves of patients with above, or below, average *MCOLN1* expression levels within their melanomas. Data were from the skin cutaneous melanoma (SKCM) cohort in TCGA (<http://portal.gdc.cancer.gov/projects/TCGA-SKCM>). Above average *MCOLN1* expression was associated with significantly worse survival. Statistical significance was assessed using a Mantel-Cox logrank test; *, $p < 0.05$.

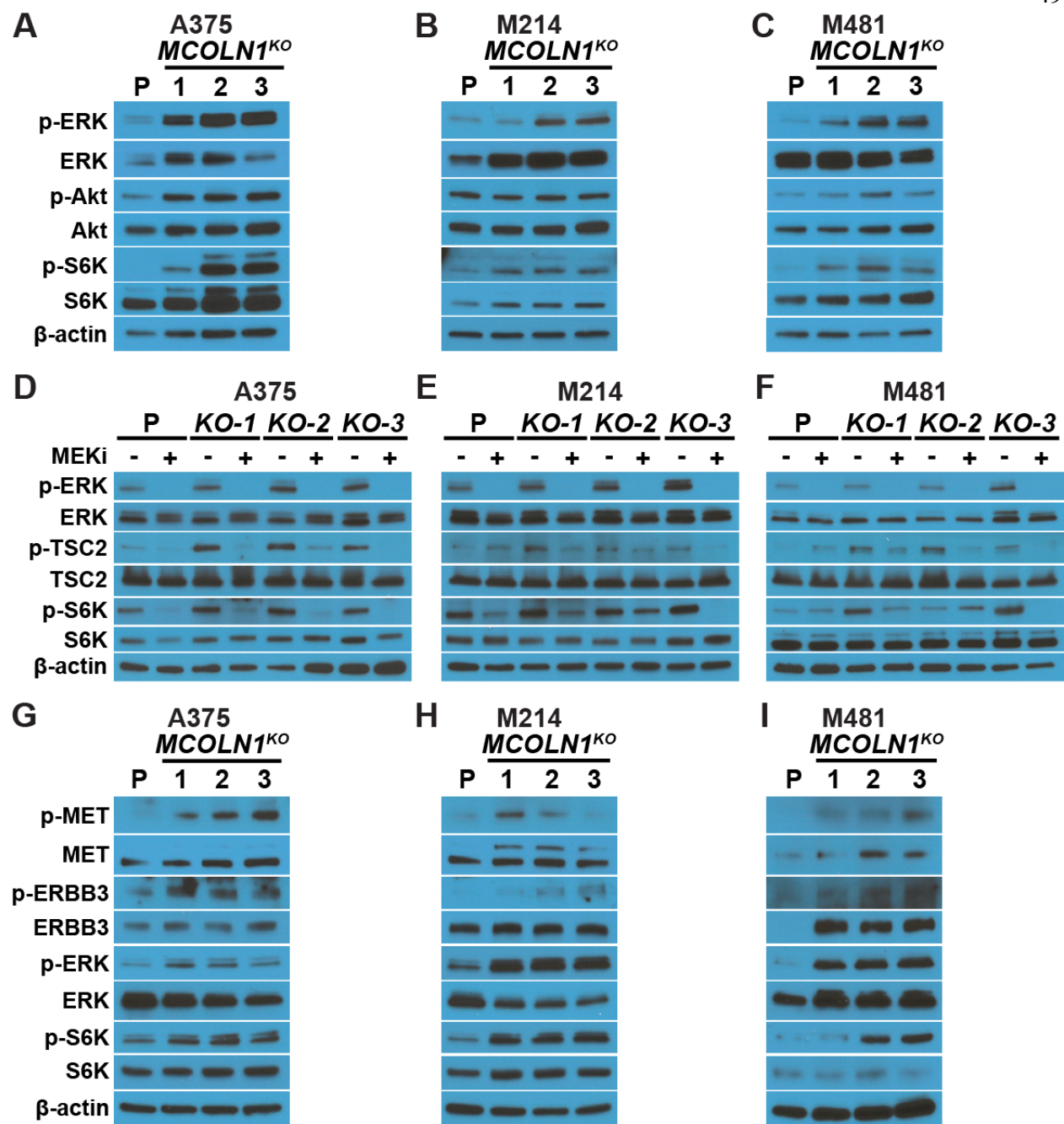


Figure 3.7. *MCOLN1*/TRPML1 deficiency activated MAPK and mTORC1 signaling, and MEK inhibition blocked the increase in ERK and mTORC1 signaling in *MCOLN1*-deficient melanoma cells. **A-C**, Western blots of p-ERK1/2 (T202/Y204), ERK1/2, p-Akt (S473), Akt, p-S6K (T389), S6K, and β -actin in cultured parental cells (P) or *MCOLN1*-deficient cells from three melanomas. **D-F**, Western blots of p-ERK1/2, ERK1/2, p-TSC2 (S664), TSC2, p-S6K, S6K, and β -actin in cultured parental cells or *MCOLN1*-deficient clones from three melanomas treated with DMSO (-) or 5nM trametinib (MEKi; +). **G-I**, Western blots of p-MET (Y1234/1235), MET, p-ERBB3 (Y1289), ERBB3, p-ERK1/2, ERK1/2, p-S6K, S6K, and β -actin in cultured parental cells or *MCOLN1*-deficient cells from three melanomas. All blots represent one representative experiment (of two performed) per melanoma.

growth of *MCOLN1*-deficient clones, possibly due to its known ability to inhibit tumor growth in all three melanomas tested (Eskiocak et al., 2016). Furthermore, BRAF mutation status did not correlate with response to *MCOLN1* loss: A375 and M481 are BRAF-mutant melanomas while M214 is a BRAF-wild type melanoma, but A375 and M214 exhibited the strongest phenotypes upon loss of *MCOLN1* (**Figures 3.3E-3.3G, 3.3J-3.3L**).

To assess why the MAPK pathway was more highly activated in *MCOLN1*-deficient as compared to parental melanoma cells, we examined the levels of phosphorylated MET and ERBB3. MET and ERBB3 are tyrosine kinase receptors that are highly expressed by melanoma cells, signal through the MAPK pathway, and promote melanoma cell proliferation (Chin, 2003; Trusolino et al., 2010; Ueno et al., 2008). Activation of these receptors by ligand binding leads to their phosphorylation and internalization into endosomes, where they signal by activating ERKs, until the endosomes fuse with lysosomes and the receptors are degraded (Citri and Yarden, 2006; Trusolino et al., 2010). Phosphorylated MET and ERBB3 levels were consistently elevated in *MCOLN1*-deficient as compared to parental melanoma cells (**Figures 3.7G-3.7I**). This suggested that *MCOLN1*-deficiency may increase MAPK pathway activation at least partly by increasing receptor signaling, perhaps as a consequence of altered endosome trafficking or fusion with lysosomes.

To test whether there was altered endosome trafficking in *MCOLN1*-deficient melanoma cells, we assessed the co-localization of MET and ERBB3 with the endosomal and lysosomal markers, Rab7 and LAMP1 (Rink et al., 2005). *MCOLN1*-

deficient cells showed significantly increased MET (**Figure 3.8A-3.8D**) and ERBB3 (**Figure 3.9A-3.9D**) colocalization with Rab7 relative to parental cells, suggesting that MET and ERBB3 accumulate in endosomes. Although *MCOLN1*-deficient cells exhibited a perinuclear accumulation of MET and ERBB3, we observed no significant increase in MET or ERBB3 colocalization with LAMP1 relative to parental cells (**Figure 3.8E-3.8H; Figure 3.9E-3.9H**). These data suggest that *MCOLN1*-deficient cells exhibited increased MAPK pathway activation due to defects in endosome trafficking or lysosomal fusion.

To test whether mTOR activation contributed to the poor proliferation and survival of *MCOLN1*-deficient melanoma cells, we treated *MCOLN1*-deficient and parental melanoma cells with the mTOR inhibitor, Torin1 (Thoreen et al., 2009). We used a relatively low concentration of Torin1, 5nM, that blocked the increase in S6K phosphorylation in *MCOLN1*-deficient cells without completely eliminating mTORC1 signaling (**Figures 3.10A-3.10C**). Torin1 treatment also completely, or nearly completely, rescued the growth of *MCOLN1*-deficient cells in culture (**Figures 3.10D-3.10F**).

To test if increased mTORC1 activation contributed to the poor growth of *MCOLN1*-deficient melanomas *in vivo*, we transplanted *MCOLN1*-deficient and parental melanoma clones subcutaneously in NSG mice. Once the tumors became palpable, we treated half of the mice daily with the mTORC1 inhibitor rapamycin. Rapamycin did not significantly affect the growth of tumors from parental lines but completely or nearly completely rescued the growth of *MCOLN1*-deficient tumors (**Figures 3.10G-3.10I**).

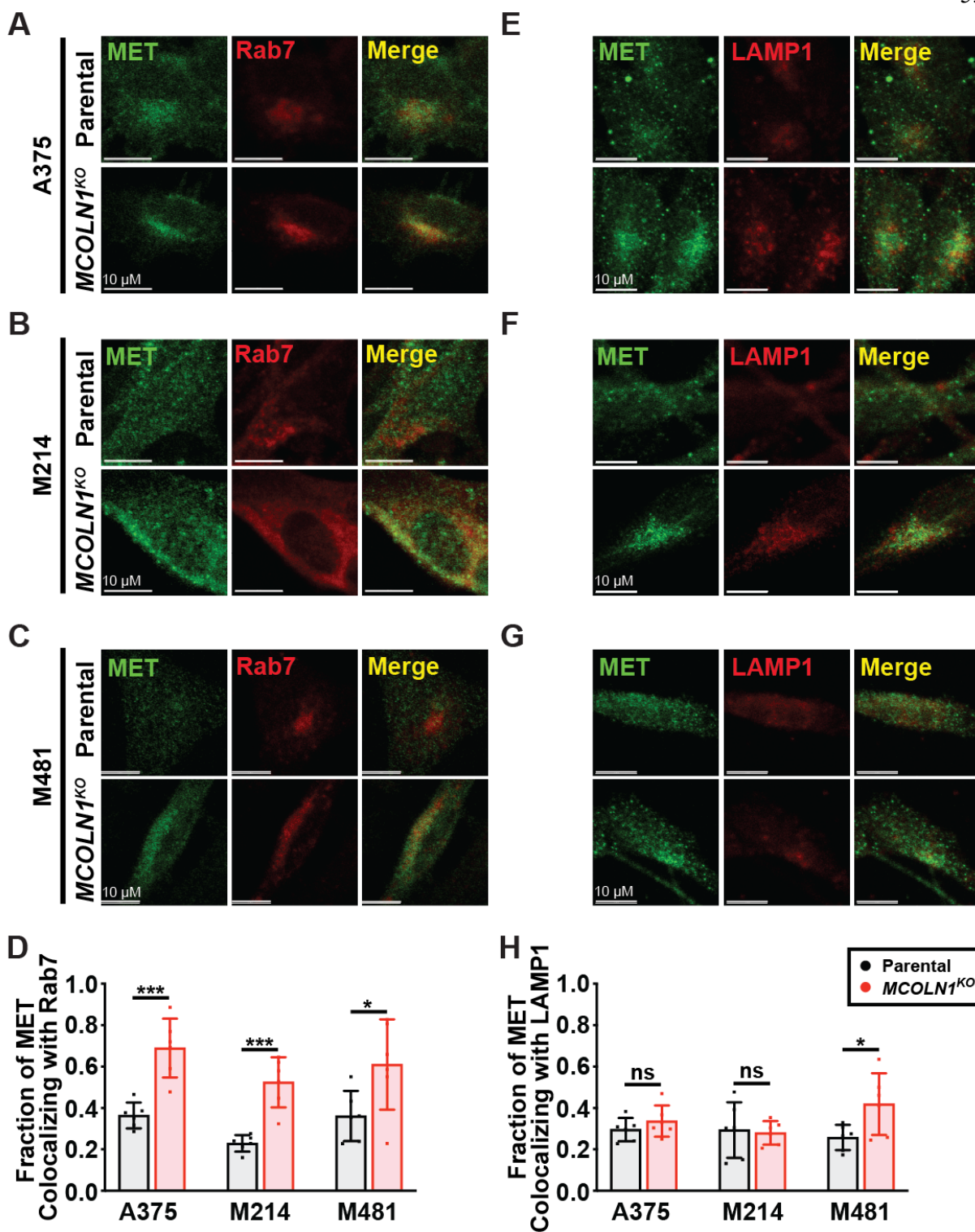


Figure 3.8. MET accumulates in endosomes in *MCOLN1*-deficient cells. **A-C**, Colocalization of MET with the endosomal marker, Rab7, in parental versus *MCOLN1*-deficient cells from three melanomas. **D**, Manders colocalization coefficients reporting the fraction of MET staining that co-localized with Rab7 staining. **E-G**, Colocalization of MET with the lysosomal marker, LAMP1, in parental versus *MCOLN1*-deficient cells from three melanomas. **H**, Manders colocalization coefficients reporting the fraction of MET staining that co-localized with LAMP1 staining. All data represent mean \pm s.d. from two independent experiments with 3 quantified cells per clone per experiment. Statistical significance was assessed using unpaired two-tailed *t*-tests; ns, not significant; *, $p < 0.05$; ***, $p < 0.001$.

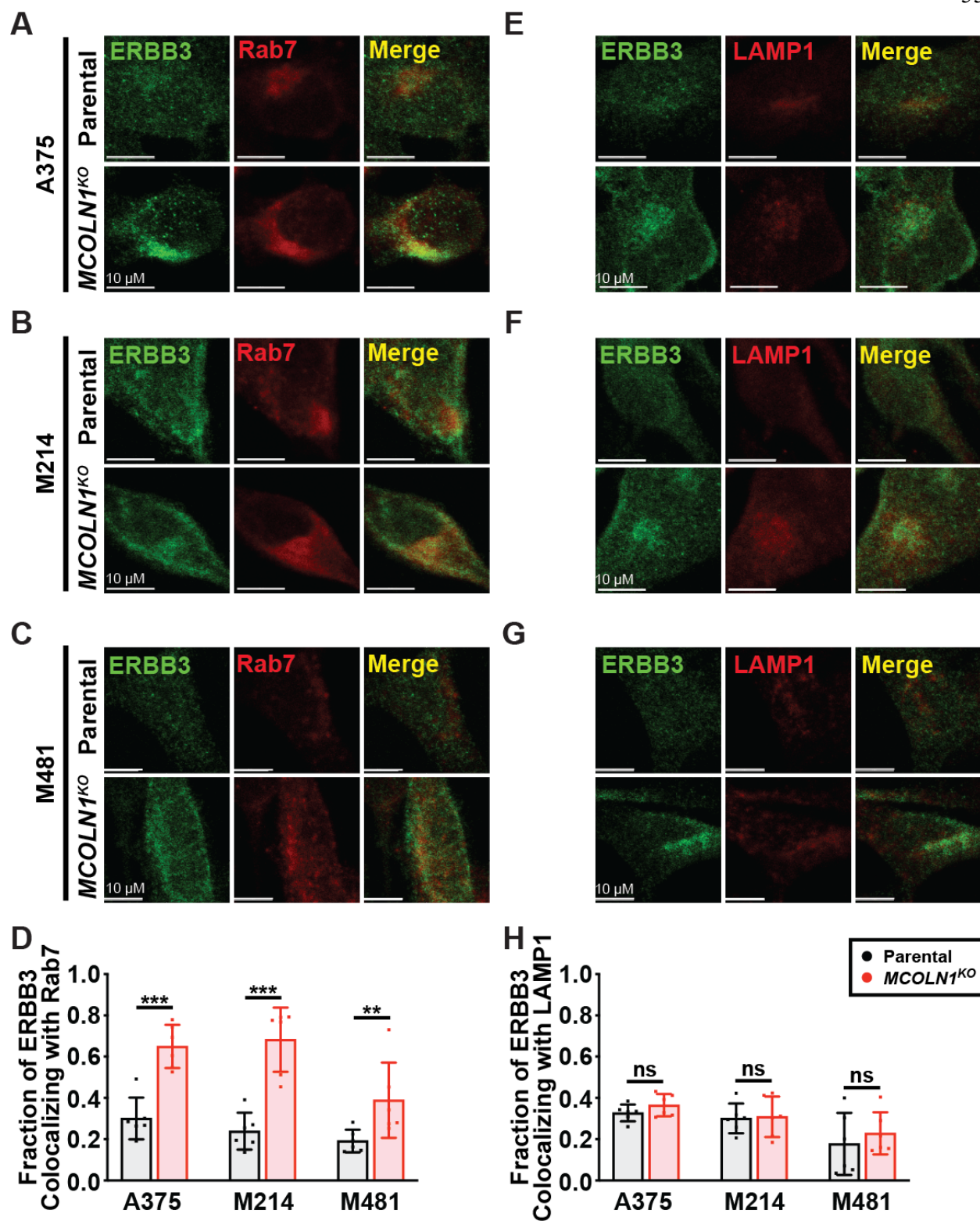


Figure 3.9. ERBB3 accumulates in endosomes in *MCOLN1*-deficient cells. A-C, Colocalization of ERBB3 with the endosomal marker, Rab7, in parental versus *MCOLN1*-deficient cells from three melanomas. **D,** Manders colocalization coefficients reporting the fraction of ERBB3 staining that co-localized with Rab7 staining. **E-G,** Colocalization of ERBB3 with the lysosomal marker, LAMP1, in parental versus *MCOLN1*-deficient cells from three melanomas. **H,** Manders colocalization coefficients reporting the fraction of ERBB3 staining that co-localized with LAMP1 staining. All data represent mean \pm s.d. from two independent experiments with 3 quantified cells per clone per experiment. Statistical significance was assessed using unpaired two-tailed *t*-tests; ns, not significant; **, $p < 0.01$; ***, $p < 0.001$.

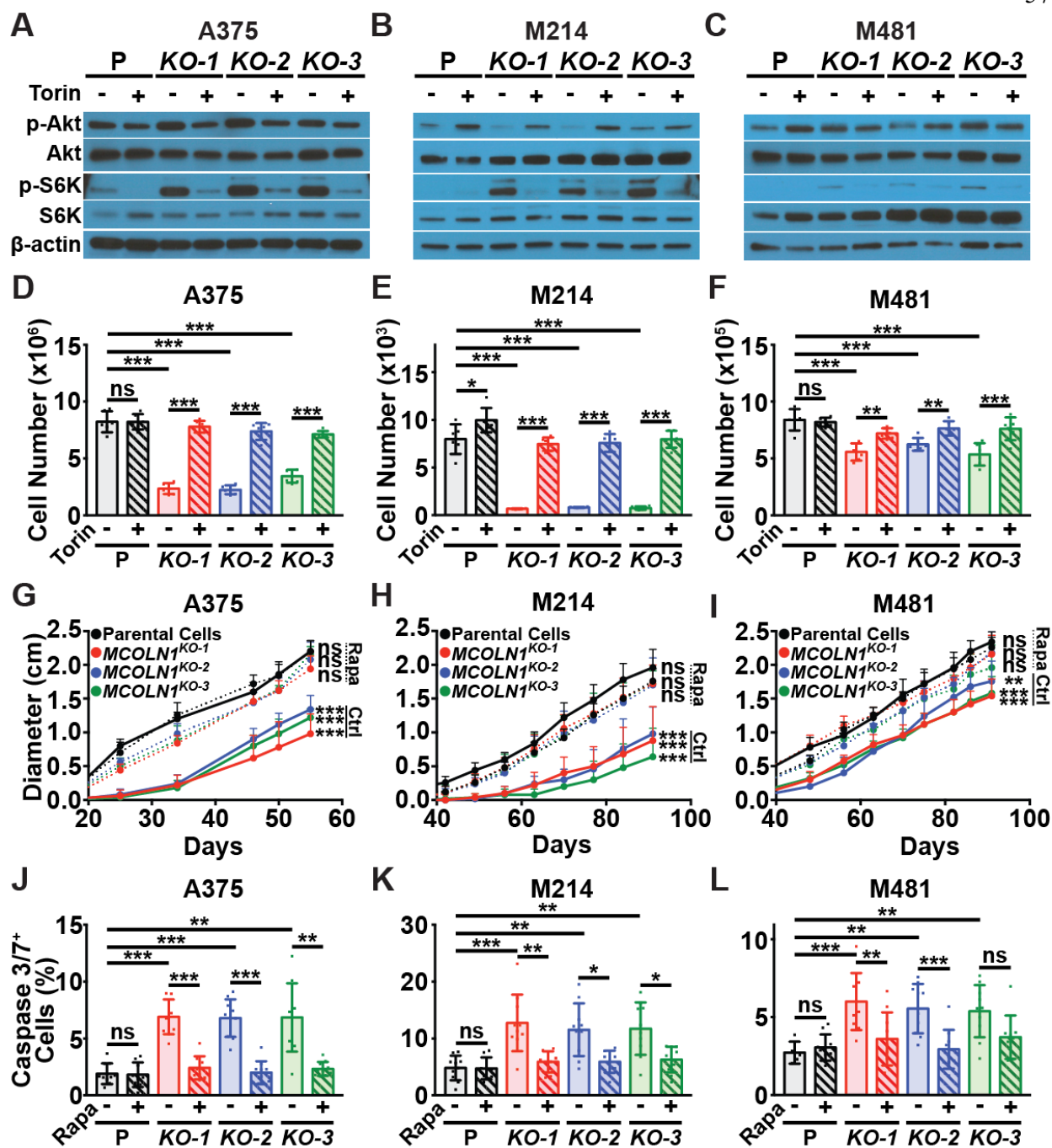


Figure 3.10. mTORC1 inhibition rescued the growth of *MCOLN1*-deficient cells. **A-C**, Western blots of p-Akt (S473), Akt, p-S6K (T389), S6K, and β -actin in cultured parental cells or *MCOLN1*-deficient clones from three melanomas treated with DMSO (-) or 5 nM Torin1 (+). The blot reflects one representative experiment (of three performed) per melanoma. **D-F**, Growth in culture of parental cells (P; black) versus *MCOLN1*-deficient clones (red, blue, and green) treated with DMSO control (solid bars) or 5nM Torin1 (striped bars) for 21 days. Torin1 treatment significantly rescued the growth of *MCOLN1*-deficient clones. The data represent mean \pm s.d. from two experiments with 3 replicate cultures per clone per experiment. **G-I**, Growth of subcutaneous tumors in mice transplanted with parental or *MCOLN1*-deficient cells and treated with DMSO Control (Ctrl, solid lines) or 5 mg/kg/day Rapamycin (Rapa, dotted lines). The data represent mean \pm s.d. from one representative experiment (of two performed) with 5 mice per clone. **J-L**, Frequency of activated caspase 3/7+ cells in subcutaneous tumors grown from parental cells or *MCOLN1*-deficient clones treated with DMSO control (solid bars) or rapamycin (striped bars). These data represent mean \pm s.d. from two independent experiments with 4 - 5 mice per clone per experiment. Statistical significance was assessed using two-way ANOVAs followed by Sidak's and Dunnett's multiple comparisons tests (**D-F**), two-way ANOVAs followed by Dunnett's multiple comparisons tests for the last time points measured (**G-I**), or Welch's one-way ANOVAs or one-way ANOVAs followed by Tamhane's T2, Dunnett's T3, Dunnett's or Sidak's multiple comparisons tests (**J-L**); ns, not significant; *, $p < 0.05$; **, $p < 0.01$; ***, $p < 0.001$.

Rapamycin treatment also rescued the increase in cell death observed in *MCOLN1*-deficient tumors (**Figures 3.10J-3.10L**). Therefore, *MCOLN1*/TRPML1 promoted tumor growth and the survival of melanoma cells by negatively regulating mTORC1 signaling.

mTORC1 activation promotes protein synthesis by increasing ribosome biogenesis and mRNA translation (Ma and Blenis, 2009; Saxton and Sabatini, 2017). We tested whether *MCOLN1*-deficient melanoma cells had increased protein synthesis as compared to parental cells by measuring the rate of O-propargyl-puromycin (OP-Puro) incorporation into cultured cells (Liu et al., 2012; Signer et al., 2014). *MCOLN1*-deficient melanoma cells exhibited significantly increased OP-Puro incorporation relative to parental cells, and this increase was blocked by treatment with Torin1 (**Figures 3.11A-3.11C**). This suggested that TRPML1 negatively regulates protein synthesis in melanoma cells by negatively regulating mTOR signaling.

To test whether the increased protein synthesis in *MCOLN1*-deficient melanoma cells contributed to their impaired growth, we treated *MCOLN1*-deficient and parental melanoma cells with a low dose of the protein synthesis inhibitor, puromycin. Treatment with puromycin blocked the increase in protein synthesis in *MCOLN1*-deficient cells (**Figures 3.12A-3.12C**) and partially rescued the increase in cell death observed in these cells (**Figures 3.12D-3.12F**) as well as their growth in culture (**Figures 3.11D-3.11F**).

To better understand the mechanism by which increased protein synthesis led to cell death, we tested whether the *MCOLN1*-deficient melanoma cells experienced proteotoxic stress. We first assessed intracellular protein aggregation using Proteostat

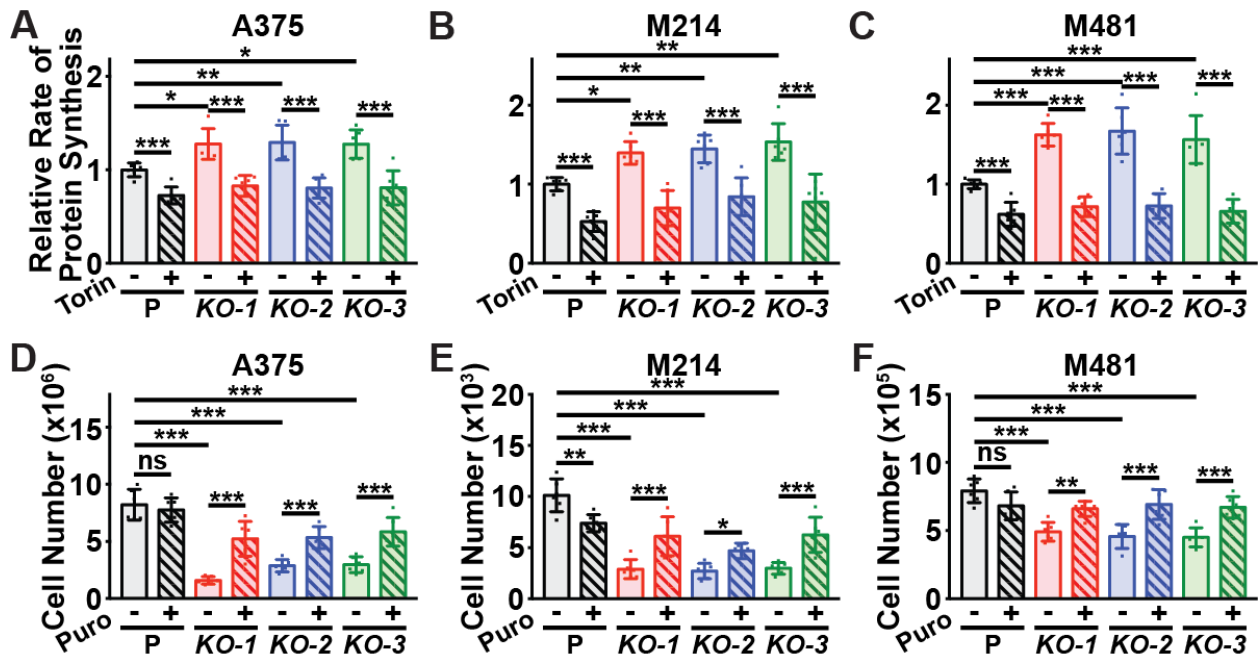


Figure 3.11. *MCOLN1*/*TRPML1* deficiency increased protein synthesis as a result of mTORC1 activation. **A-C**, Relative rate of incorporation of a pulse of OP-Puro in cultured parental cells (P; black) versus *MCOLN1*-deficient clones (red, blue, and green) treated with DMSO control (solid bars) or 5nM Torin1 (striped bars). **D-F**, Growth in culture of parental cells versus *MCOLN1*-deficient clones treated with PBS control (solid bars) or 0.5 ng/ml Puromycin (striped bars) for 21 days. Puromycin treatment significantly rescued the growth of *MCOLN1*-deficient clones. All data represent mean \pm s.d. from two independent experiments with 3 replicate cultures per treatment per clone per experiment. Statistical significance was assessed using two-way ANOVAs followed by Sidak's and Dunnett's multiple comparisons tests; ns, not significant; *, $p < 0.05$; **, $p < 0.01$; ***, $p < 0.001$.

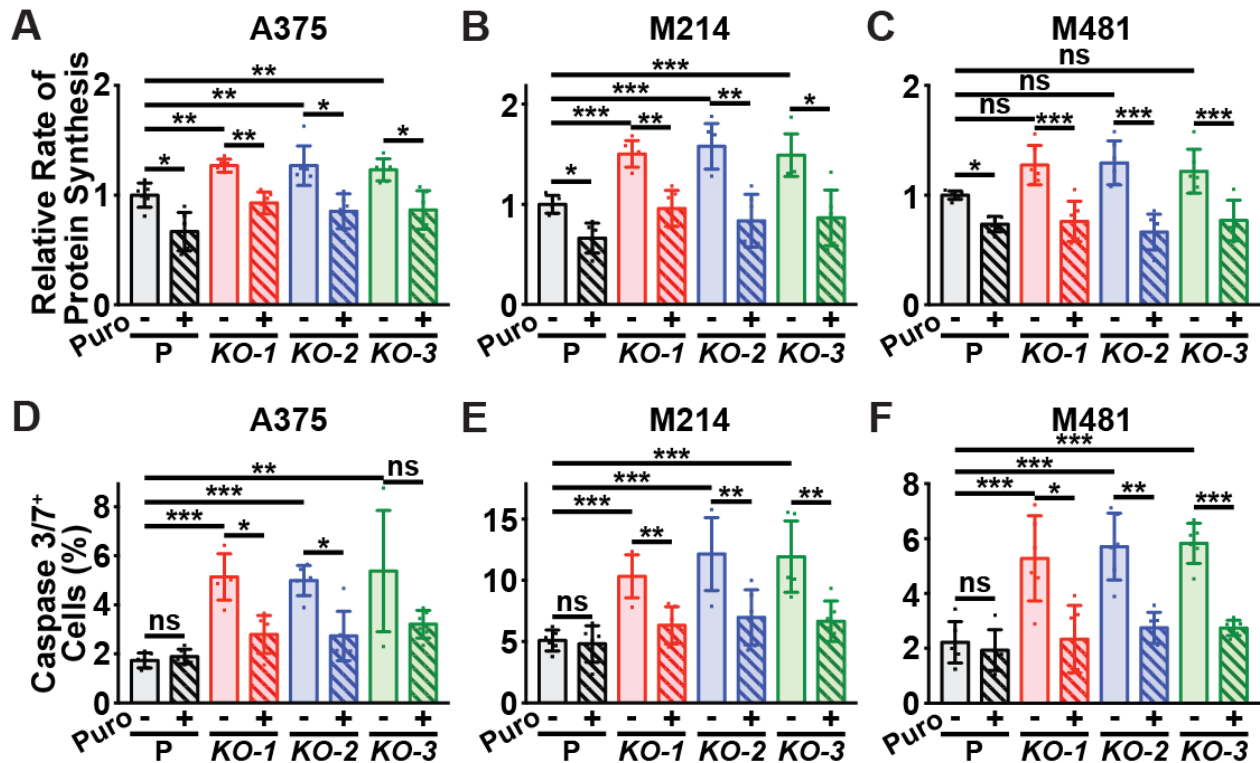


Figure 3.12. Puromycin treatment blocked the increase in protein synthesis and cell death in *MCOLN1*-deficient cells. A-F, Relative rate of protein synthesis based on the incorporation of a pulse of OP-Puro (A-C) and frequencies of activated caspase 3/7+ cells (D-F) in cultured parental cells (black) versus *MCOLN1*-deficient clones (red, blue, and green) treated with PBS (solid bars) or 0.5 ng/ml puromycin (striped bars). All data represent mean \pm s.d. from two independent experiments with 3 replicate cultures per treatment per clone per experiment. Statistical significance was assessed using one-way ANOVAs, Welch's one-way ANOVAs, or two-way ANOVAs followed by Sidak's, Dunnett's, or Tamhane's T2 multiple comparisons tests; ns, not significant; *, $p < 0.05$; **, $p < 0.01$; ***, $p < 0.001$.

dye, which fluoresces upon binding to protein aggregates (Shen et al., 2011). *MCOLN1*-deficient melanoma cells exhibited increased Proteostat staining as compared to parental cells, and this difference was rescued by Torin1 treatment (**Figures 3.13A-3.13F**). *MCOLN1*-deficient cells also exhibited increased levels of BiP (HSPA5), increased phosphorylation of EIF2 α (EIF2S1) and IRE1 α (ERN1), and increased expression of ATF4 and CHOP (DDIT3), all consistent with the activation of an unfolded protein response (Walter and Ron, 2011). Treatment with Torin1 partially or completely rescued all of these changes (**Figures 3.13G-3.13I**). This suggested that *MCOLN1*-deficient melanoma cells experience proteotoxic stress as a consequence of increased mTORC1 signaling.

To test if clearing misfolded proteins could rescue the growth of *MCOLN1*-deficient cells, we treated with a proteasome activator, PD169316, a p38 MAPK (MAPK14) inhibitor that increases 26S proteasome (SEM1) activity (Leestemaker et al., 2017). Treatment with PD169316 reduced the accumulation of protein aggregates in the *MCOLN1*-deficient cells (**Figures 3.14A-3.14C**) and partially rescued their growth in culture (**Figures 3.13J-3.13L**). Therefore, *MCOLN1*-deficiency impaired the growth of melanoma cells partly by increasing protein synthesis and inducing proteotoxic stress.

Given that *MCOLN1*-deficiency impairs endolysosomal trafficking, phagocytosis, and the fusion of phagosomes with lysosomes (Dayam et al., 2015; Samie et al., 2013) and that mTORC1 signaling can inhibit macropinocytosis (Kamphorst et al., 2015; Palm et al., 2015), we tested if *MCOLN1* was necessary for macropinocytosis by melanoma cells. Using a self-quenching albumin that fluoresces upon degradation, DQ-BSA, we

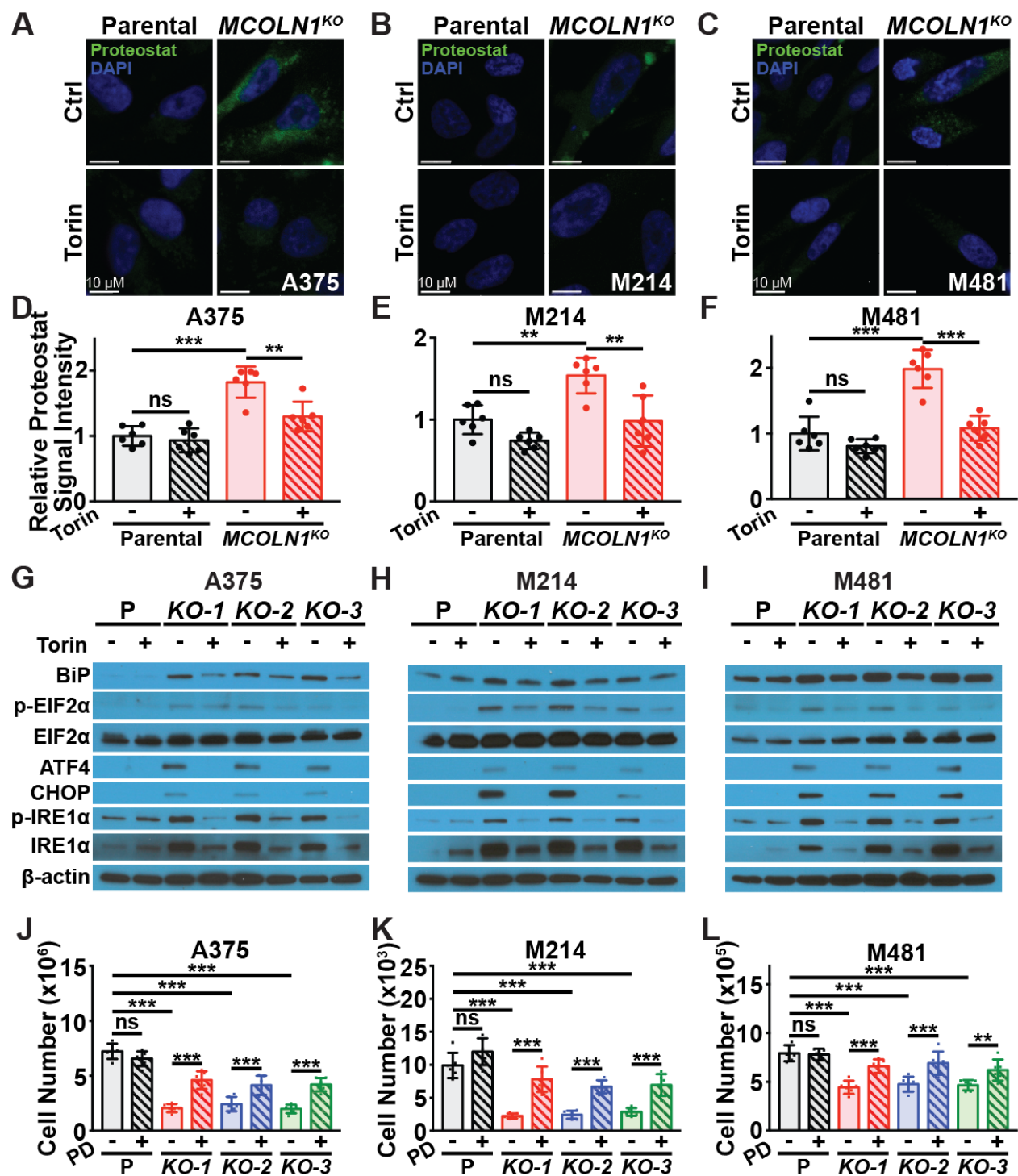


Figure 3.13. *MCOLN1*/TRPML1 deficiency increased proteotoxic stress and induced an unfolded protein response as a result of mTORC1 activation. **A-F**, Intracellular protein aggregates were visualized by staining with Proteostat Dye (**A-C**) and then quantified (**D-F**) in parental cells (black) versus *MCOLN1*-deficient clones (red) treated with DMSO control (solid bars) or 5 nM Torin1 (striped bars). Data represent mean \pm s.d. from two independent experiments with 3 replicate cultures per treatment per clone per experiment. **G-I**, Western blot analysis of BiP, p-eIF2 α (S51), total eIF2 α , ATF4, CHOP, p-IRE1 α (S724), total IRE1 α and β -actin in cultured parental cells or *MCOLN1*-deficient cells from three melanomas treated with DMSO (-) or 5 nM Torin1 (+). The blot reflects one representative experiment (of two performed) per melanoma. **J-L**, Growth in culture of parental cells versus *MCOLN1*-deficient clones treated with DMSO control (solid bars) or 5 μ M PD169316 (PD; a proteasome activator; striped bars) for 21 days. PD169316 treatment significantly rescued the growth of *MCOLN1*-deficient clones. Statistical significance was assessed using two-way ANOVAs followed by Sidak's multiple comparisons tests (**D-F**) or two-way ANOVAs followed by Sidak's and Dunnett's multiple comparisons tests (**J-L**); ns, not significant; **, $p < 0.01$; ***, $p < 0.001$.

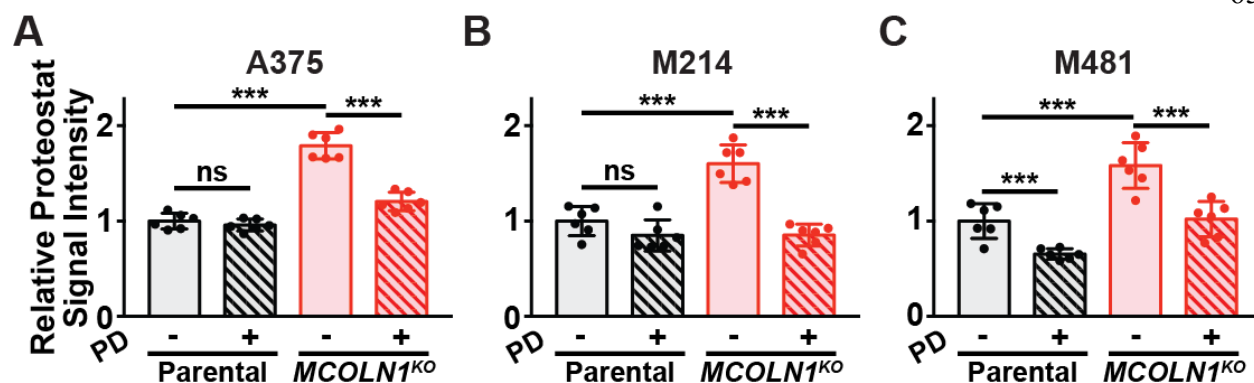


Figure 3.14. Treatment with proteasome activator reduced protein aggregation in *MCOLN1*-deficient cells. A-C, Intracellular protein aggregates were visualized by staining with Proteostat Dye and then quantified in cultured parental cells (black) versus *MCOLN1*-deficient clones (red) treated with DMSO (Ctrl; solid bars) or PD169316 proteasome activator (PD; striped bars). All data represent mean \pm s.d. from two independent experiments with 3 replicate cultures per treatment per clone per experiment. Statistical significance was assessed using one-way ANOVAs, Welch's one-way ANOVAs, or two-way ANOVAs followed by Sidak's, Dunnett's, or Tamhane's T2 multiple comparisons tests; ns, not significant; **, $p < 0.01$; ***, $p < 0.001$.

found melanoma cells engaged in significantly more macropinocytosis than melanocytes under the same culture conditions, even in medium not depleted for amino acids (**Figure 3.15**). *MCOLN1*-deficient cells exhibited significantly less macropinocytosis as compared to parental cells (**Figures 3.16A-3.16D**), and treatment with trametinib (**Figures 3.16A and 3.16C**) or Torin1 (**Figures 3.16B and 3.16D**) partially or completely rescued the reduction in macropinocytosis. *MCOLN1/TRPML1* thus promoted macropinocytosis in melanoma cells partly by negatively regulating MAPK and mTOR signaling.

We wondered if the increased protein synthesis and decreased macropinocytosis in *MCOLN1*-deficient melanoma cells would affect amino acid homeostasis. To test this, we performed metabolomics in parental and *MCOLN1*-deficient melanoma cells, with and without Torin1 treatment in culture. The only metabolite that was significantly depleted in *MCOLN1* deficient melanoma cells from all three lines, and rescued by either Torin1 or rapamycin treatment, was serine (**Figures 3.16E and 3.17A**). Serine is required for protein, nucleotide, lipid, and glutathione synthesis (Locasale, 2013), and cells can use antiporters to exchange serine for other amino acids (DeNicola et al., 2015). Metabolomic analysis of subcutaneous tumors grown from parental and *MCOLN1*-deficient melanoma cells confirmed that serine was depleted in *MCOLN1*-deficient tumors *in vivo* and that rapamycin treatment rescued this serine depletion (**Figure 3.16F**). Supplementation of the culture medium with increased L-serine (2mM versus 0.4mM in normal medium) did not significantly affect the growth of parental cells but rescued the growth of *MCOLN1*-deficient cells (**Figures 3.16G-3.16I**).

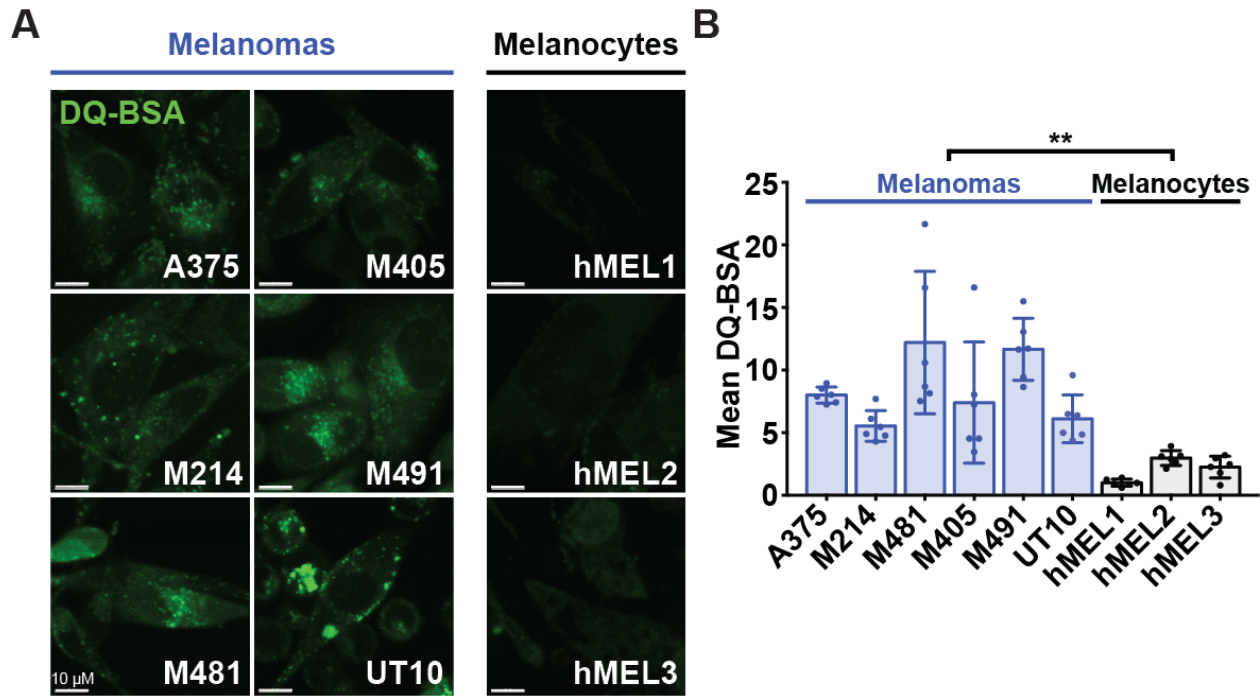


Figure 3.15. Significantly higher levels of macropinocytosis in melanoma cells as compared to normal melanocytes. **A, B,** Macropinocytosis of extracellular protein was measured by imaging (**A**) and quantified (**B**) in cultured cells from six melanomas (A375, M214, M481, M405, M491, and UT10) as well as melanocytes derived from three donors (hMEL1, hMEL2, hMEL3) by incubating cells with DQ-BSA for 6 hours, followed by confocal imaging. These data represent mean \pm s.d. from two independent experiments with 3 replicate cultures per line per experiment. Statistical significance was assessed using a nested *t*-test (**B**); **, $p < 0.01$.

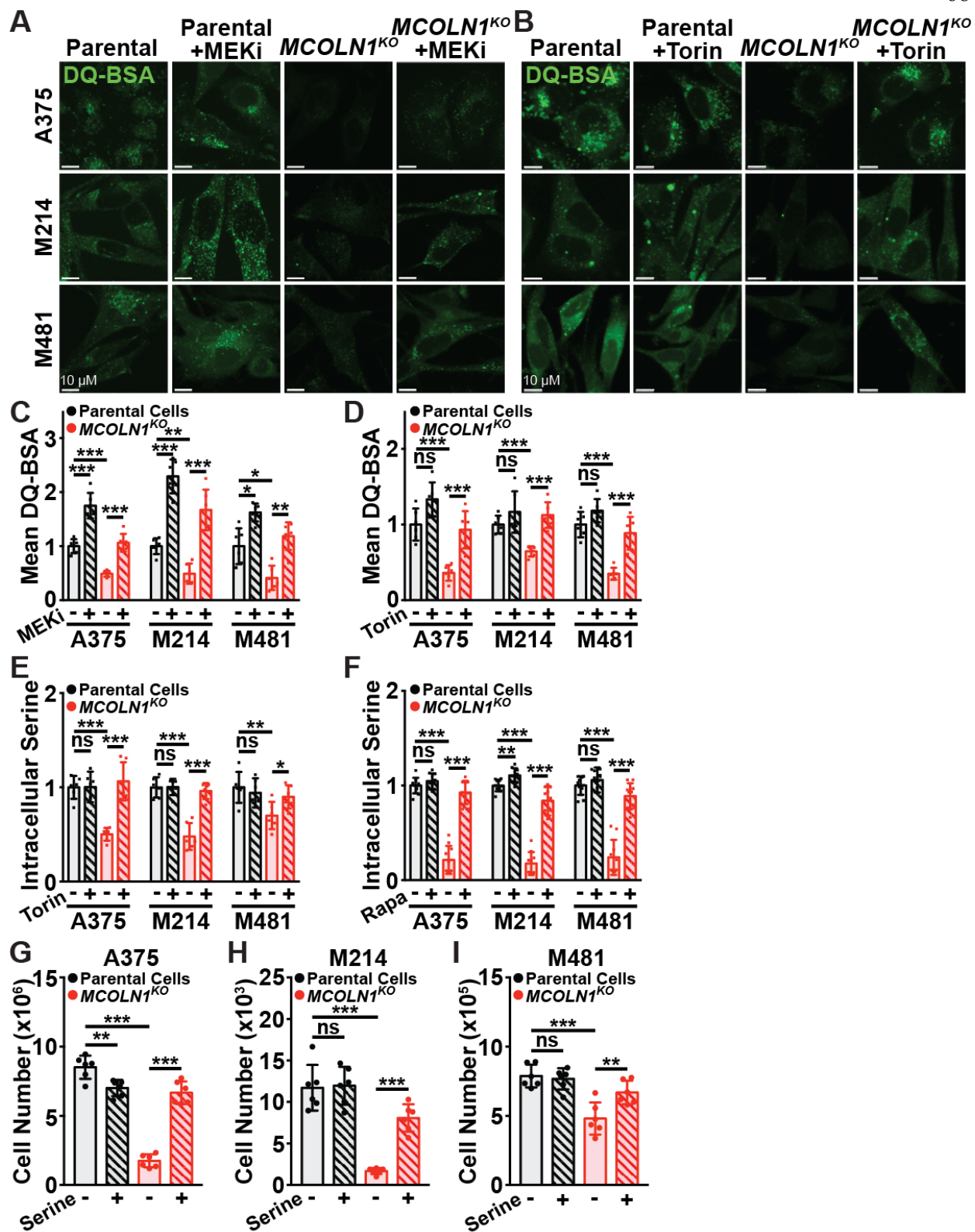


Figure 3.16. *MCOLN1*/TRPML1 deficiency impairs macropinocytosis and depletes serine. **A-D**, Macropinocytosis of extracellular protein was measured in cultured parental cells (black) or *MCOLN1*-deficient clones (red) treated with either DMSO control (solid bars) versus 5 nM trametinib (MEKi; striped bars) (**A,C**) or DMSO control (solid bars) versus 5 nM Torin1 (striped bars) (**B,D**) by incubating cells with DQ-BSA for 6 hours, followed by confocal imaging. The data represent mean \pm s.d. from two independent experiments with 3 replicate cultures per treatment per clone per experiment. **E,F**, Relative intracellular serine levels in cultured cells (**E**) or subcutaneous tumors (**F**) formed by parental cells versus *MCOLN1*-deficient cells treated with DMSO control (solid bars), Torin1 (**E**; striped bars), or rapamycin (**F**; striped bars). The data reflect two independent experiments with 3 replicate cultures per clone per treatment per experiment (**E**) or 5 mice per clone per treatment per experiment (**F**). **G-I**, Growth of parental versus *MCOLN1*-deficient cells in cultures containing 0.4mM L-serine (solid bars) or 2 mM L-serine (striped bars) for 21 days. These data represent mean \pm s.d. from two independent experiments with 3 replicate cultures per treatment per clone per experiment. Statistical significance was assessed using one-way ANOVA or Welch's one-way ANOVA followed by Sidak's or Tamhane's T2 multiple comparisons tests (**C,F**) or two-way ANOVAs followed by Sidak's and/or Dunnett's multiple comparisons tests (**D,E,G-I**); ns, not significant; *, $p < 0.05$; **, $p < 0.01$; ***, $p < 0.001$.

A

	A375	M214	M481
Serine	X	X	X
Cystathionine	X	X	
N-Acetylaspartic acid	X	X	
Uridine 5'-diphosphate	X	X	
S-Adenosylmethionine	X		
Glycine	X		
Platelet-activating factor	X		
Citrulline	X		
Carnosine	X		X
N-Acetylglutamic acid	X		
N-Acetylaspartylglutamic acid	X		
ATP		X	
N6,N6-Dimethyllysine	X		
N6,N6,N6-Trimethyllysine		X	
6-Methylnicotinamide	X		
N-Acetylneuraminic acid	X		
Inositol	X		
N-Acetylalanine	X		
Succinic acid	X		
Uridine 5'-diphosphogalactose	X		

B

	A375	M214	M481
Bethanidine	X		
Acetyl- β -methylcholine			X
Acetylcholine			X
Threonine			X
NAD+			X
Taurine			X
Hypotaurine			X
Acetylcarnitine			X
2-Amino adipic acid			X

Figure 3.17. Metabolomics of parental versus *MCOLN1*-deficient melanoma cells. **A**, Metabolites that were significantly depleted in subcutaneous tumors formed by *MCOLN1*-deficient cells as compared to parental cells, and whose levels were rescued by rapamycin treatment of the xenografted mice. **B**, Metabolites that were significantly enriched in tumors formed by *MCOLN1*-deficient cells as compared to parental cells and whose levels were rescued by rapamycin treatment of the xenografted mice.

MCOLN1/*TRPML1* thus promoted the maintenance of intracellular serine levels by negatively regulating mTORC1 signaling, reducing protein synthesis, and increasing macropinocytosis.

3.3 Materials and Methods

Melanoma specimen collection and enzymatic dissociation. Melanoma specimens were obtained with informed consent from all patients according to protocols approved by the Institutional Review Board of the University of Michigan Medical School (IRBMED approvals HUM00050754 and HUM00050085) and the University of Texas Southwestern Medical Center (IRB approval 102010-051). Single cell suspensions were obtained by mechanically dissociating tumors, enzymatically digesting in 200 U/ml collagenase IV (Worthington), DNase (50 U/ml) and 5 mM CaCl₂ for 20 min at 37°C, and filtering through a 40-µm cell strainer.

Mouse studies and xenograft assays. All mouse experiments were performed according to protocols approved by the Institutional Animal Care and Use Committee at UT Southwestern Medical Center (protocol 2016-101360). Melanoma cell suspensions were prepared for injection in 50µl of L15 medium containing 1 mg/ml bovine serum albumin, 1% penicillin/streptomycin, and 10 mM HEPES (pH 7.4), and 25% high-protein Matrigel (Fisher Scientific). Subcutaneous injections were performed in the flanks of NOD.CB17-Prkdc^{scid} Il2rg^{tm1Wjl}/SzJ (NSG) mice. Four to eight-week-old NSG mice were transplanted with 100 melanoma cells subcutaneously unless otherwise specified.

Mouse cages were randomized between treatments (mice within the same cage received the same treatment). Both male and female mice were used. Subcutaneous tumor diameters were measured weekly with calipers until any tumor in the mouse cohort reached 2.5 cm in its largest diameter. At that point, all mice in the cohort were killed for analysis. For *in vivo* treatment with mTOR inhibitor, the mice were administered rapamycin (LC Laboratories) by oral gavage beginning when the subcutaneous tumors became palpable (5 mg/kg/day in 200 μ l of 0.5% hydroxypropyl methyl cellulose with 0.2% Tween80 and 1% DMSO). Tumor growth was monitored weekly with a caliper. Mice were killed for analysis by the time the primary tumor reached 2.5 cm in its largest diameter, or when the mice exhibited signs of distress, whenever was earlier.

Primary melanoma cell cultures. A375 (ATCC; CRL-1619), M214, M481, and M491 melanoma cells and melanocytes from three donors (hMEL1 (ATCC; PCS-200-013), hMEL2 (Invitrogen; C-024-5C), hMEL3 (Lonza; CC-2586)) were cultured in tissue-culture-treated plates (Corning) with high-glucose DMEM (Gibco), 10% fetal bovine serum (FBS; Gemini) and 1% penicillin/streptomycin (Fisher). All cultures were incubated at 37°C in 5% CO₂ and constant humidity. Cells were passaged for 1 to 3 months and used for experiments. All cell lines tested negative for *Mycoplasma* using the MycoAlert detection kit (Lonza), and the identities of all cell lines were verified using short tandem repeat (STR) profiling in March 2019. To assess the effects of Torin1 (Tocris), Puromycin (Sigma), PD169316 (Sigma), or L-serine (Sigma) on the growth of

cells, 1000 parental or *MCOLN1*-deficient cells were added to each well of a 24-well plate. The small molecules were added 24 hours later, then the cells were counted using a hemocytometer (Hausser Scientific) after 7, 14, or 21 days. The medium was changed every 3-4 days.

CRISPR editing of *MCOLN1* in melanoma cells. Single guide RNAs (sgRNAs) targeting exon 2 of human *MCOLN1* were designed using publicly available tools (<http://crispr.mit.edu>):

<i>MCOLN1</i> sgRNA #1	5' – TCGCCGTCGTCTCAAATACT – 3'
<i>MCOLN1</i> sgRNA #2	5' – TGCGACAAGTTTCGAGCCAA– 3'

The sgRNAs were cloned into the U6-driven Cas9 expression vector (pX458-pSpCas9(BB)-2A-GFP; 48318, Addgene) (Ran et al., 2013). Insertion of the sgRNA was confirmed by Sanger sequencing. Approximately 100,000 – 500,000 A375 melanoma cells or melanoma cells derived from two patients (M214 and M481) were plated in tissue-culture-treated 6-well plates in DMEM plus 10% FBS and 1% penicillin/streptomycin. 1 µg of each of the two sgRNA constructs was co-transfected into the melanoma cells using polyjet (SigmaGen) according to the manufacturer's instructions. After 36-48 hours, GFP⁺ cells were flow cytometrically isolated and allowed to recover for 24-48 hours in DMEM plus 10% FBS and 1% penicillin/streptomycin. Single cells were then plated in tissue-culture-treated 96-well plates in Prime-XV tumorsphere medium (Irvine Scientific) supplemented with 2 U/ml Heparin (Sigma), 0.1 µg/ml Hydrocortisone (Sigma), 2% B27 (Thermo Fisher), 1 µM StemRegenin 1 (Stemcell Technologies), 10% charcoal stripped FBS (Thermo Fisher), 10 µg/ml Bovine

Pituitary Extract (BPE; Lonza), 10 ng/ml recombinant human IL-8 (CXCL8; Peprotech), 20 ng/ml recombinant human GRO- α /MGSA (CXCL1; Peprotech), and 25 ng/ml recombinant human HGF (Peprotech). Genomic DNA was isolated from individual clones with QuickExtract (Epicentre), and clones were screened and sequenced for *MCOLN1* deletions.

Quantitative RT-PCR Analysis. For quantitative reverse transcription PCR (qPCR), RNA from 100,000 melanoma cells was extracted (Qiagen) and reverse transcribed into cDNA using SuperScript III (Invitrogen). qPCR was performed using a Roche LightCycler480. The primers used for qPCR analysis for *MCOLN1* were: 5'-CTGATGCTGCAAGTGGTCAAG-3' (Forward) and 5'-GGTGTCTCTTCCCGGAATGTC-3' (Reverse).

Antibody staining and flow cytometry. All melanomas expressed DsRed and were identified and isolated by flow cytometry (Piskounova et al., 2015). All antibody labeling was performed for 20 min on ice, followed by washing with HBSS and centrifugation at 200xg for 5 min. Cells were stained with directly-conjugated antibodies against mouse CD45 (75-0451-U100; 30-F11-violetFluor450; Tonbo), mouse CD31 (48-0311-82; 390-eFluor450; eBiosciences), mouse Ter119 (75-5921-U100; TER-119-violetFluor450; Tonbo) and human HLA-A, B, C (555555; G46-2.6-APC; BD Biosciences). Human melanoma cells were identified and isolated as cells that were positive for DsRed and HLA and negative for mouse CD45, CD31, and Ter119. Cells were resuspended in 4',6-

diamidino-2-phenylindole (DAPI; 1 µg/ml; Sigma) to eliminate dead cells from sorts and analyses. Cells were analyzed or sorted on a FACS Fusion cell sorter (Becton Dickinson), a FACS Aria II SORP cell sorter (Becton Dickinson), or a FACS Canto RUO cell analyzer (Becton Dickinson). For flow cytometric analysis of activated Cas3/7 staining, cultured melanoma cells were trypsinized with a 0.25% trypsin solution (Fisher) or tumors were enzymatically dissociated as described above. Equal numbers of melanoma cells (500,000-2,000,000) were loaded with 1 µM CellEvent Caspase-3/7 Green in HBSS (Ca²⁺- and Mg²⁺-free). Cells were stained for 15-30 min at 37°C. Staining was assessed by flow cytometry, gating on live melanoma cells (positive for human HLA and DsRed and negative for DAPI and mouse CD45/CD31/Ter119).

Ki-67 staining to evaluate proliferation. To assess Ki-67 staining in cultured cells, melanoma cells were grown in 8-well Lab-Tek II Chamber Slides (Thermo). Cells were washed with cold PBS and fixed in 4% paraformaldehyde (Fisher) for 15 min at room temperature. For *in vivo* experiments, tumor specimens were fixed in 4% paraformaldehyde overnight at 4°C, cryoprotected in 30% sucrose (Sigma) overnight, and frozen in OCT (Fisher). Sections (10 µm) were cut using a cryostat. Cells or tissue sections were permeabilized with PBS supplemented with 0.05% Triton X-100 for 5 min, washed with PBS, and blocked in 5% goat serum (JacksonImmuno) in PBS for 1 hour at room temperature. Cells or tissue sections were then stained with anti-Ki67 antibody (M7240, Dako, 1:100) overnight at 4°C, washed in PBS, stained with secondary antibody (Alexa Fluor 488-AffiniPure F(ab')₂ Fragment goat anti-mouse IgG; Life

Technologies; 1:1000) for 1 hour in the dark at room temperature, washed again in PBS, stained with 1 µg/ml DAPI, and mounted with Fluoromount-G (SouthernBiotech) for confocal imaging.

Lentiviral shRNA library transduction. Lentiviral shRNA constructs against ion channels and transporters from throughout the human genome were assembled from multiple sources. The GIPZ Human Ion Channel shRNA library (1,881 shRNAs; Dharmacon, RHS6045) was supplemented with two custom libraries comprised of shRNAs targeting channels and transporters that were not included in the Ion Channel shRNA library (301 shRNAs from Dharmacon and 393 shRNAs from the pGIPZ shRNAmir library from Dharmacon). For *MCOLN1* knockdown, Dharmacon shRNA clones V3LHS_338980 and V2LHS_249668 were used. For *MCOLN1* overexpression, the human *MCOLN1* open reading frame (HsCD00732386, DNAsu) was cloned into a lentiviral expression construct (pLOC-tRFP-IRES-tGFP; Dharmacon) using the In-Fusion HD cloning system (Clontech). The *MCOLN1* gain and loss-of-function constructs were verified by Sanger sequencing. For virus production, 0.9 µg of the appropriate plasmid along with 1 µg of helper plasmids (0.4 µg pMD2.G and 0.6 µg of psPAX2) were transfected into 293T cells using polyjet. The viral supernatants were collected 48 hours after transfection and filtered through a 0.45 µm filter. Freshly dissociated melanoma cells (300,000 to 1,000,000) were infected with viral supernatants supplemented with 10 µg/ml polybrene (Sigma) for 4 to 6 hours and cultured in DMEM plus 10% FBS and 1% penicillin/streptomycin for 48 hours to allow

GFP expression. DsRed⁺/GFP⁺ cells were sorted and transplanted into NSG mice to assess tumor growth.

***In vivo* shRNA screens.** shRNA drop-out screens were conducted as previously described (Gargiulo et al., 2014). For the primary screen, a library of 2,589 shRNAs was divided into 27 pools of ~100 shRNAs/pool. Two negative control scrambled shRNAs (Dharmacon, RHS4349 and RHS4346) and three positive control shRNAs targeting *EIF3A* (Dharmacon, V2LHS_23910, V2LHS_23911, and V2LHS_23913) were spiked into each pool to serve as internal controls. For each pool, shRNA lentivirus was produced in 293T cells as described above, and 5-10 million freshly dissociated melanoma cells from each of three patients (M214, M481, and M491) were transduced. Three different melanoma lines were used to ensure that the screen was robust. All three melanomas were fast-growing and efficiently-metastasizing. After 48 hours in culture, GFP⁺ cells were sorted. We have previously demonstrated that at least 1 in 4 human melanoma cells form tumors after subcutaneous transplantation into NSG mice (Quintana et al., 2008). Based on this, 100,000 GFP⁺ melanoma cells were subcutaneously injected into each of 4 NSG mice per shRNA pool per melanoma so that an average of 1,000 melanoma cells would express each shRNA in each pool injected into a single mouse in the primary screen, and that at least 250 melanoma cells expressing each shRNA would have an opportunity to contribute to each tumor. Once the tumors reached 1.0 – 1.5 cm in diameter, they were surgically excised, and genomic DNA was isolated (Zymo) from equal numbers of input cells and tumor cells. Two

aliquots of 100,000 cells per pool per melanoma were analyzed to quantify shRNA abundance among input cells. shRNA barcodes were PCR amplified. The resulting PCR products were purified by gel extraction (Qiagen) and sequenced using a NextSeq 500 (Illumina) to compare the abundance of each shRNA in the input cells as compared to the tumors. Sequencing results were analyzed as previously described (Gargiulo et al., 2014). Raw sequences were trimmed using cutadapt (Martin, 2011) and mapped using Bowtie 2 (Langmead and Salzberg, 2012). Raw reads for each shRNA were normalized to the total number of reads in the corresponding sample. *t*-tests were performed on the \log_2 -transformed counts with multiple comparisons adjustments to compare the normalized abundance of each shRNA in the input cells as compared to tumors. shRNAs that had a \log_2 -transformed tumor abundance minus input of abundance of ≤ -1 in at least 2 out of 3 melanomas and a significant *p*-value ($p \leq 0.05$) were considered to be significantly depleted in the screen. Candidate genes also had to be detectably expressed by melanoma cells and at least 2 unique shRNAs against the same target gene had to exhibit depletion in the screen. For the secondary screen, 210 shRNAs targeting the 40 candidate genes identified in the primary screen were assembled into a new library, which was then divided into 18 pools of ~17 shRNAs each (including 2 negative and 3 positive control shRNAs, as described above, in each pool). Virus production, transduction, and sorting of melanoma cells were performed as described above. 10,000 GFP⁺ cells were subcutaneously injected into each of 3 NSG mice per pool per melanoma so that an average of nearly 600 melanoma cells would express each shRNA upon injection into each mouse, and that approximately 150 melanoma

cells expressing each shRNA would have an opportunity to contribute to the formation of each tumor. Three aliquots of 100,000 cells per pool per melanoma were analyzed as input cells. Genomic DNA isolation, barcode amplification, and sequencing were performed as described above.

Western blot analysis. For culture experiments, melanoma cells were grown adherently, washed with PBS, and directly lysed in the culture dishes using RIPA Buffer (Cell Signaling Technology) or Triton lysis buffer (50 mM Tris HCl, pH 7.4, 150 mM NaCl, 1 mM EDTA, 1% Triton X-100) supplemented with phenylmethylsulphonyl fluoride (Sigma) and protease and phosphatase inhibitor cocktail (Roche). For *in vivo* experiments, tumors were surgically excised and snap frozen in liquid nitrogen. Tumor samples were lysed in lysis buffer in 1.7 ml Eppendorf tubes with disposable pestles (Kontes). The bicinchoninic acid (BCA) protein assay (Thermo) was used to quantify protein concentrations. Equal amounts of protein (5–20 μ g) were loaded into each lane and separated on 4-20% polyacrylamide tris glycine SDS gels (BioRad), then transferred to polyvinylidene difluoride (PVDF; BioRad) membranes. Membranes were blocked for 1 hour at room temperature with 5% bovine serum albumin (BSA) in TBS supplemented with 0.1% Tween20 (TBST) and then incubated with primary antibodies overnight at 4°C. Membranes were then washed and incubated with horseradish peroxidase conjugated secondary antibody (Cell Signaling Technology) for 1h at room temperature, then washed again. Signals were developed using Clarity Western ECL Substrate (BioRad) or SuperSignal West (Thermo Fisher). Blots were sometimes

stripped using Restore stripping buffer (Thermo Fisher) and re-stained with other primary antibodies.

Colocalization studies. For analysis of colocalization between receptor tyrosine kinases (MET and ERBB3) and late endosomal or lysosomal markers (Rab7 and LAMP1, respectively), 10,000 to 30,000 melanoma cells were plated in 8-well Lab-Tek II Chamber Slides (Thermo). Cells were washed with cold PBS and fixed in 4% paraformaldehyde (Fisher) for 15 min at room temperature, permeabilized with PBS supplemented with 0.05% Triton X-100 for 5 min, washed with PBS, and blocked in 5% donkey serum (JacksonImmuno) in PBS for 1 hour at room temperature. Cells or tissue sections were then co-stained with either rabbit anti-MET (8198, Cell Signaling, 1:200) or rabbit anti-ERBB3 (12708, Cell Signaling, 1:200) combined with mouse anti-Rab7 (95746, Cell Signaling, 1:100) or mouse anti-LAMP1 (sc-20011, Santa Cruz, 1:100) primary antibodies overnight at 4°C. The next day, cells were washed in PBS, stained with secondary antibodies (Alexa Fluor 488 donkey anti-rabbit IgG and Alexa Fluor 647 donkey anti-mouse IgG; Life Technologies; 1:1000) for 1 hour at room temperature, washed again in PBS, stained with 1 µg/ml DAPI, and mounted with Fluoromount-G (SouthernBiotech) for confocal imaging. Randomly selected melanoma cells were imaged using Z-stacks with a 40x objective and 2048 x 2048 pixel resolution on a Zeiss LSM780 Inverted confocal microscope. Deconvolution of the Z-stack images was performed using the Bitplane Imaris v7.7.2 and AutoQuant X3 softwares. Background was subtracted from each image using Imaris v7.7.2. Colocalization was assessed in

individual cells using the Imaris surface function and a 3D colocalization analysis was performed using the Imaris Coloc tool. Manders colocalization coefficients were used to quantify the degree of colocalization of two fluorophores per cell (Dunn et al., 2011; Manders et al., 1993).

Measurement of the rate of protein synthesis. For analysis of the rate of protein synthesis in culture, 100,000 – 500,000 melanoma cells were plated in 12-well tissue-culture-treated plates containing DMEM plus 10% FBS and 1% penicillin/streptomycin. When specified, cells were cultured for 24 hours in 5 nM Torin1 or 0.5 ng/ml puromycin prior to addition of OP-Puromycin to assess the rate of protein synthesis. 50 μ M OP-Puromycin (Medchem Source) was added to the culture medium for 30 minutes. Cells were washed twice in cold PBS, trypsinized, and centrifuged at 300xg for 5 minutes to pellet. The cells were resuspended in 250 μ l of 1% paraformaldehyde (Affymetrix) in PBS for 15 min on ice. Cells were then washed in PBS, and permeabilized in 100 μ l of PBS supplemented with 3% FBS and 0.1% saponin (Sigma) for 5 min at room temperature. The azide-alkyne cycloaddition to quantify OP-Puro incorporation into nascent peptides was performed using the Click-iT Cell Reaction Buffer Kit (Thermo Fisher) with azide conjugated to Alexa Fluor 555 (Life Technologies) at 5 μ M final concentration. After the 30 min azide-alkyne cycloaddition reaction, the cells were washed twice in PBS supplemented with 3% FBS and 0.1% saponin, then resuspended in PBS with 1 μ g/ml DAPI and analyzed by flow cytometry.

Measurement of protein aggregation. Protein aggregation was measured with the Proteostat Aggresome Detection Kit (Enzo). Melanoma cells were plated in 8-well Lab-Tek II Chamber Slides (Thermo) in DMEM plus 10% FBS and 1% penicillin/streptomycin. When specified, cells were cultured for 24 hours in 5 nM Torin1 or 5 μ M PD169316 proteasome activator before being fixed. Cells were washed with PBS, fixed in 4% formaldehyde (Fisher) for 30 min at room temperature, washed twice with PBS, permeabilized in 1X Assay Buffer (Enzo) supplemented with 0.5% Triton X-100 and 3 mM EDTA, pH 8.0, for 30 min at 4°C, and washed twice with PBS. Cells were then stained with the Proteostat Dual Detection Reagent (Enzo) for 30 min in the dark at room temperature. Cells were carefully washed twice in PBS, stained with 1 μ g/ml DAPI, and mounted with Flouromount-G for confocal imaging. Protein aggregation was quantified by calculating the integrated signal density per cell in randomly chosen fields of view throughout each sample using ImageJ.

Measurement of macropinocytosis in culture by imaging of live cells. As previously described (Palm et al., 2015), melanoma cells or human melanocytes were plated in 8-well chamber slides (Ibidi) containing DMEM plus 10% FBS and 1% penicillin/streptomycin. When specified, cells were pre-treated with 5 nM Torin1 or trametinib (Selleckchem) for 24 hours before addition of DQ-BSA (0.3 mg/ml DQ Green BSA; Thermo) to the culture medium to quantify macropinocytosis. Cells were imaged after 5-6 hours of incubation with DQ-BSA using a Zeiss LSM780 Inverted confocal microscope. One hour before imaging, 0.2 μ g/ml Hoechst 33342 (Thermo) was added

to visualize nuclei. Cellular degradation of fluorescently labeled albumin was determined by calculating the integrated signal density per cell in randomly chosen fields of view throughout each sample using ImageJ.

LC-MS/MS metabolomic analysis. Cultured melanoma cells or subcutaneous tumor fragments were homogenized using pestles in 1.7 ml Eppendorf tubes in ice-cold 80:20 methanol:water (vol:vol) and vortexed vigorously. The supernatant was collected into fresh Eppendorf tubes after a 15 min centrifugation at 17,000xg at 4°C and placed directly into autosampler vials for analysis by LC/MS without drying in a speed-vac. Metabolite measurements were carried out on a Thermo Scientific (Bremen, Germany) QExactive HF-X hybrid quadrupole orbitrap high resolution mass spectrometer (HRMS) coupled to a Vanquish UHPLC. Chromatographic separation of metabolites was achieved using a Millipore (Burlington, MA) ZIC-pHILIC column (5 µm, 2.1 x 150 mm) with a binary solvent system of 10 mM ammonium acetate in water, pH 9.8 (Solvent A) and acetonitrile (Solvent B) with a constant flow rate of 0.25 ml/minute. For gradient separation, the column was equilibrated with 90% Solvent B. After injection, the gradient proceeded as follows: 0-15 minutes linear ramp from 90% B to 30% B; 15-18 minutes isocratic flow of 30% B; 18-19 minutes linear ramp from 30% B to 90% B; 19-27 minutes of column regeneration with isocratic flow of 90% B. HRMS data were acquired with two different methods. Individual samples were acquired with an HRMS full scan (precursor ion only) switching between positive and negative polarities. Polarity-switching HRMS full scan data were acquired with a resolving power of 60,000 FWHM and a mass range

of 50-750 Daltons; the AGC target was set to 10^6 and a maximum injection time of 100 ms. Pooled samples, which were used for structural verification of the identity of metabolite peaks, were generated from an equal mixture of all individual samples and were analyzed using individual positive- and negative polarity data-dependent high-resolution tandem mass spectrometry (ddHRMS/MS) for high confidence metabolite identification. For ddHRMS/MS methods, precursor ion scans were acquired at a resolving power of 60,000 FWHM, with a mass range of 50-750 Daltons. The Automated Gate Control (AGC) target value was set to 10^6 , with a maximum injection time of 100 ms. Product ion spectra were acquired at a resolving power of 15,000 FWHM without a fixed mass range. The AGC target value was set to 2×10^5 with a maximum injection time of 150 ms. Data dependent parameters were set to acquire the top 10 ions with a dynamic exclusion of 15 seconds and a mass tolerance of 5 ppm. Isotope exclusion was turned on and the normalized collision energy was set to a constant value of 30. Settings remained the same in both polarities.

Statistical Methods. Generally, multiple melanomas derived from different patients or cell lines were tested in multiple independent experiments performed on different days. Mice were allocated to experiments randomly and samples processed in an arbitrary order, but formal randomization techniques were not used. Prior to analyzing the statistical significance of differences among treatments, we tested whether data were normally distributed and whether variances were similar among treatments. To test for normality, we performed the Shapiro–Wilk tests when $3 \leq n < 20$ samples or the

D'Agostino tests when $n \geq 20$ samples. To test whether variability significantly differed among treatments, we performed F -tests (for experiments with two treatments) or Levene's median tests (for experiments with more than two treatments). When the data were not significantly deviated from normality ($p \geq 0.01$) and variability not significantly differed among treatments ($p \geq 0.05$), we performed parametric tests such as student's t -tests (for experiments with two treatments) or one-way ANOVAs (for experiments with more than two treatments) on the original data. When the data were not significantly deviated from normality, but variability significantly differed among treatments, we performed parametric tests with the Welch's method for variance adjustment. When the data were significantly deviated from normality, we \log_2 -transformed the data and tested again for normality and variability. If the transformed data no longer significantly deviated from normality, we then performed parametric tests with or without the Welch's method for variance adjustment on the transformed data. If the \log_2 -transformation was not possible or the transformed data still significantly deviated from normality, we performed non-parametric tests on the non-transformed data. Ratio data were always \log_2 -transformed before any statistical tests were performed. Statistical tests were always two-tailed when this option was applicable. For experiments with two factors and data significantly deviated from normality, we reduced the factors to one when no appropriate non-parametric, two-way statistical tests were available. To assess the enrichment of shRNAs in the input cells as compared to tumors in the shRNA screen, we performed multiple unpaired, two-tailed t -tests on the \log_2 -transformed, total-count normalized data (Gargiulo et al., 2014). To assess differences in tumor growth or cell

growth in culture, we performed one-way or two-way ANOVAs on the last time point measured. To assess the difference between survival curves, we performed the Mantel-Cox's log-rank test. To assess the reproducibility of shRNA screen experiments, we performed the Spearman's correlation test. To assess the difference between two groups comprised of multiple different melanoma or melanocyte lines, we performed the two-tailed, nested *t*-test. When applicable, multiple-comparisons adjustments were always performed after statistical tests. All statistical analyses were performed with Graphpad Prism 8 or R 3.5.1 with the stats, fBasics and car packages. All data represent mean \pm standard deviation. No data were excluded. Mice sometimes died during experiments, presumably due to the growth of metastatic tumors. In those instances, data that had already been collected from those mice in interim analyses were included (such as subcutaneous tumor growth measurements over time).

3.4 Acknowledgments

S.J.M. is a Howard Hughes Medical Institute Investigator, the Mary McDermott Cook Chair in Pediatric Genetics, the Kathryn and Gene Bishop Distinguished Chair in Pediatric Research, the director of the Hamon Laboratory for Stem Cells and Cancer, and a Cancer Prevention and Research Institute of Texas Scholar. The research was supported by the Howard Hughes Medical Institute, the Cancer Prevention and Research Institute of Texas (RP170114, RP170633, and RP180778), and the Once Upon a Time Foundation. S.Y.K. and D.B. were each supported by Ruth L. Kirschstein National Research Service Award Predoctoral Fellowships from the National Cancer

Institute (F30 CA216885 and F31 CA239330). A.T. was supported by the Leopoldina Fellowship Program (LPDS2016-16) of the German National Academy of Sciences. We thank Jian Xu for sequencing, N. Loof of the Moody Foundation Flow Cytometry Facility, and K. Luby-Phelps and A. Bugde of the Live Cell Imaging Facility at UT Southwestern. We also thank the UT Southwestern BioHPC (high-performance computing) cluster. Graphics were created using BioRender.

CHAPTER FOUR

Discussion and future directions

4.1 Targeting ion channels and transporters in cancer

Ion channels and transporters regulate intracellular volume, pH, proliferation, migration, and signaling, all of which are dysregulated in cancer cells. Previous studies have identified specific channels and transporters that are overexpressed, amplified, or mutated in cancer and have demonstrated that inhibition of these channels or transporters reduces tumor growth and metastasis.

However, because aberrantly functioning channels and transporters alter so many aspects of cellular physiology, they likely promote cancer through multiple direct and indirect mechanisms. For example, I found that *MCOLN1*, a lysosomal cation channel important for endosomal and lysosomal fusion and trafficking, was required by melanoma cells to negatively regulate MAPK and mTORC1 signaling, to maintain protein homeostasis, and to promote tumor growth. My work shows that channels and transporters can have secondary effects on oncogenic signaling by affecting the trafficking or function of endosomes and lysosomes. Regardless of the exact mechanism, specific ion channels and transporters may be targeted to treat cancer.

How can we more effectively target ion channels and transporters to treat cancer patients? Ion channels and transporters often reside on the cell surface and existing clinically-approved drugs target them. However, there are also major limitations. A large number of ion channels and transporters are broadly required by all cells to regulate fundamental processes. Thus, it is critical to identify channels and transporters that are

overexpressed or mutated in cancer cells and then to functionally test whether they are preferentially required by cancer cells as compared to normal cells.

Though some studies have extensively investigated the mechanisms downstream of oncogenic ion channels and transporters (Beuschlein et al., 2013; Choi et al., 2011; Eskiocak et al., 2016; Scholl et al., 2013; Takahashi et al., 2018), additional work will be required to understand the mechanisms by which they promote the survival or proliferation of cancer cells.

A general challenge is that many of the available pharmacological agents target entire classes of channels or transporters. These pharmacological inhibitors and activators may show activity against cancer cells in culture but may not possess adequate specificity to avoid side effects in the heart or the brain, where many ion channels and transporters are expressed. Although some inhibitors that target specific ion channels and transporters have been developed, they are often not suitable for use *in vivo*. For example, many only function at high micromolar concentrations in culture that cannot be achieved *in vivo* and/or do not possess adequate pharmacokinetic properties. Therefore, it will be critical to develop potent and specific inhibitors to more effectively target channels and transporters that drive tumor growth.

4.2 The role of TRPML1 in melanoma

I identified TRPML1 as an ion channel that is required by melanoma cells but not by normal melanocytes. TRPML1 promotes melanoma growth by negatively regulating MAPK and mTORC1 signaling to maintain protein homeostasis and macropinocytosis,

and to sustain intracellular serine levels (**Figure 4.1**). While cancer cells traditionally depend upon the activation of oncogenic signaling pathways like the PI3K, MAPK, and mTOR pathways, overactivation of these pathways can have deleterious consequences that impair proliferation and survival (Bartkova et al., 2006; Braig et al., 2005; Chen et al., 2005; Evan et al., 1992; Peterson et al., 2009). Melanoma cells almost always exhibit MAPK pathway activation (Nazarian et al., 2010) but appear to upregulate TRPML1 to avoid overactivation. The increased MAPK pathway and mTORC1 activation in TRPML1 deficient melanoma cells reduced macropinocytosis, increased protein synthesis, depleted serine, and induced proteotoxic stress, ultimately causing cell death.

TRPML1 is also required for the proliferation of head and neck cancer cells with HRAS mutations (Jung et al., 2019). However, in contrast to my results, *MCOLN1*/TRPML1 deficiency reduced MAPK pathway activation in those cells by attenuating HRAS clustering. In melanoma, TRPML1 deficiency increased MAPK pathway activation. Increased MAPK and PI3K pathway activation were also observed in astrocytes from *Mcoln1* deficient mice, though it is unclear whether this reflected a cell-autonomous effect of TRPML1 deficiency or increased levels of inflammatory cytokines (Weinstock et al., 2018). The opposite results in different cell types may reflect distinct effects of TRPML1 on HRAS signaling, which is not mutated in melanoma (Hodis et al., 2012), or other differences between cells.

It is striking that melanoma cells increase both macropinocytosis and TRPML1 expression relative to normal melanocytes, even in the absence of amino acid

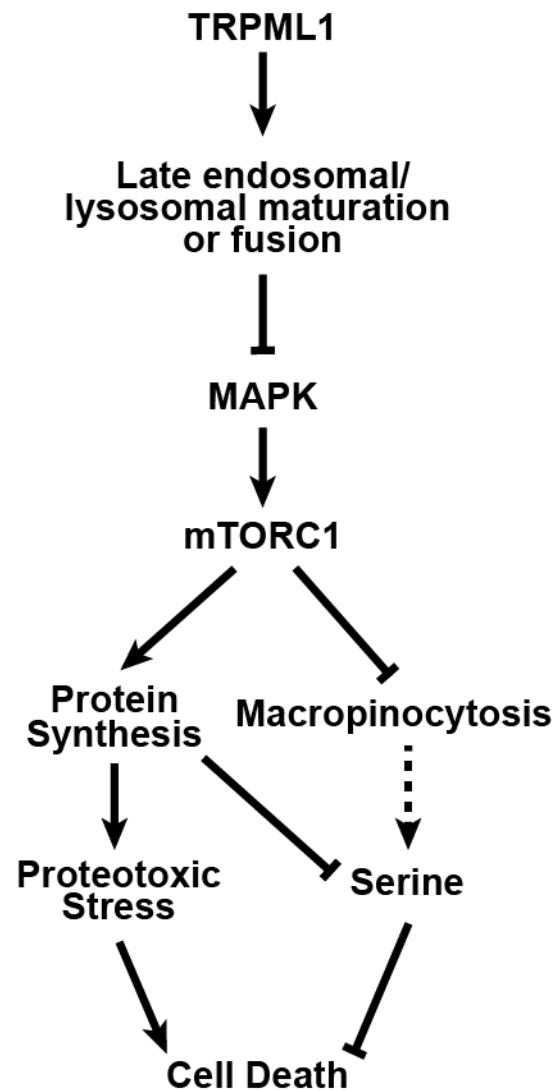


Figure 4.1. Model of TRPML1 function in melanoma cells. TRPML1, which is required for proper endosomal and lysosomal trafficking, negatively regulates the MAPK and mTORC1 pathways to sustain macropinocytosis and to protect cells against proteotoxic stress, serine depletion, and apoptotic cell death.

starvation. Their dependence upon TRPML1 to attenuate MAPK/mTORC1 signaling, to sustain macropinocytosis, and to prevent proteotoxic stress reveals a new vulnerability. These data highlight the potential of therapeutic approaches that induce proteotoxic stress, such as proteasome inhibitors, autophagy or lysosomal inhibitors, or chaperone inhibitors.

4.3 The combination of TRPML1 inhibition with other therapies

Both shRNA-mediated knockdown and deletion of TRPML1 significantly inhibited melanoma growth, demonstrating the potential of TRPML1 as a therapeutic target in melanoma. Several chemical inhibitors of TRPML1 have been identified and shown to inhibit cell proliferation in *HRAS*-mutant cancers in culture (Jung et al., 2019) but may not possess the specificity and pharmacokinetic properties for *in vivo* use. To improve our ability to target TRPML1, new pharmacological inhibitors of TRPML1 optimized for *in vivo* use must be developed.

Melanoma is notorious for developing resistance to targeted therapies such as BRAF and MEK inhibitors. Moreover, deletion of TRPML1 reduced, but did not completely block, tumor growth. Thus, it will be important to consider TRPML1 therapy in the context of combination therapies. I found that loss of TRPML1 increases proteotoxic stress in melanoma cells. Activation of the proteasome can partly rescue this cell death, raising the possibility that the combination of TRPML1 inhibition with proteasome inhibition could produce an even larger inhibition of tumor growth.

Immunotherapy has become an effective treatment for melanoma. Patients treated with a combination of two checkpoint inhibitors had a four-year survival rate of 53%, a vast improvement over other melanoma therapies (Hodi et al., 2018). Based on this finding, I have started to assess whether TRPML1 deficiency influences melanoma cell immunogenicity and responsiveness to immunotherapy. I performed transcriptional profiling of parental and TRPML1-deficient melanoma cells and discovered that TRPML1-deficient melanoma cells highly upregulate the expression of SPANX family proteins that are not normally expressed by melanoma cells or melanocytes. One of these proteins, SPANX-B, is immunogenic when expressed by cancer cells. SPANX-B expression increases CD4⁺ and CD8⁺ T-cell responses against cancer cells in culture (Almanzar et al., 2009). Future work should test if TRPML1 loss makes melanoma cells more immunogenic as a result of the increased expression of tumor associated antigens like SPANX-B. To answer this question, one could transplant parental and TRPML1-deficient Yale University Mouse Melanoma (YUMM) cell lines (Meeth et al., 2016) into both immunocompetent and NSG mice. If the TRPML1-deficient tumors exhibit greater growth defects in immunocompetent mice as compared to NSG mice and if TRPML1-deficient tumors demonstrate increased immune cell infiltration compared to parental tumors, then TRPML1 loss may make melanoma cells more immunogenic and thus more sensitive to checkpoint inhibition.

4.4 mTOR inhibition in cancer

mTOR is activated in many cancers, promoting tumor growth and progression (Guertin and Sabatini, 2007). However, mTOR inhibitors have so far been ineffective in the treatment of many cancers, including melanoma (Dancey, 2010; Margolin et al., 2005; Sabatini, 2006). One explanation is that mTOR inhibition relieves negative feedback on other signaling pathways such as the PI3K, Akt, and MAPK pathways (Dancey, 2010; Guertin and Sabatini, 2007; Sabatini, 2006). The activation of these pathways may negate the effects of mTOR inhibition, allowing cancer cells to grow and proliferate. An ongoing question is whether there are additional mechanisms by which cancer cells circumvent mTOR inhibition.

I found that activation of mTORC1 as a result of TRPML1 loss was detrimental to melanoma cells and that mTORC1 inhibition rescued the growth of TRPML1-deficient melanomas. Melanoma cells required TRPML1 to prevent the overactivation of the MAPK and mTORC1 pathways and to sustain macropinocytosis. My data suggest that melanoma cells are dependent on macropinocytosis and the increased mTORC1 activation in the absence of TRPML1 inhibits macropinocytosis. Thus, mTOR inhibitors may be ineffective in melanoma because they promote macropinocytosis, enhancing the ability of melanoma cells to acquire nutrients, such as amino acids. To explain why melanoma cells are dependent on macropinocytosis, isotope tracing using ¹⁵N-labeled albumin could determine what metabolites are derived from the uptake of extracellular proteins. If mTOR inhibition increases macropinocytosis in melanoma cells, adding

macropinocytosis or lysosome inhibitors to mTOR inhibitor therapy may increase effectiveness.

4.5 Implications for patients with mucopolysaccharidosis type IV

Patients who have loss-of-function mutations in *MCOLN1* present in infancy with a lysosomal storage disorder called mucopolysaccharidosis type IV (MLIV), which is characterized by severe psychomotor retardation, ophthalmologic abnormalities, and achlorhydria (Amir et al., 1987; Bargal et al., 2000; Chen et al., 1998; Sun et al., 2000). There is currently no specific treatment for MLIV, and the mechanism by which loss of TRPML1 function leads to the neurodevelopmental deficits is unknown.

I investigated the effects of TRPML1 deficiency in melanoma cells and found that the phenotypes caused by TRPML1 loss in melanoma cells were rescued by mTORC1 inhibition. These data raise the possibility that MLIV patients also exhibit mTORC1 activation in their tissues and that their symptoms are at least partly caused by mTORC1 hyperactivation. Consistent with my data, other lysosomal storage disorders such as mucopolysaccharidoses types I, VI, and VII exhibit mTORC1 hyperactivation, resulting in skeletal deformities (Bartolomeo et al., 2017). It will be important in future studies to determine whether *Mcoln1*^{-/-} mice, which exhibit neurological defects similar to MLIV patients, exhibit MAPK or mTORC1 activation in their tissues and whether long-term treatment with rapamycin can alleviate their neurological symptoms. If so, then mTOR inhibitors may ameliorate the symptoms of MLIV.

4.6 Final remarks

In this work, I discovered that TRPML1, a lysosomal cation channel, is required for melanoma cell survival and tumor growth because it negatively regulates MAPK and mTORC1 signaling to protect cells from proteotoxic stress and to sustain macropinocytosis. I hope that the insights I have gained about the function of TRPML1 in melanoma will create opportunities to develop new therapies for both melanoma and MLIV. There is still much to learn about the roles that TRPML1 and other ion channels and transporters play in cancer and disease, but we are one step closer.

APPENDIX A

Log₂-transformed tumor shRNA enrichment for the primary shRNA screen

shRNA	Tumor shRNA enrichment		
	M214	M481	M491
MCOLN1	-2.45	-4.44	-2.61
MCOLN1	-1.82	-1.81	-2.08
MCOLN1	-4.41	-5.21	-5.00
MCOLN1	-3.92	-2.69	-2.43
ABCC8	-0.27	-0.23	-0.27
ABCC9	-1.16	-1.21	-0.81
ABCC9	-0.46	0.37	-0.05
BTBD10	0.16	-0.66	-0.15
C5ORF62	0.01	-0.18	-0.17
CACNA1A	-0.54	-0.17	-1.14
CACNA1C	0.43	0.19	0.21
CACNA1D	0.34	-0.80	-0.48
CACNB3	-0.57	-0.45	-0.72
CATSPER3	-0.68	-1.86	0.02
CFTR	-0.17	-1.34	-0.71
CHRM5	0.34	-0.23	0.00
CHRM5	0.33	-0.65	0.06
CHRM5	-1.08	-2.52	-1.68
CHRM5	0.16	0.15	0.27
CHRM5	0.45	0.74	0.05
CHRNA4	-1.34	-2.55	-1.67
CHRNA5	0.30	-0.02	-0.07
CHRNA5	-0.81	-0.27	-0.41
CLCA1	-0.55	-0.70	-0.63
CLCN4	-0.93	-1.51	-0.84
CLCNKB	-1.35	-2.26	-1.21
CLIC5	0.23	-0.25	-0.21
CNGB3	-0.38	-0.30	0.14
CNGB3	-0.54	-0.85	-0.92
ELK1	-1.03	-0.55	-1.57
ELK1	-0.03	-0.23	-0.17
ELK1	-0.11	-0.26	-0.34
ELK1	0.47	0.07	0.17
GABRA2	-0.51	-0.84	-1.05
GABRE	-0.91	-1.36	-0.45
GABRG2	-0.43	0.13	-0.43
GABRQ	-0.01	0.32	0.12
GAR1	-0.86	-0.14	-1.22
GLRA2	-0.50	-0.31	-0.37
GPM6A	0.15	0.16	0.17
GRID2	-0.27	-1.83	-0.69
GRIN2C	-0.44	-0.90	-0.58
GRM7	-0.44	-2.05	-0.91
GRM7	-0.10	0.12	0.12
GRM7	-0.55	-0.08	-0.67
GRM7	0.06	0.13	0.17
HCN1	-0.04	-0.04	0.13
HTR3A	0.70	0.16	-0.10
HTR3A	0.13	-1.47	-0.67
HTR3A	-0.09	-0.90	-0.09
HTR3A	-0.15	-0.27	-0.62
HTR3B	-0.68	-0.35	-0.82
HTR3B	0.19	-0.44	-0.22
HTR3B	0.31	0.03	-0.07
ITPR3	-1.33	-1.24	-1.53
KCNA10	-0.90	-2.39	-0.10
KCNA3	-0.10	-0.07	0.38
KCNA4	0.22	-0.12	0.12
KCNB1	0.27	-0.23	-0.09

shRNA	Tumor shRNA enrichment		
	M214	M481	M491
KCND1	-0.12	-0.66	-0.99
KCNG1	-1.24	-1.18	-1.67
KCNG3	-0.33	-0.36	-0.28
KCNH5	-0.26	-0.59	-0.87
KCNH7	-0.38	-1.91	-0.41
KCNJ3	0.05	-0.16	-0.23
KCNJ4	-0.29	-0.65	-0.95
KCNK13	-0.35	-0.60	-0.66
KCNK2	-0.31	0.28	-0.45
KCNK9	-0.65	-0.52	-0.37
KCNMA1	0.21	-0.43	-0.04
KCNN2	-0.02	0.20	0.18
KCNQ3	0.01	-0.47	-0.67
KCNQ4	-0.84	-0.81	-0.07
KCTD7	-0.23	-0.58	-0.24
KCTD7	0.13	0.06	0.15
KCTD7	-0.90	-0.17	-0.79
KCTD7	-0.55	-0.84	-0.81
KCTD7	-1.77	-1.97	-0.91
MCOLN2	-0.09	0.10	-0.25
MCOLN3	-0.18	-0.41	-0.28
MCOLN3	-1.01	-0.70	-0.28
MLC1	-0.44	-1.53	-1.11
NALCN	0.39	0.16	-0.16
NOX5	0.16	0.30	-0.45
P2RX5	-0.40	-0.52	-0.12
PKD2L1	-0.46	-0.66	-0.14
PKD2L1	-0.45	-1.30	-0.91
PKD2L2	-0.38	0.09	0.16
RYR2	-0.03	-0.51	-0.60
SCN2A	0.32	0.12	0.07
SCN4B	-0.32	-0.63	-0.35
SCN8A	-0.92	-1.24	-0.61
SETD1A	-0.53	-0.53	-1.58
TPCN1	-0.47	-2.09	-1.20
TPTE	0.03	0.43	0.38
TRPA1	0.12	-0.20	0.36
TRPC1	-0.35	-0.12	-0.21
TRPC3	-0.22	-0.66	-0.78
TRPC6	0.31	0.27	0.35
CACNA1D	0.14	0.33	0.43
CACNA2D3	0.21	0.27	0.27
CACNA2D3	-0.72	-1.47	-0.73
CACNB1	0.26	0.45	-0.29
CACNB1	-1.14	-0.77	-0.20
CACNB1	-0.95	-1.38	-1.57
CACNB1	-1.48	-1.52	-0.96
CACNG3	-0.85	-1.01	-0.85
CATSPER3	-1.34	-1.82	-0.21
CHRM5	0.03	0.46	0.36
CHRM5	-0.38	-0.49	-0.40
CHRNA2	-0.23	-0.49	-0.50
CHRNA2	-0.63	-0.95	-0.46
CHRNA2	-0.70	-1.52	-0.51
CLCN7	-0.45	-1.56	-1.69
CLCN7	-0.50	-2.90	-0.84
CLCN7	0.53	-0.08	0.09
CLNS1A	-0.75	-1.50	-0.74
CNGB3	-0.56	-0.21	-0.54

shRNA	Tumor shRNA enrichment		
	M214	M481	M491
ELK1	-0.22	-0.03	-0.28
FXYD1	-1.27	-2.59	-1.83
FXYD1	-1.24	-1.17	-0.35
GABRA4	0.04	0.00	0.05
GABRA4	-0.03	-0.29	-0.54
GABRA4	-0.24	-0.24	-0.42
GABRD	-1.73	-1.70	-1.05
GABRR1	-2.00	-2.84	-0.85
GABRR1	-0.14	0.32	0.02
GABRR1	-0.35	-0.10	-0.02
GRIK2	0.14	-0.48	-0.63
GRIK2	0.23	-0.61	-0.73
GRIK2	-0.72	-0.26	0.08
GRIN2B	-0.68	-0.05	0.06
GRIN2B	-0.66	-0.72	-0.22
GRM7	0.27	-0.95	-0.61
GRM7	-0.07	0.12	0.24
GRM7	-1.01	-1.93	-1.67
HCN1	-0.90	-0.70	-0.43
HCN1	-1.27	-3.37	-1.94
HCN1	0.40	0.65	0.39
HTR3A	-0.34	0.19	-0.30
HTR3A	-0.75	-0.96	-0.54
HTR3A	0.15	-0.06	-0.26
HTR3B	-0.66	-0.31	-0.74
HTR3B	0.42	0.17	0.03
HTR3B	-0.03	-0.47	-0.07
HTR3B	0.18	0.20	-0.13
KCNIP2	-1.02	-1.87	-0.97
KCNC3	-0.41	-1.11	-1.55
KCNC3	-0.79	-0.80	-1.92
KCNF1	-0.81	-1.58	-2.62
KCNJ10	0.25	0.23	0.28
KCNJ16	-0.02	0.08	-0.43
KCNJ16	-0.47	0.20	0.02
KCNJ3	-0.04	0.00	0.01
KCNJ3	-0.12	-0.25	-0.78
KCNJ3	0.26	-0.06	0.10
KCNK7	-0.27	-1.10	-0.72
KCNN1	-1.25	-1.42	-1.63
KCNQ3	-0.85	-0.77	0.14
KCNT2	0.05	0.17	-0.08
KCNT2	-0.49	-0.17	-0.06
KCTD10	-1.02	-0.51	-0.47
KCTD10	0.07	-0.51	-0.09
KCTD13	-0.31	-0.62	-0.49
KCTD7	-0.47	-0.53	-0.31
MCOLN2	-0.55	0.21	0.11
NOX5	-0.36	-0.59	-0.54
NOX5	-0.68	-1.06	-0.98
NOX5	-0.05	-0.98	-1.42
NUDT9	0.09	-1.61	-0.16
P2RX6	0.47	-0.05	-0.27
P2RX6	0.03	-1.38	-0.90
P2RX7	-0.15	0.23	0.16
P2RX7	-0.05	0.18	0.21
PKD1L2	-0.39	-0.27	-0.17
SCN11A	-0.36	-0.62	-0.02
SCN11A	0.12	0.06	0.23
SCN9A	-0.47	-1.01	-0.37
SCN9A	-1.32	-2.74	-1.11
STX1B	-1.05	-0.31	-0.76
STX1B	-0.81	-1.59	-0.98
STX1B	-1.19	-0.56	-0.10
TOMM40	-0.14	0.47	0.08
TOMM40	-1.21	-2.77	-2.00

shRNA	Tumor shRNA enrichment		
	M214	M481	M491
TOMM40	-1.28	-1.26	-1.76
TRPM2	-1.99	-2.13	-1.96
TRPV1	-1.38	-1.20	-0.84
TRPV1	-0.63	-0.09	-0.41
TRPV5	-0.63	-1.56	-0.82
TRPV5	-0.17	0.39	0.31
TRPV5	-0.29	-1.56	-1.22
TRPV5	-1.15	-2.54	-0.39
TRPV5	-1.43	-0.49	-0.60
TTYH1	-0.72	-2.34	-1.88
VDAC1	0.27	0.32	-0.23
ABP1	-0.46	-0.44	0.03
AVEN	-2.92	-1.30	-0.94
AVEN	-0.34	-0.05	0.17
AVEN	0.11	0.27	0.21
CACNA1D	-0.02	0.09	-0.18
CACNB1	-1.22	-0.80	-0.53
CACNG2	-1.10	-1.28	-2.15
CACNG3	-0.31	-0.14	-0.61
CATSPER3	-0.67	-0.20	-0.82
CHRNA2	-0.86	-0.77	-0.83
CHRNA2	-0.46	-0.02	0.26
CHRNA3	0.07	-2.04	-2.50
CHRNA3	0.03	-0.17	-0.27
CHRNA2	-1.26	-1.70	-1.33
CLCN1	-0.34	-0.54	-0.39
CLCN1	0.20	-0.26	-0.05
CLCN1	-0.21	0.09	-0.39
CLCN1	-2.65	-1.63	-2.55
CLCN2	-1.16	-3.13	-1.71
CLCN7	-0.98	-1.47	-2.33
CLNS1A	-0.22	-0.08	-0.06
CLNS1A	-0.44	-0.16	-0.36
CLNS1A	-0.07	0.03	-0.54
CLNS1A	0.39	0.40	0.26
FXYD3	-0.95	-1.16	-0.93
GABRA5	0.16	-1.06	-0.93
GABRD	-0.78	-1.20	-0.92
GABRD	-0.46	-1.32	-0.76
GABRE	-0.28	-0.64	-0.94
GABRR1	-1.15	-0.40	-1.42
GLRB	-0.18	-0.21	-0.04
GLRB	-0.55	0.22	-0.18
GLRB	0.49	-0.72	-0.20
GRM7	-1.07	-0.24	-0.49
GRIA3	-0.13	0.09	-0.42
GRIK2	-0.08	-0.16	-0.09
GRIK3	-0.47	-1.07	-0.86
GRIN2B	-0.29	-0.44	-0.45
GRM7	0.04	0.24	0.05
HCN1	-0.17	-0.53	-0.31
HTR3A	0.12	-1.37	-1.07
KCNA6	-1.08	-2.04	-2.57
KCNA6	-0.04	-0.04	-0.52
KCNC3	-1.90	-0.12	-1.48
KCNE4	-0.56	-0.18	-0.74
KCNF1	-0.55	-1.12	-0.30
KCNF1	0.65	0.11	0.37
KCNG1	-0.76	-0.70	-1.05
KCNH8	-0.39	0.05	-0.48
KCNIP2	-1.01	-1.00	-1.25
KCNIP4	-0.96	0.06	-0.08
KCNJ16	-0.36	-0.01	-0.26
KCNJ16	-0.05	0.34	0.51
KCNJ4	-1.90	-3.26	-1.82
KCNK1	0.93	-0.41	-0.22

shRNA	Tumor shRNA enrichment		
	M214	M481	M491
KCNK13	-0.01	0.23	0.05
KCNK13	-0.17	0.01	-0.18
KCNN1	-1.05	-0.88	-1.87
KCNN1	-1.58	-1.60	-0.27
KCNQ3	-2.07	-2.08	-1.51
KCNQ3	-0.93	-0.90	-0.57
KCNS1	0.01	-0.49	-0.90
KCNT1	-0.67	-0.50	-2.56
KCTD10	-0.04	0.20	0.29
KCTD13	-0.48	-0.91	-0.71
KCTD13	-1.07	-1.74	-0.25
KCTD2	-0.56	-1.37	-0.92
NOX5	-0.76	-1.71	-2.44
NOX5	-0.41	-1.37	-1.21
NUDT9	-0.25	-0.75	-0.44
NUDT9	-0.55	-0.06	-0.58
P2RX6	-0.05	0.10	0.01
VDAC1	-0.32	-0.09	0.03
PKD1L2	-0.90	-0.99	-0.73
PKD1L2	-0.02	-0.03	-0.46
RYR1	-0.03	0.13	-0.29
RYR2	-1.03	-0.18	-0.86
SCN11A	0.17	-0.05	-0.18
SCN11A	-0.25	-1.05	-0.14
SCN3A	-0.41	-0.59	-0.18
SCN3A	-0.57	-0.64	-0.77
SCN9A	0.38	-0.93	0.20
SCN9A	-0.14	0.08	0.10
SLC26A7	-0.43	-0.72	0.07
SNAP25	0.79	0.11	0.14
TOMM40	-2.93	-0.94	-1.74
TRPC6	-0.23	0.08	0.13
TRPM2	-0.84	-0.31	-0.97
TRPM7	0.06	-0.25	0.04
TRPM7	-0.15	-0.25	0.00
TRPM7	-0.37	0.14	-0.26
TRPM7	-0.16	-0.30	-0.14
TRPV1	0.54	-0.48	0.06
TRPV1	-0.37	-0.27	-0.29
TTYH1	-0.66	-1.27	-2.10
VDAC1	0.42	0.57	0.07
ABP1	-0.03	-0.55	-0.23
ABP1	-0.03	-0.13	0.07
CACNB2	0.11	-0.42	-0.13
CACNB2	0.25	-0.47	-0.20
CACNB2	-0.73	-0.40	0.02
CACNG2	0.06	-0.35	-0.15
CACNG2	0.40	-0.49	-0.25
CACNG2	0.47	-1.81	-0.88
CACNG5	-0.43	-0.43	-0.45
CACNG5	-0.61	0.03	0.04
CACNG5	0.10	-0.13	0.16
CACNG5	0.26	-0.05	0.49
CACNG5	-0.20	-0.28	-0.74
CATSPER4	-0.66	-0.13	-0.10
CCT8L2	-0.01	-0.09	0.12
CCT8L2	0.61	-0.10	0.07
CCT8L2	-0.31	-0.17	-0.23
CFTR	-0.08	0.16	-0.43
CHRNA3	-0.43	-0.80	-1.39
CHRNA3	-0.18	-0.41	-0.30
CHRN3	-0.20	0.35	0.71
CHRN3	-0.62	-0.18	-0.28
CLCN2	0.02	-0.68	-0.84
CLCN2	0.50	-0.13	-0.63
CLCNKA	-0.89	-0.87	-0.64

shRNA	Tumor shRNA enrichment		
	M214	M481	M491
CLCNKA	-0.38	-0.33	-0.11
CLCNKA	0.47	0.09	0.19
CLIC4	-0.40	-1.16	-1.82
CLIC4	0.23	0.03	0.41
CLIC4	-0.49	0.29	-0.01
CNGB1	-0.48	0.03	0.28
CNGB1	-0.27	-0.35	-1.16
FXYD3	-0.44	-0.55	-0.21
GABRA5	-0.91	-0.24	-0.34
GABRA5	-0.05	0.09	0.05
GABRA5	-0.24	-1.32	-1.26
GABRR2	-0.66	0.04	-0.22
GRIA4	-0.27	-0.14	0.12
GRIA4	-0.78	-0.88	0.07
GRIA4	0.34	-0.09	-0.11
GRIA4	0.49	0.14	0.76
GRIK3	-0.52	0.16	0.40
GRIK3	-0.84	-0.55	0.34
KCNA1	0.35	0.27	0.45
KCNA7	-0.71	-0.53	-1.07
KCNAB2	-0.21	0.16	0.44
KCNC4	0.09	-1.33	-0.66
KCNC4	0.44	-0.05	0.58
KCNC4	-1.30	-2.51	-1.88
KCNC4	-0.55	-1.95	-1.02
KCNC4	-0.90	-0.18	0.34
KCNE1L	-0.07	-0.77	-0.64
KCNE1L	-0.73	-0.70	-1.53
KCNE1L	-0.26	0.03	-0.15
KCNE4	-0.68	-1.39	-3.18
KCNE4	-1.06	-0.59	-1.95
KCNG1	-0.60	-1.57	-2.25
KCNG1	-0.52	-1.61	-1.44
KCNG1	0.11	0.23	0.38
KCNG3	-0.22	0.37	0.15
KCNG3	-0.61	-0.32	-0.26
KCNH8	-0.76	-0.81	-0.85
KCNIP4	0.16	-0.70	-0.82
KCNJ4	0.01	-0.35	0.27
KCNK13	0.26	0.01	0.66
KCNK17	0.24	0.05	0.06
KCNK17	0.91	-1.12	-1.46
KCNK7	0.61	0.31	-0.38
KCNK7	-0.39	-1.77	-1.43
KCNK7	-0.62	0.02	-0.09
KCNN2	0.15	-0.70	-0.18
KCNQ1	0.08	-0.10	0.40
KCNS1	-0.13	-0.28	-0.23
KCNV1	-0.03	-1.01	-0.80
KCNV1	0.12	0.18	0.12
KCNV1	-0.54	-0.58	-0.99
KCTD14	-0.63	0.04	-0.21
NOX1	-0.24	-0.16	-0.04
NOX1	0.29	0.08	0.02
NOX1	-0.25	-0.22	-0.08
SCN3B	0.08	-0.02	-0.95
SCN4A	-0.78	-1.04	-2.89
SLC26A7	0.07	-0.27	-0.02
SLC26A7	-0.03	-0.05	0.01
SNAP25	0.03	0.26	0.45
SNAP25	-0.49	-0.16	0.17
SNAP25	0.19	-0.02	0.24
TRPM2	0.08	-1.47	-1.23
TRPM2	-1.00	-0.45	-0.17
TRPM4	-0.02	-0.50	-0.40
TRPM8	-0.19	0.19	-0.31

shRNA	Tumor shRNA enrichment		
	M214	M481	M491
TRPM8	0.86	0.01	0.53
TRPM8	-0.47	-0.84	-1.54
VDAC2	-0.01	-0.29	0.77
ZACN	0.58	-1.04	-0.29
ZACN	-0.96	-0.67	-1.48
ABP1	-0.85	0.65	0.21
ACCN1	-1.14	-1.28	-1.06
AQP7	-0.14	-0.11	-0.11
BSND	-1.09	-1.01	-1.59
C5ORF62	0.58	-0.31	-0.79
CACNA1E	-0.77	-0.25	-0.87
CACNA1E	-0.50	-0.53	0.25
CACNA1E	0.14	-0.09	-0.24
CACNA2D2	-0.32	-0.97	-0.91
CACNA2D2	-0.40	-0.94	-1.55
CACNB4	-0.20	-0.27	-0.51
CACNG2	-1.29	-0.37	-0.62
CACNG6	0.01	-0.09	-0.16
CACNG8	-0.95	-1.95	-1.25
CACNG8	-1.26	-0.69	-0.75
CFTR	-1.39	-0.86	0.04
CHRNA5	-0.36	0.51	-0.99
CHRNA5	0.06	0.44	0.40
CHRN3	-0.33	-0.02	0.06
CLCN4	-0.99	-0.27	-0.77
CLCNKA	-1.84	-1.77	-1.43
CLIC4	0.82	0.40	0.22
CNGA2	-1.09	-0.01	-0.15
CNGA2	0.56	-0.84	-0.91
CNGA2	-1.21	-0.29	-0.59
CNGB1	-0.22	-0.25	-0.52
CNGB1	-0.20	-0.83	-0.33
VDAC2	-1.22	-0.69	-0.37
FXD3	-1.48	-0.92	-2.17
FXD6	-0.01	-0.06	-0.43
GABRA5	-1.42	-2.04	-0.88
GABRE	-1.03	-0.72	-1.28
GABRG2	0.22	-0.76	0.04
GABRR2	-1.27	-0.53	0.05
GABRR2	-0.48	0.47	0.66
GRIA4	-1.23	-0.29	-0.67
GRIA4	-0.30	-0.39	-0.01
GRID2	0.76	-1.22	-0.80
GRIK5	-1.25	-1.79	-1.43
GRIK5	-0.88	-0.88	-1.32
GRIN2C	-1.18	-0.83	-0.60
GRIN2C	-0.47	-0.77	-0.09
GRIN3A	-1.51	-0.65	-0.82
GRINA	-0.19	0.62	-0.20
HTR3C	-0.45	-0.24	-0.14
HTR3C	-0.06	0.16	-0.01
HVCN1	0.22	0.09	0.02
HVCN1	0.36	0.49	0.49
KCNAB2	-0.99	-0.67	-1.25
KCNAB2	-0.84	-1.32	-0.81
KCNB1	-0.21	-1.08	-0.61
KCNE1L	-1.32	-1.81	-2.06
KCNE1L	-0.20	-0.07	-0.17
KCNG2	-0.90	-1.68	-1.59
KCNG2	-2.40	-2.52	-2.00
KCNH8	-0.62	-0.55	-0.33
KCNIP4	-0.90	-0.56	-0.31
KCNJ11	-0.77	-0.80	-0.67
KCNJ11	-0.72	0.04	-0.30
KCNJ11	0.49	-0.24	-0.35
KCNJ4	-1.74	-1.46	-1.38

shRNA	Tumor shRNA enrichment		
	M214	M481	M491
KCNJ4	-0.82	-0.52	-0.73
KCNK13	-0.19	-0.22	-0.17
KCNK17	-1.41	-1.36	-0.81
KCNK7	0.02	-1.20	-0.19
KCNN2	-0.83	0.60	-0.07
KCNN2	-0.50	-0.15	-0.04
KCNQ1	-0.02	0.07	-0.20
KCNS1	-1.52	-0.21	-0.53
KCNS1	-0.73	-0.24	-0.42
KCNS3	-0.91	-1.21	-0.42
KCNS3	-1.04	-0.98	-0.76
KCNT1	-0.45	0.21	-0.14
KCNT1	1.11	-0.48	-0.44
KCNT1	-1.09	-0.24	-0.89
KCTD14	-2.33	-1.39	-0.62
KCTD14	-1.48	-1.31	-1.23
KCTD15	-2.97	-3.18	-2.12
NOX1	-1.18	-1.55	-0.29
RYR2	-0.44	-0.48	-0.20
SCN10A	-0.31	-0.87	0.09
SCN10A	-0.91	0.03	-0.62
SCN10A	0.25	-1.52	-1.67
SCN1B	-0.49	0.33	0.27
SCN4A	-1.90	-1.47	-1.00
SCNN1B	0.56	-0.12	0.37
SCNN1B	0.95	0.53	0.48
SETD1A	-1.46	-2.54	-2.26
SETD1A	0.23	-0.28	-0.40
SLC26A7	-0.94	-0.12	0.23
SNAP25	-0.51	-0.77	-0.88
TRPC3	0.21	0.07	-0.24
TRPM2	1.26	-2.48	-0.40
TRPM3	-0.56	-0.20	-0.25
TRPM3	-0.20	-0.39	-0.24
VDAC2	-0.87	-0.11	-0.21
ACCN1	-1.20	-1.59	-1.86
AQP7	-0.92	-1.91	-2.68
AQP7	-0.99	-1.00	-1.28
AQP7	-0.70	-0.47	-1.43
AQP7	-2.33	-3.26	-2.20
BEST3	1.02	0.74	0.96
BEST3	0.15	-0.12	0.15
BEST3	0.05	0.34	0.42
BSND	-0.79	-1.44	-2.06
C5ORF62	-0.20	-0.43	-0.80
CACNA1A	-1.39	-1.50	-1.57
CACNA1A	-0.14	-2.10	-2.37
CACNA1I	0.12	0.06	-0.61
CACNA1I	-0.84	-1.74	-2.07
CACNA1S	-3.19	-1.89	-0.61
CACNA2D2	-1.02	-0.34	-0.67
CACNA2D2	-0.15	-0.58	-0.96
CHRNA5	0.50	0.21	0.46
CHRNA6	-0.22	-0.30	-0.47
CHRNA6	0.53	0.25	0.56
CHRND	-0.42	-1.04	-1.29
CLCC1	0.38	0.37	0.08
CLCN4	-1.11	-0.21	-0.64
CLCN4	-0.91	-1.55	-2.10
CLCN4	0.06	0.07	0.33
CNGA2	0.20	-0.39	-0.56
FXD6	-1.98	-1.45	-2.14
GABRB1	-0.32	-0.84	-0.74
GABRB1	0.56	0.07	0.15
GABRB1	0.00	-0.10	0.15
GABRG2	-0.08	0.12	-0.93

shRNA	Tumor shRNA enrichment		
	M214	M481	M491
GRID2	0.61	0.35	0.82
GRID2	-2.11	-1.88	-1.89
GRIN3A	-0.27	0.01	1.05
GRIN3A	-1.05	-1.76	-2.91
GRINA	-1.66	-3.33	-1.46
GRINA	0.35	0.40	0.89
HTR3C	-0.50	-0.44	-1.45
HVCN1	-0.62	-1.25	-0.63
ITPR2	0.00	0.24	0.21
ITPR2	0.17	0.31	0.52
ITPR2	0.49	0.24	0.54
ITPR2	0.06	-0.59	-0.59
KCNA3	0.34	0.28	0.65
KCNA3	0.63	0.22	0.61
KCNAB3	-0.64	-0.10	-1.18
KCNAB3	0.66	-0.69	0.34
KCNAB3	-1.83	-4.52	-1.83
KCNAB3	-1.82	-2.48	-1.73
KCNB1	0.27	0.26	0.68
KCND2	-1.15	-0.80	-1.24
KCNH2	-0.58	-1.73	-3.08
KCNH2	-1.75	-1.59	-2.19
KCNH7	-0.36	-0.85	-1.82
KCNH7	0.01	0.04	0.17
KCNIP1	0.79	0.29	0.79
KCNIP1	0.21	0.23	0.50
KCNJ13	-1.02	-3.22	-2.72
KCNJ13	0.30	0.03	0.07
KCNJ6	-0.11	-0.31	0.46
KCNK3	0.14	-0.94	-0.91
KCNK3	-2.82	-2.95	-2.87
KCNK3	-0.71	-0.58	-1.36
KCNK6	0.19	0.01	-0.05
KCNK6	-1.97	-4.91	-3.33
KCNK9	-1.01	-1.38	-3.02
KCNMB3	0.16	-0.21	-0.24
KCNMB3	0.04	0.20	0.02
KCNN4	-0.04	0.07	-0.32
KCNS3	-1.17	-0.27	-0.66
KCNS3	-0.56	-1.42	-1.45
KCNU1	1.18	0.35	-0.06
KCNU1	0.95	-0.20	0.51
KCTD15	-2.12	-1.46	-1.27
KCTD15	0.26	-0.39	-0.02
NMUR2	-0.29	-0.13	-0.43
NMUR2	0.31	0.16	-0.67
NMUR2	0.59	-0.26	-0.30
ORAI1	-0.62	-3.05	-0.74
ORAI1	0.12	0.00	0.41
PKD2	-1.14	-1.10	-1.36
SCN1B	-0.83	-0.30	-0.72
SCN5A	-0.14	-0.44	-1.55
SCN5A	-1.55	-1.75	-1.29
SCN5A	-0.65	-0.64	-1.40
SCNN1B	-0.09	-0.17	-0.05
SCNN1B	-0.36	-0.82	-0.95
SCNN1B	1.00	0.46	1.17
TRPC3	0.43	-0.03	-0.72
TRPC3	0.49	0.08	0.25
TRPM3	0.73	0.27	0.59
TRPM5	-0.89	-0.41	-1.30
TRPM5	-0.54	-0.01	-1.01
TTYH3	-1.18	-1.74	-3.43
TTYH3	-1.06	-1.96	-2.75
TTYH3	-0.33	-0.90	-1.32
ABCC9	-0.89	-0.85	-0.69

shRNA	Tumor shRNA enrichment		
	M214	M481	M491
ACCN1	0.05	0.35	-0.09
BEST3	-0.19	-0.08	-0.54
C5ORF62	0.32	0.06	-0.16
CACNA1A	-0.21	-0.18	-0.24
CACNA1I	-0.80	-2.38	-1.12
CACNA1I	-0.08	0.11	-0.02
CACNA1I	-2.61	-4.59	-2.19
CACNA1S	-1.07	-0.95	-1.93
CACNA2D2	-0.29	-1.87	-1.83
CACNG6	-1.10	-2.04	-2.19
CACNG6	-0.65	-1.03	-2.47
CATSPER1	-0.65	-2.26	-1.98
CHRNA5	0.30	0.39	0.35
CHRNA6	-0.55	-0.62	0.03
CHRNA6	-0.20	0.29	0.39
CHRND	-0.67	-0.97	-0.48
CHRNE	-0.92	-4.12	-3.00
CLCC1	-0.11	-0.06	0.03
CLCC1	-1.09	-0.58	-0.06
CLCC1	0.08	-0.25	-0.10
CNGA2	-0.87	-0.48	-0.75
FXYD5	-1.19	-1.60	-1.39
FXYD5	0.19	-1.38	-1.23
FXYD6	-0.36	-0.04	-0.66
GABRA1	0.08	0.29	0.47
GABRA1	-0.34	0.41	0.31
GABRA2	-0.28	-0.10	0.57
GABRA2	0.37	0.23	0.52
GABRB1	-0.87	-0.96	-1.22
GABRB1	-0.07	0.12	0.03
GABRG2	-0.10	0.06	0.06
GPM6A	-0.91	-1.12	-1.83
GPM6A	-0.24	-0.63	-0.29
GRIK5	-0.99	-1.66	-1.23
GRIN1	-0.57	-1.98	-1.45
GRIN3A	-0.39	-0.89	-0.10
GRIN3A	-0.28	-0.20	-0.38
HTR3C	0.37	-0.25	-0.23
HTR3E	-0.20	-1.54	-0.50
HTR3E	-0.39	-0.30	-0.42
ITPR2	-0.08	0.56	0.11
KCNA3	0.21	0.44	0.45
KCNAB1	0.51	0.36	0.51
KCNAB3	-0.77	-0.73	-1.47
KCNB1	0.05	-0.23	0.17
KCNC1	-0.27	0.32	0.05
KCND2	-0.45	-1.22	-1.39
KCNIP1	0.21	-0.18	0.01
KCNJ6	-0.42	-0.46	-0.52
KCNJ6	-0.33	-0.81	-1.43
KCNJ6	-0.06	-1.35	-1.00
KCNJ6	-0.33	-0.35	-0.51
KCNJ8	-0.26	-0.01	-0.53
KCNK10	0.39	0.63	0.51
KCNK10	-0.71	-1.39	-1.03
KCNK3	-0.35	-1.79	-1.81
KCNK6	-1.24	-2.37	-1.02
KCNK9	-1.15	-2.93	-1.60
KCNK9	-0.73	-0.86	-1.43
KCNK9	-1.36	-0.58	-1.43
KCNMB3	-0.38	-0.38	-1.10
KCNMB3	0.17	0.27	0.26
KCNN4	-1.29	-1.54	-1.88
KCNN4	0.37	-0.52	-0.49
KCNN4	0.77	-1.01	-0.81
KCNQ1	-0.74	-1.20	-1.41

shRNA	Tumor shRNA enrichment		
	M214	M481	M491
KCNU1	0.10	0.28	0.40
KCTD15	-1.62	-4.08	-1.16
KCTD20	0.74	-0.13	0.02
KCTD5	0.10	0.29	0.85
KCTD5	-0.51	-1.31	-1.01
MCOLN3	-0.09	0.32	0.37
NMUR2	-0.72	-0.56	-0.39
P2RX3	0.05	0.09	0.17
P2RX3	-1.77	-2.54	-3.03
P2RX3	-0.64	-1.71	-1.14
P2RX4	-0.77	-0.35	-1.28
PKD2	-0.39	-1.60	-0.60
PKD2	-0.02	0.02	-0.17
PKD2L2	-1.06	-1.31	-1.19
PKD2L2	0.49	-0.12	-0.05
SCN1B	-0.61	-0.57	-0.34
SCN2A	0.23	-0.35	-0.28
SCN5A	-0.42	-0.44	-0.39
SCNN1D	0.10	-1.70	-1.74
SLC9A2	0.56	-0.07	-0.10
SLC9A2	-0.72	-2.00	-1.84
SLC9A3	-0.27	-1.25	-0.92
TCTN1	0.11	0.11	-0.08
TNFAIP1	-0.02	-0.04	-0.08
TPCN1	0.20	-0.13	-0.33
TRPC4	0.18	-0.51	-0.76
TRPM5	-1.82	-1.91	-3.07
TRPM5	-0.27	-0.71	-0.47
TRPM5	-0.85	-1.18	-1.42
ACCN2	-0.33	0.11	-1.18
ACCN2	-0.84	0.42	-2.25
ACCN3	-1.15	0.22	-2.18
ACCN3	-0.91	-0.90	-1.95
ACCN3	-3.50	-2.07	-4.56
ACCN3	-1.19	-1.44	-1.57
CACNA1B	-0.32	-0.64	-0.99
CACNA1H	-0.38	-0.33	-1.02
CACNA1H	-0.83	-0.71	-1.87
CACNA1H	0.22	-1.29	-0.55
CACNA1H	0.07	0.71	-0.75
CACNG1	-0.33	-0.70	-1.15
CACNG1	-0.55	-1.79	-3.52
CACNG1	-0.05	-0.67	0.11
CATSPER1	-0.41	-0.05	-1.26
CHRNA7	-0.51	-1.25	-0.77
CHRNA7	0.12	-1.15	-0.18
CLCA2	0.39	0.66	0.40
CLCN5	-0.28	-0.21	-0.60
CLIC1	0.34	0.03	-0.97
CLIC1	0.08	-0.08	-0.48
CNGA3	-1.17	-0.47	-2.00
CNGA3	-0.26	0.02	0.01
CUL5	0.41	-0.06	1.23
CUL5	0.02	0.13	0.81
FXYD5	-0.41	0.02	-0.96
FXYD5	-0.08	-0.42	-0.45
FXYD5	-0.12	-0.71	-0.84
GABRB2	-0.44	-0.05	0.63
GABRG3	0.30	0.71	0.53
GABRG3	0.23	0.09	0.18
GABRG3	-0.72	-0.52	-1.38
GABRG3	0.19	-0.09	0.37
GLRA1	0.23	0.28	-0.47
GLRA1	0.11	-0.37	0.40
GLRA1	0.20	-0.01	0.13
GRIA1	0.01	-0.61	0.50

shRNA	Tumor shRNA enrichment		
	M214	M481	M491
GRIN1	0.01	0.07	-0.62
GRIN1	-2.18	-0.54	-2.29
GRIN3B	-0.71	-0.65	-3.99
GRIN3B	0.09	0.61	0.40
GRIN3B	0.20	0.22	0.52
ITPR3	-1.03	0.24	-3.58
ITPR3	0.04	-0.32	0.33
ITPR3	-0.72	-1.45	-1.93
KCNA4	-0.21	0.75	-0.70
KCNA4	0.24	-0.14	0.06
KCNAB1	0.17	-0.44	-0.27
KCNAB1	-0.12	0.02	-0.12
KCNC1	0.10	-0.13	0.48
KCNC1	0.66	-0.11	0.40
KCNC1	0.04	-0.05	-0.21
KCNC1	-1.26	-0.64	-1.61
KCND3	-0.16	-0.82	-1.92
KCND3	-1.20	-2.13	-1.47
KCND3	0.03	0.09	0.30
KCNG4	-0.43	-0.52	-0.29
KCNG4	-0.79	-0.85	-1.16
KCNJ1	-0.13	-0.16	-0.25
KCNJ1	-0.02	-0.31	0.47
KCNJ1	-0.27	-0.80	-0.42
KCNJ1	-0.32	-1.30	-0.62
KCNJ14	-0.11	0.19	0.56
KCNJ14	0.28	-0.02	0.47
KCNJ14	0.03	0.36	-0.24
KCNK10	-0.26	-0.25	-0.19
KCNK16	0.14	-0.32	-0.05
KCNMB4	0.01	0.36	-0.06
KCNQ1	-0.19	-1.06	-0.78
KCNQ1	0.18	-0.10	0.30
KCTD20	0.19	-0.82	-0.05
KCTD20	0.07	-1.23	-0.56
MCOLN3	-0.34	-0.36	-0.95
P2RX4	-0.86	-0.45	-0.87
PKD1L2	-0.72	1.02	-2.34
PKD2L2	-0.21	-0.18	0.02
SCN2A	-1.34	0.03	-1.03
SCN7A	-1.10	-0.89	-0.89
SCN7A	0.37	-0.21	0.64
SCNN1D	-1.18	-0.28	-1.24
SLC9A3	-3.90	-0.07	-3.87
SLC9A3	-1.12	-0.78	-2.29
TMEM37	-0.24	-0.45	-1.18
TMEM37	-0.43	-0.71	-1.00
TMEM37	0.37	0.28	0.41
TNFAIP1	-0.16	0.20	-0.03
TNFAIP1	-0.64	-0.92	-1.66
TPCN1	0.67	0.45	0.12
TPCN2	-0.68	-0.10	-2.12
TPCN2	0.01	-0.54	-0.54
TRPC4	0.04	-0.24	0.62
TRPC4	0.00	-0.71	0.11
TRPM6	-0.14	-0.12	-0.35
TRPM6	-0.66	-0.48	0.17
TRPM6	0.32	0.15	0.50
TRPV6	-0.20	-0.39	-0.54
ACCN2	-0.10	-0.63	-0.74
CACNA1B	-1.81	-4.13	-1.39
CACNA1B	-0.07	-1.11	-0.29
CACNA1H	-0.10	-0.03	0.59
CACNA2D1	-0.06	0.03	0.66
CACNA2D1	0.34	-0.72	-0.48
CACNG1	-0.80	-3.39	-1.57

shRNA	Tumor shRNA enrichment		
	M214	M481	M491
CATSPER1	-0.75	-1.22	-0.66
CATSPER1	-0.98	-0.71	-1.56
CHRM5	-0.14	-0.09	0.51
CHRNA1	0.00	-0.59	-0.62
CHRNA7	0.14	-0.33	0.15
CHRNA7	-1.32	-2.50	-1.51
CHRNA7	-0.70	-0.89	-1.60
CHRNE	-0.77	-2.00	-2.52
CLCA2	-0.13	-0.29	-0.10
CLCA3P	0.29	0.76	0.98
CLCA4	-0.07	-0.40	-0.32
CLCN5	-1.08	-0.11	0.38
CNGA4	-0.80	-4.83	-2.68
CUL5	0.30	-0.92	-0.11
FXYD2	0.65	-0.03	0.31
FXYD5	0.57	-2.48	-1.29
GABRA2	-0.69	-0.31	-0.70
GABRA2	0.10	-1.37	-0.66
GABRG3	0.09	-1.58	-0.66
GLRA1	0.26	0.36	-0.52
GLRA1	0.15	-0.02	-0.81
GLRA3	-0.08	-0.21	0.66
GRIA1	-0.68	-1.74	-2.02
GRIA3	0.17	-2.95	-1.55
GRIN1	-0.07	-1.46	-0.68
GRIN1	0.91	0.73	-0.62
GRIN3B	-0.90	-4.81	-3.56
ITPR3	-0.63	-1.58	-0.61
KCNA4	0.28	-0.46	-0.31
KCNA4	-1.25	-3.65	-2.51
KCNA5	-0.95	-1.04	-2.22
KCNAB1	-0.73	-1.44	-1.53
KCNC1	-0.16	0.06	0.50
KCND3	-1.27	-1.14	-2.40
KCNE2	0.23	0.73	0.60
KCNG4	-0.76	-2.38	-2.06
KCNG4	0.19	-0.10	0.07
KCNH3	0.29	-0.23	0.04
KCNH3	-0.37	-0.96	-2.21
KCNH4	-1.34	-1.87	-1.50
KCNH4	-0.28	-1.64	-1.15
KCNH4	-0.13	-1.50	-0.59
KCNH4	-0.47	-2.48	-2.85
KCNJ1	-0.05	0.09	0.36
KCNJ15	0.02	-0.10	0.49
KCNJ8	-0.11	-1.49	-0.29
KCNJ9	-0.49	-2.72	-1.29
KCNJ9	-0.63	-3.34	-0.25
KCNK10	-0.29	-2.03	-0.77
KCNK16	-1.14	-3.19	-1.60
KCNK18	0.03	0.06	-0.07
KCNK18	0.08	-0.24	0.57
KCNMA1	-0.60	-1.00	-2.19
KCNMA1	-0.05	0.46	0.63
KCNMA1	-0.45	-0.91	-1.03
KCNMB1	-0.22	-1.56	-2.58
KCNMB4	-0.41	-2.06	-1.43
KCNQ1	0.13	-0.54	-0.18
KCNQ5	-0.07	0.40	0.37
KCNQ5	-0.30	-0.17	0.41
KCNV2	-0.50	-1.90	-0.58
KCNV2	-2.02	-3.34	-1.98
KCNV2	0.60	-2.10	-2.19
KCNV2	-0.18	-0.07	0.64
MCOLN3	-0.58	-0.53	-1.05
MCOLN3	0.31	0.36	-0.07

shRNA	Tumor shRNA enrichment		
	M214	M481	M491
P2RX4	-0.74	-2.30	-1.69
P2RX4	-1.14	-2.36	-0.98
P2RX4	-1.46	-2.30	-2.53
P2RX5	-1.01	-1.10	-1.30
PKD1L2	-0.20	-0.95	-1.24
PKD1L2	-0.13	-0.94	-0.46
PKD2L2	-0.42	-0.62	-1.13
SCN7A	-0.21	-0.26	0.68
SCNN1D	-0.81	-2.29	-1.96
SCNN1G	-0.07	-0.11	0.22
SCNN1G	-0.43	-1.57	-1.40
TMEM37	-0.81	-1.58	-1.60
TMEM37	-0.04	0.37	0.54
TNFAIP1	0.35	-0.46	0.12
TPCN1	0.19	-0.24	0.12
TPCN1	-0.26	-0.11	0.74
TPCN2	-0.19	-1.11	-0.50
TPCN2	-0.63	-0.51	-1.14
TRPC4	-0.94	-2.15	-2.15
TRPM6	-0.82	-1.28	-1.44
TRPV6	0.56	-1.53	-2.04
TRPV6	-0.29	-0.78	-0.32
ABCC8	-0.13	-0.19	-1.01
ACCN5	0.41	0.11	0.52
ACCN5	-0.47	-0.08	-0.23
CACNA1C	-0.95	-2.07	-2.75
CACNA1C	-0.25	-1.70	-2.51
CACNA1G	-0.93	-0.60	-0.62
CHRN1B1	-2.81	-2.81	-3.48
CHRN1B1	-0.98	-2.13	-1.34
CHRNA1G	-2.15	-0.52	-2.74
CHRNA1G	-0.26	-0.42	-0.73
CHRNA1G	-0.84	-0.96	-1.21
CHRNA1G	-0.69	-0.91	-1.54
CLCA1	0.26	0.60	-0.03
CLCA3P	0.32	0.09	0.00
CLCA3P	0.22	-0.30	-0.69
CLCA3P	0.60	0.14	0.47
CLCN6	0.42	0.08	-0.23
CLCN6	0.29	0.07	0.29
CLCN6	-2.55	-1.60	-2.38
CLCN6	-0.02	-0.11	-0.32
CLIC5	-0.93	-1.04	-1.37
CLIC5	0.21	-0.06	-0.15
CLIC5	-0.78	0.03	-0.44
CLIC6	-0.18	0.05	0.11
CNGA4	-0.12	-1.33	-1.33
ELK1	-2.60	-2.25	-2.17
FXYD2	0.65	0.50	0.45
FXYD2	-0.91	-0.72	-0.93
FXYD4	-2.06	-2.72	-2.37
GABRA3	-0.21	0.42	0.04
GABRB3	-0.48	-0.80	-1.15
GABRB3	-0.43	-0.23	-0.49
GABRB3	-0.17	-0.09	0.29
GABRP	-0.53	-0.29	-1.09
GABRQ	0.78	0.84	0.45
GABRQ	0.03	0.08	0.13
GLRA2	-0.51	-0.04	0.26
GLRA2	-0.05	0.12	0.23
GLRA2	1.01	0.57	0.56
GLRA3	0.68	0.71	1.05
GLRA3	0.14	-0.04	0.16
GLRA3	0.77	0.56	0.32
GLRA4	0.75	0.21	-0.43
GLRA4	0.18	-0.14	-0.64

shRNA	Tumor shRNA enrichment		
	M214	M481	M491
GRIA2	-0.25	0.05	-0.25
GRIA2	-0.53	-0.59	-1.24
GRIK1	-0.07	-0.13	0.05
HCN2	0.23	0.02	-0.56
HCN2	-1.18	-0.78	-1.35
HCN4	-0.11	-0.33	-0.08
KCNA5	-0.42	0.07	0.68
KCNB2	-0.98	0.14	0.68
KCNC2	-0.14	0.27	0.65
KCNE1	-1.46	-1.27	-1.29
KCNE1	-0.32	0.02	0.11
KCNE3	0.44	0.18	-0.16
KCNE3	-0.31	0.01	0.61
KCNE3	-0.29	-0.06	0.13
KCNH3	-1.17	-1.78	-3.20
KCNH5	0.41	0.32	0.13
KCNJ2	-0.05	-0.14	-0.05
KCNJ2	-0.42	-0.34	-0.50
KCNJ9	-1.28	-0.96	-1.68
KCNK15	0.19	0.00	-0.30
KCNK15	-2.44	-1.04	-2.61
KCNK15	-2.09	-1.75	-2.86
KCNK15	-2.58	-1.88	-1.94
KCNK15	-4.01	-3.16	-3.37
KCNMB1	-1.70	-0.49	-1.54
KCNMB2	-0.76	-0.31	-0.11
KCNQ2	-0.28	-1.89	-1.96
KCNQ2	-1.03	-0.81	-1.91
KCNQ4	-1.35	-1.22	-3.02
KCNQ5	-1.51	-1.55	-1.08
KCNQ5	0.81	0.93	0.29
KCTD3	0.73	-0.20	-0.05
TRPA1	-0.60	-0.33	-0.67
P2RX2	0.60	0.16	-0.04
P2RX2	-0.82	0.21	0.22
P2RX2	-0.93	-1.78	-2.30
P2RX5	-0.34	-0.19	-0.49
P2RX5	-1.89	-2.26	-2.88
P2RX5	-1.23	-1.11	-1.57
P2RX5	0.49	-0.01	-0.31
SCN2B	-0.49	0.11	-0.77
SCN2B	0.07	-0.55	-0.17
SCN8A	-0.34	0.16	0.68
SCNN1G	-0.88	0.10	0.51
SCNN1G	0.84	0.20	0.12
TRPA1	-0.42	-0.71	-1.04
TRPA1	-0.86	0.15	-0.64
TRPC5	0.24	-0.01	-0.43
TRPM1	-0.97	-1.51	-1.83
TRPV2	0.50	0.43	0.32
TRPV2	-1.05	-1.71	-1.07
TRPV4	0.09	0.22	-0.65
ANXA7	-0.60	0.13	-0.67
ANXA7	0.32	-0.40	-0.64
BTBD10	0.49	-0.32	0.25
CACNA1G	-2.37	-0.14	-2.43
CACNA1G	-0.48	-1.27	-0.91
CACNG4	-0.15	-1.11	-0.46
CACNG7	-0.82	-1.75	-2.87
CACNG7	-0.28	-0.63	-1.31
CHRNA4	-0.90	0.43	-0.42
CHRNA9	0.40	-0.21	0.55
CHRNA9	0.75	0.35	0.81
CHRNA1	-0.53	0.13	-0.42
CHRNA4	0.21	0.30	0.43
CHRNA4	-0.38	-0.82	-1.04

shRNA	Tumor shRNA enrichment		
	M214	M481	M491
CHRNA4	-0.40	0.11	-1.24
CHRNA4	-1.16	-2.97	-1.70
CHRNA4	-0.37	-0.96	-0.31
CLCA1	-0.39	-0.05	0.06
CLCN3	0.48	0.24	0.29
CLCN3	-0.20	-0.29	-0.32
CLCNKB	-0.36	-0.72	-0.76
CLIC3	0.19	-0.08	0.02
CLIC6	-0.95	-1.27	-1.55
CNGA4	-0.42	-0.44	-0.08
FXYD7	-0.31	-0.89	-1.20
FXYD7	-0.59	-1.13	-1.57
GABRA3	-0.34	-0.83	-1.36
GABRB3	-0.92	-1.21	-0.74
GABRG1	0.07	-0.18	0.64
GABRP	0.14	-0.02	0.46
GABRQ	-0.79	-1.34	-1.32
GLRA2	-0.10	-0.03	0.37
GLRA4	0.12	-0.16	-0.01
GRID1	-1.40	-0.83	-1.17
GRIK4	0.12	-0.23	-1.06
GRIN1	-1.72	-0.67	-1.08
HCN2	-0.22	-0.27	-0.33
HCN4	-0.49	-0.32	-0.44
HCN4	0.02	0.14	-0.38
ITPR1	0.29	-0.13	0.27
ITPR1	-0.99	-1.74	-0.72
KCNA10	-1.26	-2.04	-1.18
KCNA10	-0.21	-0.41	-0.18
KCNC2	0.25	0.02	0.72
KCNC2	0.24	0.18	0.44
KCND1	-1.25	-1.78	-2.32
KCND1	0.19	0.01	-0.02
KCNE2	0.06	0.18	0.00
KCNH1	-1.91	-1.92	-0.76
KCNH1	-0.35	-0.50	-0.60
KCNH6	-1.46	-1.56	-2.60
KCNIP2	-0.52	0.30	0.72
KCNJ15	0.34	0.60	0.67
KCNJ2	-0.79	-1.30	-0.44
KCNJ5	-1.73	-2.57	-1.61
KCNJ5	-0.66	-0.61	-0.95
KCNJ9	-1.19	-1.11	-2.00
KCNK12	-2.54	-2.76	-1.08
KCNK2	0.66	0.28	0.11
KCNK5	0.35	-0.27	-0.35
KCNK5	0.00	0.20	0.68
KCNMB1	-0.21	-1.13	-0.56
KCNMB2	-0.10	0.46	0.37
KCNN3	0.26	0.26	0.68
KCNQ2	-1.60	-1.84	-1.12
KCNQ2	-0.88	-0.21	-0.58
KCNQ4	-0.60	-0.59	0.02
KCNRG	-0.34	-0.49	-0.44
KCNS2	0.15	0.49	-0.21
KCNS2	-0.89	0.08	-0.80
KCTD12	-0.49	-0.44	-0.80
KCTD3	-0.09	0.19	-0.28
MLC1	0.08	0.25	0.59
MLC1	-0.18	-2.03	-1.71
MS4A2	0.23	-0.04	-0.03
NALCN	0.38	-0.33	0.21
NALCN	0.43	-0.05	0.27
NOX1	-0.43	-0.07	-0.05
P2RX1	-1.24	-1.51	-2.90
P2RX1	-0.95	-0.78	-1.25

shRNA	Tumor shRNA enrichment		
	M214	M481	M491
SCN1A	-0.90	-0.55	-1.06
SCN2B	0.37	0.54	0.11
SCN4B	-1.61	-0.81	-1.55
SCN8A	0.13	0.24	-0.36
SCNN1A	0.46	0.55	0.96
SCNN1A	-1.29	-2.85	-0.54
SHROOM2	-0.63	-2.08	-1.49
TRPC1	0.15	-0.07	0.10
TRPC1	-1.00	-0.14	-1.00
TRPM1	0.72	0.70	0.26
TRPM1	0.71	0.62	0.64
TRPV2	0.27	-1.00	-1.48
TRPV2	-0.32	-0.96	-0.56
TRPV3	0.85	0.86	0.84
TRPV3	-2.05	-2.98	-1.30
ACCN4	0.13	-1.25	0.15
ACCN4	-0.77	-1.74	-1.84
ANXA7	0.01	-0.43	-0.29
BTBD10	0.01	-0.34	-0.95
CACNA1F	-0.39	-1.84	-1.68
CACNA1F	-0.49	-1.26	-1.90
CACNA1F	-0.62	-1.10	-1.80
CACNB3	0.50	-0.39	-0.90
CACNB3	-1.41	-2.33	-3.28
CACNB3	-0.23	0.31	-0.24
CACNB3	0.07	-0.43	-0.26
CACNG4	-0.28	0.02	-0.15
CACNG4	0.35	-0.19	-0.60
CACNG7	-1.04	-1.11	-0.91
CACNG7	0.27	0.07	0.43
CATSPER2	-0.03	0.09	-0.08
CATSPER2	-0.97	-2.84	-1.67
CHRNA4	-0.66	-3.19	-2.63
CHRNA4	-0.04	-0.15	-1.15
CLCN3	0.16	-0.46	-0.70
CLCNKB	-0.74	-1.77	-1.62
CLCNKB	-1.63	-2.82	-1.33
CNGA1	0.09	-0.13	-0.30
CNGA1	-0.03	-0.81	-0.48
CNGA1	-0.97	-0.83	-1.38
CNGA1	-0.20	-0.11	-0.14
FXYD7	-1.71	-1.09	-2.20
FXYD7	0.31	0.13	0.65
GABRA6	-0.30	-0.18	-1.26
GAR1	-0.21	0.47	0.47
GRID1	0.85	0.03	0.96
GRIK4	0.63	-0.68	-1.76
GRIN2D	-0.82	-1.92	-2.31
GRIN2D	-2.13	-0.93	-1.55
GRIN2D	0.00	0.24	0.10
HCN3	-0.32	-1.27	-1.38
HCN3	-1.27	-1.13	-1.46
HTR3B	-0.48	-0.38	-0.45
KCNA2	0.01	0.21	0.59
KCNA2	-0.30	-0.60	-1.02
KCND1	-0.84	-0.45	-0.48
KCNH1	0.26	-0.57	-0.49
KCNH1	-1.17	-1.40	-1.33
KCNH6	-0.85	-0.31	-0.85
KCNH6	0.59	-0.28	-0.51
KCNH6	-0.41	-2.04	-2.14
KCNIP2	-0.77	-0.23	-1.74
KCNIP2	-0.32	-2.15	-2.15
KCNIP2	-0.15	0.05	-0.91
KCNJ12	-2.91	-3.61	-4.22
KCNJ12	-0.33	-0.02	-0.49

shRNA	Tumor shRNA enrichment		
	M214	M481	M491
KCNJ5	-0.95	-2.00	-2.65
KCNJ5	-0.28	0.18	0.18
KCNK2	-0.12	0.20	0.40
KCNK5	-1.01	-2.82	-2.56
KCNK5	0.53	0.42	0.80
KCNN3	-1.33	-1.07	-1.30
KCNRG	-0.13	0.42	0.46
KCNRG	-0.21	-0.04	0.31
KCNRG	-0.73	-1.06	-1.15
KCNRG	0.01	0.37	-0.01
KCTD6	-0.39	0.18	0.21
MLC1	-1.67	-2.74	-2.33
MLC1	0.32	-0.73	-1.32
MS4A2	-0.07	0.20	0.77
MS4A2	0.33	-0.76	-0.63
MS4A2	-0.16	0.59	0.19
MS4A2	0.18	-0.19	-0.25
MS4A2	-0.31	-0.19	-0.46
NALCN	0.49	-0.21	-0.37
P2RX1	0.12	-0.68	-0.47
PKD1	-2.02	-1.52	-1.86
PKD1	-0.52	-0.64	-0.44
PKD2L1	-0.14	0.35	0.26
PKD2L1	-0.87	-1.08	-1.49
PKDREJ	0.06	0.26	1.23
PKDREJ	-0.15	0.08	0.17
RYR3	-0.23	0.02	-0.09
RYR3	-0.39	-0.45	0.13
RYR3	0.30	0.47	0.86
SCN1A	0.13	0.09	-0.02
SCN1A	0.40	-0.08	-0.34
SHROOM2	-0.06	-0.23	-0.03
SLC9A1	0.52	0.07	0.05
SLC9A1	-1.06	-4.59	-2.46
SLC9A1	-1.38	-2.63	-2.83
SLC9A1	0.89	0.02	0.13
SLC9A1	0.19	0.43	0.86
TRPC1	-0.53	-0.63	-1.28
TRPC1	-0.20	-0.13	-0.18
TRPC1	0.16	-0.09	0.13
TRPV3	0.42	0.17	0.76
TSPO	-0.75	-2.22	-2.52
TSPO	0.02	-0.86	-1.04
TSPO	-0.92	-2.28	-2.73
VDAC3	0.34	0.21	0.57
ABCC8	0.08	0.38	0.48
ABCC9	-0.30	0.10	-0.19
ACCN4	-1.65	-3.58	-2.18
ACCN5	-0.11	0.32	-0.17
CACNA1C	-0.76	-0.57	-0.81
CACNB4	-0.10	0.33	0.25
CACNB4	0.65	-0.03	0.41
CACNG3	0.42	0.19	0.38
CACNG8	-0.42	-3.13	-1.34
CACNG8	-1.44	-1.30	-2.11
CATSPER2	-0.22	-1.20	0.00
CATSPER4	-0.56	-1.21	-0.65
CATSPER4	-0.03	-0.64	-1.21
CHRNA1	-0.18	-0.58	-1.28
CHRNA1	-0.15	-0.03	-0.01
CHRNA4	-1.24	-0.22	-2.20
CHRNA9	0.52	-0.12	0.22
CHRNA9	0.07	-0.26	0.03
CLCA4	0.09	-0.11	-0.55
CLCA4	-0.62	-0.13	-0.10
CLCA4	-0.24	0.24	0.27

shRNA	Tumor shRNA enrichment		
	M214	M481	M491
CLCN3	0.29	0.12	-0.10
CLCN5	-0.70	0.03	-0.25
CLIC3	-0.12	-0.41	-0.35
CLIC3	-0.98	-1.09	-0.79
CLIC3	-2.07	-2.40	-4.23
CLIC6	0.07	0.29	0.46
CNGA3	-1.41	-1.73	-1.08
CNGA1	-0.25	-0.21	0.05
CNGA3	-2.74	-3.44	-1.54
CNGA3	-0.68	0.15	-0.17
CNGB3	0.01	0.05	0.14
FXYD4	-1.18	-0.33	-1.83
FXYD4	-2.01	-3.15	-2.96
GABRA6	-0.06	-0.15	-0.31
GABRP	-0.58	-0.73	-1.04
GABRR3	-0.10	-0.93	0.10
GAR1	-0.44	-0.16	0.15
GRIA2	0.07	-0.30	-0.59
GRIA3	-0.19	-0.14	0.21
GRIA3	-0.38	-0.53	-1.11
GRID1	-0.97	-2.77	-2.37
GRIK4	-2.19	-1.46	-2.14
HCN3	-0.10	-2.70	-2.42
ITPR1	0.42	0.06	0.25
KCNA1	-0.31	0.04	-0.31
KCNA10	0.08	-0.37	-0.02
KCNA2	-0.34	-0.38	-0.85
KCNA7	-1.58	-2.08	-4.48
KCNB2	-0.34	-1.04	-2.32
KCNE2	-0.24	-0.64	-0.20
KCNH2	-1.14	-1.82	-1.40
KCNH6	-1.02	-0.99	-1.10
KCNIP2	-1.27	-2.27	-1.79
KCNIP2	0.69	0.32	0.35
KCNK1	-0.03	-0.48	-0.46
KCNK18	-0.29	0.47	-0.09
KCNK4	-1.51	-4.29	-2.23
KCNK4	-0.59	-1.29	-1.50
KCNMB2	0.09	-0.48	0.19
KCNMB2	-0.22	-0.59	-0.66
KCNN3	-0.42	-0.60	-0.36
KCNRG	-0.01	-0.18	-0.09
KCNS2	0.13	0.30	0.63
KCNT2	0.10	0.13	0.11
KCTD2	-2.79	-1.94	-2.42
KCTD3	-0.03	-0.32	-0.52
KCTD6	0.15	-0.44	0.17
KCTD6	-0.05	0.11	0.48
KCTD7	-1.95	-2.05	-1.49
MCOLN2	-0.17	-0.73	-0.38
MCOLN2	-0.60	-2.11	-1.42
MCOLN2	-0.78	-0.07	-0.45
NOX1	-0.21	0.04	-0.02
P2RX1	-1.39	-1.52	-2.09
P2RX7	0.02	-0.35	0.17
PKD1	-0.90	-1.67	-1.50
PKD2L1	-0.11	-0.52	-0.34
PKD2L1	0.29	0.39	0.58
RYR3	-0.15	-0.24	-0.56
SCN2A	-0.21	0.16	0.52
SCN3A	0.75	-1.20	0.00
SCN4B	-0.35	-0.36	-1.09
SCN8A	-0.05	-0.41	-0.41
SCNN1A	-0.19	-0.20	-1.33
SLC9A2	0.18	-0.01	0.13
TRPC5	-0.84	-1.48	-0.82

shRNA	Tumor shRNA enrichment		
	M214	M481	M491
TRPC5	-0.03	0.21	-0.13
TRPC7	-0.03	-0.04	-0.30
TRPC7	-0.25	-0.61	-0.28
TRPM4	0.04	0.10	-0.07
TRPM4	-0.65	-0.88	-0.26
TRPV3	0.66	-0.20	0.17
VDAC3	0.26	-0.15	-0.37
VDAC3	0.57	0.34	0.21
ABCC8	0.59	-0.07	-0.30
ABCC8	-0.23	-0.30	0.61
ABCC9	-0.42	-1.36	-1.28
BEST3	-0.01	-0.28	1.15
CACNA1C	-0.51	0.65	-1.21
CACNA2D2	-1.12	-2.46	-1.78
CACNA2D3	-1.63	-0.76	-2.40
CACNB4	-0.03	-0.97	-1.54
CACNG3	0.14	0.40	0.95
CATSPER2	-0.28	-0.64	-1.12
CATSPER2	0.93	0.17	0.98
CATSPER4	0.05	0.08	0.10
CHRNA1	-0.27	-0.13	-0.85
CHRNA9	0.90	-0.26	0.14
CLCA2	0.72	0.27	-0.47
CLCA2	0.38	-0.13	-0.23
CLCN1	0.02	-0.04	-0.34
CLCNKB	-0.95	-0.06	-2.12
CLIC3	-0.64	-0.01	0.48
CLIC6	-0.46	-0.14	-0.53
CLNS1A	0.07	0.31	-0.95
CNGB3	-0.93	-0.66	-1.25
CNGB3	-0.21	-0.86	-1.62
FXYD1	0.35	-0.14	-1.25
FXYD1	-0.69	-0.65	-1.94
FXYD4	-0.39	-3.11	-3.96
FXYD4	-0.12	-0.33	-0.04
GABRB2	0.44	-1.65	-1.80
GABRB2	-0.85	-1.53	-1.99
GABRR3	-0.43	-0.14	-0.83
GABRR3	-1.45	-2.66	-2.99
GAR1	0.32	0.21	0.80
GPM6A	-0.97	0.09	-0.44
GPM6A	0.30	0.31	0.37
GRIA3	-0.13	-0.20	0.35
GRIA3	-0.41	0.40	0.47
GRIA3	0.41	-0.07	1.19
GRIA3	-0.15	-1.19	-0.99
GRIK1	-1.82	-0.01	-2.42
GRIK1	-0.36	-1.13	-1.74
GRIN2A	0.11	-0.53	-0.97
GRIN2A	-1.54	-2.11	-2.81
GRIN2A	0.03	0.30	0.91
GRIN2A	0.02	-0.88	-1.96
KCNA1	-0.71	-0.34	-1.66
KCNA5	-1.11	-1.84	-3.90
KCNA5	0.00	0.18	0.76
KCNA5	-0.53	-0.51	0.35
KCNA7	-0.39	-0.05	0.02
KCNA7	-1.71	-0.48	-5.22
KCND2	-0.70	-2.04	-1.37
KCNE1	-0.84	-1.35	-1.94
KCNE3	-0.08	0.47	1.46
KCNG1	-2.58	-3.39	-4.80
KCNH1	0.31	0.06	1.18
KCNH2	-0.35	-0.63	-0.89
KCNH2	-0.53	0.62	1.76
KCNH5	-0.32	0.30	-0.83

shRNA	Tumor shRNA enrichment		
	M214	M481	M491
KCNH6	-2.63	-1.82	-3.29
KCNH7	-1.10	-1.13	-1.23
KCNJ12	-2.42	-2.91	-2.85
KCNJ2	-0.39	0.92	-0.76
KCNJ8	-0.35	-0.41	-0.16
KCNK1	-1.11	-2.18	-3.27
KCNK12	0.03	-0.13	-0.76
KCNK18	-0.20	-0.48	-0.42
KCNK4	-1.62	-1.39	-3.88
KCNMB2	0.24	0.24	0.11
KCNS2	-0.54	-0.62	-0.18
KCNT2	-1.47	-1.64	-1.60
KCNT2	-0.06	-0.02	0.72
KCTD12	-1.60	-4.81	-1.78
KCTD3	-0.31	-0.47	-1.45
KCTD4	-0.71	-0.27	-1.42
KCTD4	0.06	0.22	1.60
KCTD4	0.41	0.12	0.25
PKDREJ	0.24	0.41	0.21
RYR1	-0.47	-0.19	-1.63
RYR1	-0.88	-0.80	-2.32
SCN2A	-0.20	-0.19	1.60
SCN3A	-1.74	-3.01	-3.51
SCN3B	0.44	-0.08	-2.90
SCN3B	-0.91	-2.80	-2.41
SCN3B	0.33	-0.20	0.30
SCN8A	-0.42	-0.06	0.07
SHROOM2	-0.97	-1.36	-1.39
SLC9A2	-0.22	-0.20	0.97
STRC	0.26	-0.59	-1.22
TPTE	0.64	0.30	0.69
TRPC3	-0.28	0.24	-0.09
TRPC3	-0.78	-0.10	0.42
TRPC6	-2.24	-1.73	-2.16
TRPC6	0.08	0.07	0.97
TRPM4	-1.08	-1.83	-2.20
TRPV3	-1.47	-3.06	-5.05
VDAC3	0.03	1.04	0.04
ACCN2	-0.64	-0.39	-0.35
ANXA7	-1.13	-0.61	-1.41
CACNA1A	-1.53	-2.70	-1.01
CACNA1C	-0.22	0.03	0.24
CACNA1E	-0.08	0.18	0.56
CACNA1E	-0.25	-0.93	-1.07
CACNA1H	0.13	0.34	0.09
CACNA2D1	-0.63	-0.61	-0.78
CATSPER2	0.08	0.13	-0.22
CHRNA1	-1.41	-0.97	-2.08
CHRNA1	0.09	-0.26	0.03
CLCA1	-0.07	0.14	-0.34
CLCA1	-0.99	-1.12	-0.88
CLCA4	0.09	0.10	0.15
CLCC1	-0.23	-0.22	-0.27
CLCC1	-0.06	0.32	0.22
CLCN2	-1.24	0.06	-0.94
CLCN5	-0.29	0.43	-0.38
CLCN6	-0.14	0.17	-0.07
CLIC1	-0.42	-0.02	0.43
CLIC3	-0.25	-4.13	-2.35
CNGA2	-2.72	-3.43	-3.67
CNGA3	0.75	0.43	0.20
CUL5	0.22	0.37	0.27
FXYD3	-0.93	-1.11	-0.66
GABRA3	0.03	-0.34	-0.68
GABRA5	-1.14	-3.43	-0.60
GABRB2	-1.09	-0.76	-0.29

shRNA	Tumor shRNA enrichment		
	M214	M481	M491
GABRB3	-0.39	-0.04	-0.62
GABRE	-1.01	-2.49	-0.80
GABRP	0.08	-0.05	-0.34
GABRQ	-0.16	-0.32	-0.09
GABRR1	-1.83	-0.76	-0.79
GLRA1	0.40	0.01	0.40
GPM6A	0.11	0.08	0.52
GRIA2	0.55	-0.34	0.62
GRIA3	-0.23	0.53	0.30
GRIA3	-1.53	-0.93	-1.68
GRID2	-0.02	-0.07	0.28
GRIK1	-0.40	0.50	0.39
GRIK1	-0.42	-0.88	-1.20
GRIK3	-0.60	-0.90	-0.81
GRIN3B	-1.06	-1.85	-1.80
HCN3	-0.94	-2.13	-1.42
HCN4	-0.50	0.20	0.09
SCN1A	-0.93	0.12	-0.30
HTR3A	-1.76	-2.83	-1.75
ITPR1	-0.69	-0.33	-0.09
ITPR2	0.24	-0.03	-0.39
ITPR2	-0.18	0.00	-0.07
ITPR2	0.18	-0.27	0.00
KCNA10	-0.41	-0.67	-0.28
KCNA4	0.58	-0.15	-0.09
KCNC1	-0.26	0.00	0.16
KCNC1	-1.24	-1.67	-1.53
KCND2	-1.17	-0.55	-0.99
KCND2	-1.28	-1.52	-0.92
KCND3	-0.36	-1.88	-1.62
KCNE1L	0.54	0.22	0.74
KCNE3	0.39	-0.09	0.28
KCNE4	0.08	-0.23	-0.47
KCNH2	-0.52	-1.36	-0.64
KCNH6	-0.43	-1.19	-1.24
KCNJ6	-0.22	-0.15	-0.17
KCNK4	-0.90	-0.70	-0.57
KCNK4	-0.77	-2.21	-1.04
KCNMA1	-0.52	-1.20	-0.57
KCNMB2	0.15	0.25	0.11
KCNN3	-0.54	-0.37	-0.79
KCNS1	-0.57	0.02	-0.15
KCNS3	-0.29	0.43	0.07
KCTD14	-1.23	-0.13	-1.72
MLC1	-0.01	0.23	0.13
NUDT9	0.25	0.52	0.08
P2RX7	-0.67	-1.35	-3.17
PKDREJ	0.35	0.58	0.27
PKDREJ	0.29	0.46	0.48
RYR3	0.31	-1.05	-0.92
SCN3A	-0.68	-0.56	-0.78
SCN4A	-0.42	-2.02	-1.83
SCN7A	0.19	0.22	0.34
SCN7A	0.24	0.13	-0.21
SCN7A	0.32	0.31	0.57
SHROOM2	-0.57	0.41	-1.23
TPCN1	-0.14	-0.55	-0.39
TPCN2	-0.39	-0.41	-0.37
TPTE	-0.19	-0.51	0.02
TRPC4	0.06	0.09	0.64
TRPC5	-0.02	-0.09	0.30
TRPC6	0.31	0.39	-0.07
TRPC6	-0.16	0.31	0.30
TRPM1	-0.78	-0.42	-0.84
TRPV1	-0.56	-0.11	-0.07
TRPV1	-0.30	-2.12	-1.50

shRNA	Tumor shRNA enrichment		
	M214	M481	M491
TTYH1	-0.01	-0.14	-0.54
VDAC2	0.18	0.19	0.07
ABCC8	-0.49	-1.37	-2.91
ACCN1	-1.22	-0.54	-0.65
ACCN4	0.00	0.21	0.49
ACCN4	-1.54	-0.54	-1.30
BEST3	-0.17	0.13	-0.62
BTBD10	0.06	0.12	0.27
CACNA1E	-1.04	-2.13	-3.07
CACNA1I	-0.07	0.25	-0.17
CACNB1	-0.23	0.19	-0.85
CACNB3	-0.80	-0.64	-1.29
CACNG6	-0.35	-0.64	-0.05
CATSPER2	-0.82	-1.40	-1.96
CATSPER3	-1.23	-2.27	-2.11
CATSPER3	-0.16	0.13	0.13
CCT8L2	0.46	0.04	-0.03
CHRNA6	0.17	0.53	-0.05
CLCA1	0.57	0.04	0.40
CLCN3	-0.33	-0.26	-0.82
CLCN5	-0.43	-0.98	-1.34
CNGA1	0.56	-0.86	-0.42
CNGA2	-0.33	-1.71	-2.09
CUL5	0.76	0.34	0.57
FXYD2	-0.97	-0.87	-0.43
FXYD3	0.04	0.02	0.31
GABRA4	0.20	0.39	0.46
GABRB2	-0.86	-0.87	-0.93
GABRG1	0.41	-0.42	-0.23
GABRQ	-0.59	-0.45	-0.95
GABRR1	-0.84	-0.93	-0.58
GABRR2	-0.10	-0.46	-0.55
GLRB	-0.06	-0.57	-0.38
GRIA1	-0.05	0.19	-0.41
GRIK4	-0.52	-0.51	-0.99
GRIN2A	-0.66	-0.75	-0.54
GRIN2B	-1.20	-0.78	-1.82
GRIN2B	2.51	-4.04	-1.73
GRIN2D	-1.43	-0.40	-0.93
GRIN3A	0.10	-0.36	-0.32
GRIN3A	-0.23	0.42	-0.11
GRM7	-0.10	0.66	0.34
HTR3E	-0.99	-1.03	-1.02
HTR3E	-0.40	-0.11	-0.57
ITPR1	-1.20	-0.96	-0.38
ITPR2	-0.75	-1.20	-2.11
ITPR3	0.09	-0.88	-1.07
KCNA1	0.68	-0.02	0.45
KCNA2	-0.39	-1.54	-1.20
KCNA4	-0.87	-1.17	-0.77
KCNA4	0.34	0.23	0.34
KCNA5	-0.57	-3.08	-2.38
KCNA5	-0.45	-0.04	-0.37
KCNA6	-0.84	-0.93	0.17
KCNAB3	-1.26	-3.55	0.15
KCNC1	-0.42	-1.21	-1.08
KCNC3	-0.60	-0.80	-1.32
KCNG2	-0.58	0.06	-0.93
KCNG3	-1.06	-1.76	-1.26
KCNH1	0.28	-0.16	-0.07
KCNIP1	-0.39	-1.53	-1.47
KCNJ10	0.26	-0.91	-1.44
KCNJ13	-0.03	-1.51	-0.49
KCNJ14	-0.77	-0.67	-1.51
KCNJ2	0.26	0.19	-0.19
KCNK13	-0.66	-1.45	-1.82

shRNA	Tumor shRNA enrichment		
	M214	M481	M491
KCNK9	-0.88	-1.42	-0.24
KCNMB4	-0.33	-0.35	-0.82
KCNQ4	0.15	0.79	0.19
KCNS1	-0.68	-0.60	-1.13
KCNS2	-1.08	-0.96	-0.94
KCNV1	-0.62	0.26	0.09
KCTD10	0.00	-0.93	-0.79
KCTD10	-0.10	-0.85	-0.87
KCTD12	-0.24	0.12	0.49
KCTD12	-1.00	-1.17	-1.81
KCTD14	0.23	0.39	-0.34
KCTD20	-0.80	-0.67	-1.38
FXYD5	-0.06	0.39	0.14
NMUR2	-0.85	-0.24	-1.22
NMUR2	-0.39	-0.40	0.46
P2RX3	-0.18	0.09	-0.49
PKD2L2	-0.07	0.37	0.32
SCN10A	-0.31	-0.70	-0.55
SCN11A	-0.22	-0.58	1.09
SCN3B	-0.30	-0.15	-0.74
SCN8A	0.96	0.66	0.26
SCN9A	0.17	0.35	-0.16
SCNN1A	-1.05	-1.23	0.18
SHROOM2	-0.85	-0.03	-0.52
TRPC5	-0.06	0.00	-0.01
TRPC7	0.29	0.28	0.21
TRPM1	0.06	0.54	-1.01
TRPM2	-0.04	-0.68	0.39
TRPM3	-0.27	-0.02	-1.54
VDAC2	-0.50	0.42	-0.01
ACCN3	-0.07	0.37	-0.29
AQP7	-2.09	-2.03	-0.51
AVEN	-0.30	-1.11	-1.44
AVEN	-0.70	-0.03	0.16
CACNA1F	-0.73	-1.00	-1.53
CACNA1S	0.19	-0.04	0.46
CACNA2D2	-0.13	-0.29	-0.15
CACNG3	-0.26	-0.16	0.32
CACNG6	0.35	0.49	0.64
CATSPER2	-0.10	0.08	0.41
CHRNA3	-0.19	-0.04	-0.40
CHRNA3	-0.56	0.26	-0.61
CLCA1	0.00	0.26	-0.02
CLCA2	0.44	0.05	0.72
CLCA2	0.13	0.12	0.34
CLCA4	0.93	-0.23	-0.15
CLCN2	-0.26	-0.90	-1.23
CLCN3	-1.00	-0.62	-1.06
CLCN3	-0.40	-1.00	-0.09
CLCN6	0.62	0.14	0.09
CLIC1	-1.66	-0.83	-2.38
CLIC6	0.10	-0.43	-0.11
CLNS1A	-0.30	-1.94	-0.95
CNGA1	-0.33	-0.70	-0.81
CNGA3	-1.42	-2.36	-0.86
CNGB3	0.36	0.30	-0.22
ELK1	0.35	-0.58	0.15
GABRA1	0.04	0.43	-0.41
GABRA2	-0.20	0.29	0.12
GABRA4	-0.13	0.48	0.39
GABRE	-0.05	0.34	0.14
GABRG1	-0.18	-1.16	-0.87
GABRG3	0.04	0.16	-0.19
GABRR3	0.08	-0.49	-0.84
GLRA2	-0.05	0.02	0.68
GLRA3	-0.49	-2.22	-0.36

shRNA	Tumor shRNA enrichment		
	M214	M481	M491
GRIA1	-1.16	-0.51	-0.73
GRIA4	0.08	-0.46	-0.59
GRIK2	0.04	-0.30	-0.31
GRIK3	-1.19	-2.90	-3.03
GRIN2C	-0.97	-0.65	-0.52
HCN4	-0.64	-0.27	-0.19
HTR3E	0.09	0.18	-0.08
ITPR1	0.08	0.06	-0.23
KCNA10	-0.81	-1.15	-1.95
KCNA10	-1.35	-3.30	-2.84
KCNA2	-0.09	-2.39	-1.27
KCNA3	-0.30	-0.27	0.05
KCNA4	0.24	-1.19	-1.63
KCNA5	-0.22	-1.27	-1.26
KCNAB3	-0.88	-2.83	-1.45
KCNC2	-0.45	-1.21	-0.69
KCND2	-0.23	-0.34	-0.98
KCND3	-1.08	-2.74	-2.34
KCNE2	-0.51	-3.68	-1.76
KCNF1	-0.35	-0.32	-0.23
KCNG3	-0.39	-1.99	-1.43
KCNH4	-0.63	-1.74	-1.45
KCNH8	-0.29	0.30	-0.42
KCNJ10	0.13	0.30	0.86
KCNJ9	-0.01	-0.04	-0.11
KCNK13	0.27	0.56	0.05
KCNK13	-0.23	-1.32	-1.13
KCNMA1	0.17	-0.01	-0.54
KCNMA1	-0.37	-0.17	0.00
KCNMB1	0.05	0.44	0.92
KCNMB2	-0.72	-1.28	-1.15
KCNN2	0.32	0.35	0.41
KCNN4	0.50	-1.39	-0.79
KCNQ4	-1.57	-0.31	-1.17
KCNV2	-0.83	-0.85	-1.22
KCTD20	0.14	-0.17	0.17
KCTD3	0.12	-0.41	0.05
KCTD6	0.13	0.44	-0.46
MCOLN3	0.03	0.17	0.80
MS4A2	-0.30	-0.75	-0.78
PKD1L2	-0.12	-0.47	-0.28
RYR1	-0.89	-0.86	-1.50
SCN1A	-0.89	0.26	-1.75
SCN1A	0.31	0.35	0.43
SCN9A	-0.40	-0.51	-0.35
SCNN1G	-0.82	-3.62	-2.43
STX1B	-0.21	-0.15	0.59
TOMM40	-1.53	0.34	-0.63
TPCN2	-1.91	-1.73	-1.17
TRPC3	-0.25	-0.08	-0.93
TRPC4	0.01	0.33	0.27
TRPC4	-0.75	-1.87	-0.69
TRPM3	0.26	-0.16	0.15
TRPM3	-0.56	-0.15	-1.58
TRPM4	-0.07	-0.36	-0.27
TRPM6	0.41	-0.51	-2.18
TRPM6	-0.71	-0.12	-0.73
TRPM8	0.82	-0.42	-0.69
TRPV2	-0.61	-0.80	-1.13
TRPV6	-0.03	-0.09	-0.57
ABCC9	1.12	0.57	1.08
ANXA7	-0.06	0.27	0.14
CACNA1B	-1.14	-2.57	-2.74
CACNA1C	-1.43	-1.95	-2.49
CACNA1E	-0.74	-2.42	-1.60
CACNA1E	-2.04	-1.45	-1.36

shRNA	Tumor shRNA enrichment		
	M214	M481	M491
CACNA1G	-0.99	-3.58	-3.07
CACNB2	-0.68	0.13	-0.85
CACNG1	-0.34	0.26	-0.13
CACNG7	-0.53	-0.16	-0.69
CACNG8	-2.74	-3.03	-2.63
CCT8L2	-2.37	-1.89	-2.61
CFTR	-0.50	-0.11	-0.14
CHRM5	0.05	-0.09	-0.04
CHRN2	-1.70	-2.53	-2.74
CLCC1	-1.23	-0.61	-1.18
CLCN4	-0.75	-1.83	-1.36
CLCN5	0.93	0.60	0.38
CLIC3	-0.40	0.48	0.04
CLIC4	1.07	0.40	0.73
CLIC6	-2.99	-0.58	-2.09
CNGB1	-2.25	-2.20	-1.56
GABRA1	0.42	0.26	0.31
GABRA2	-0.82	-0.51	-0.93
GABRA3	0.41	0.05	-0.03
GABRA6	-0.13	-0.53	0.26
GABRB1	0.58	0.69	0.31
GABRG1	-1.40	-0.97	-0.26
GABRG2	-0.22	-0.65	-1.02
GLRA3	-0.07	-0.30	-0.26
GRID1	-1.15	-0.54	-1.12
GRID2	-0.30	0.03	-0.61
GRIK2	1.20	0.57	0.52
GRIK3	0.52	0.18	0.44
GRIN2D	-0.73	-0.97	-1.53
HCN4	-0.81	-2.94	-2.22
HTR3B	-0.03	-0.16	0.18
HTR3B	-0.25	-0.33	0.33
ITPR1	-0.69	-0.89	-0.88
KCNA1	-0.17	-0.57	-1.31
KCNA2	-0.57	-1.19	-1.53
KCNB2	-1.16	0.16	-0.91
KCNC1	-1.57	-1.75	-1.53
KCNC3	-0.47	-0.40	-0.59
KCNE3	-0.05	0.08	0.45
KCNG3	-0.81	-0.56	-0.76
KCNG4	-1.95	-4.34	-2.49
KCNH1	0.91	0.08	0.14
KCNH1	-0.04	-0.93	-0.16
KCNH5	-0.81	-0.67	-0.54
KCNH7	0.29	0.32	0.45
KCNH7	-1.87	-0.98	-1.90
KCNH8	-0.52	-0.55	-0.62
KCNJ13	1.46	0.29	1.06
KCNJ16	-0.59	-0.23	0.29
KCNJ16	0.95	0.58	0.84
KCNJ5	-0.19	0.11	-0.38
KCNJ9	-1.91	-0.91	-1.03
KCNK15	-1.06	-3.34	-2.19
KCNK3	-0.37	0.20	-1.05
KCNK9	1.06	-0.22	0.25
KCNMB3	-1.44	-0.18	-1.69
KCNQ3	-0.06	-0.07	-0.29
KCNQ5	0.35	0.59	0.25
KCNS2	-1.14	-0.82	-1.46
KCNS3	0.17	0.92	0.33
KCNT1	-0.13	0.03	-0.24
KCNV1	-0.09	0.03	-0.26
KCNV1	-0.05	0.08	-0.09
KCNV1	0.41	0.17	0.35
KCTD10	-0.03	-0.10	-0.06
KCTD12	-0.20	-0.46	-0.27

shRNA	Tumor shRNA enrichment		
	M214	M481	M491
KCTD14	-0.33	-0.50	-0.43
KCTD3	-1.03	-0.35	-0.32
KCTD5	-0.15	-0.17	-0.30
MCOLN3	-2.52	-2.22	-2.10
NALCN	-1.25	-0.94	-1.75
NMUR2	0.64	0.32	0.11
PKD2	-0.12	0.03	0.16
PKD2	-0.02	-0.31	-0.16
PKD2	-1.50	-1.84	-2.39
SCN1A	-1.01	-2.72	-0.98
SCN1B	-0.78	-1.51	-1.53
SCN2A	-0.36	0.25	0.21
SCN4B	-0.64	-0.31	-0.31
SCN5A	0.17	-0.19	-0.18
SCNN1G	-0.11	0.55	-0.16
SCNN1G	-1.49	-0.29	-1.00
TPCN2	-1.17	-0.87	-1.66
TPTE	0.54	0.15	0.21
TPTE	0.47	0.10	0.23
TRPC3	-0.45	0.22	-0.20
TRPC5	-1.96	-2.70	-1.58
TRPM7	-1.19	-0.69	-1.13
TRPV6	-1.38	-1.75	-2.01
ACCN5	-0.12	0.05	0.00
CACNA1E	0.02	0.08	0.12
CACNA1G	-1.86	-0.44	-1.75
CACNA1H	-0.88	-0.76	-1.30
CACNA2D3	-0.82	-1.45	-1.16
CACNB4	-0.92	-0.74	-0.60
CACNG2	-0.58	-0.22	-0.57
CACNG3	-1.10	-1.01	-0.83
CHRNA9	0.41	0.06	0.32
CHRNA9	-0.64	-0.80	-1.98
CLCA1	-0.53	0.02	-0.12
CLCA2	-1.33	-1.02	-1.16
CLCN2	-0.41	-0.92	-0.85
CLCN6	-0.89	-0.23	-0.95
CLIC4	1.09	0.46	0.93
CLIC5	-1.10	-0.71	-0.47
CLIC6	-0.68	-0.37	-0.96
CNGB1	0.42	0.34	0.17
CNGB3	-1.14	-1.00	-1.47
CUL5	-0.91	-0.80	-0.48
FXYD4	-1.09	-1.38	-1.46
FXYD7	-0.11	-0.47	0.13
GABRA4	-0.93	-1.92	-1.33
GABRA6	-0.45	0.09	-0.23
GABRB2	-1.03	-0.52	-0.74
GABRG2	-0.15	0.09	-0.31
GABRQ	-0.45	0.08	0.40
GABRR3	-0.35	0.29	-0.10
GLRB	-0.99	-0.44	-0.58
GRIA2	-0.85	-0.36	-0.76
GRIA3	-2.35	-1.32	-1.71
GRIN2B	-1.31	-2.51	-1.08
HCN1	-0.03	-0.38	-0.73
HCN3	-1.66	-3.25	-2.04
HTR3C	0.46	-0.15	0.00
HVCN1	-1.59	-0.84	-0.88
KCNA2	-0.70	-0.43	-0.01
KCNA2	0.69	-0.36	-0.29
KCNA3	-0.40	-1.03	-0.39
KCNC2	-0.82	-1.71	-1.84
KCND2	-0.13	-0.45	-0.87
KCNE1L	0.73	0.48	0.05
KCNG3	0.59	0.32	0.07

shRNA	Tumor shRNA enrichment		
	M214	M481	M491
KCNG3	0.67	-0.04	0.69
KCNH8	-2.55	-1.89	-3.35
KCNJ1	0.01	-0.21	0.07
KCNJ14	0.55	0.24	0.14
KCNJ16	0.78	0.36	0.50
KCNJ3	-0.65	-0.62	-0.67
KCNJ6	-0.72	-1.59	-0.95
KCNJ6	-0.53	-0.42	-0.63
KCNK1	0.63	0.37	0.51
KCNK1	0.02	-0.06	-0.59
KCNK12	0.64	-0.04	0.01
KCNK2	0.79	0.25	0.08
KCNK5	-1.61	-1.06	-1.05
KCNK6	-2.21	-2.55	-1.99
KCNMA1	-1.33	-0.58	-1.07
KCNMA1	-0.69	-0.30	-0.38
KCNMB1	0.00	0.09	-0.51
KCNMB3	0.55	0.12	0.82
KCNN1	-1.80	-1.27	-1.56
KCNQ1	-0.93	-0.80	-0.43
KCNQ1	-0.72	-0.61	-0.23
KCNQ2	-2.05	-1.07	-1.39
KCNQ3	-0.75	-0.51	-0.64
KCNQ4	-2.98	-2.61	-1.75
KCNRG	-0.16	0.10	-0.41
KCNS2	-1.89	-0.56	-1.03
KCTD12	0.11	-0.70	-0.07
KCTD7	-0.64	-0.63	-1.04
KCTD7	-1.76	-0.49	-1.36
MCOLN3	0.03	-0.57	-0.16
NOX5	-1.58	-0.88	-1.10
P2RX2	-1.46	-1.60	-0.88
P2RX2	-1.22	-1.56	0.00
P2RX6	0.40	-0.29	0.17
PKDREJ	-0.42	-0.05	0.00
RYR1	-0.80	-1.79	-1.78
RYR1	-1.87	-1.84	-1.63
RYR2	0.61	0.25	0.65
SCN11A	-2.64	-1.44	-2.76
SCN3B	-0.61	-0.42	-1.27
SCN8A	0.98	0.50	0.09
SCN9A	-2.52	-1.67	-2.76
SCNN1A	-0.29	-0.27	-0.52
SLC9A2	0.89	0.46	0.63
TNFAIP1	0.54	0.52	-0.02
TPCN1	-1.12	-1.49	-0.70
TPCN1	1.07	0.50	0.41
TRPC4	0.24	0.27	0.14
TRPC4	0.21	0.00	-0.03
TRPV1	0.59	0.05	0.22
TRPV1	0.30	0.54	0.47
TRPV2	-0.47	-0.81	-1.29
CACNA1G	-0.18	-0.32	-0.85
CACNA1G	0.30	-0.08	-0.37
CACNA2D1	-0.10	-0.18	-0.81
CACNA2D3	-0.04	-0.35	-0.35
CACNG4	-0.14	-0.19	-0.28
CACNG4	-0.23	0.29	0.13
CATSPER2	-0.05	-0.16	-0.24
CHRNA2	-0.32	-0.81	-0.90
CLCN5	-0.64	-1.00	-2.07
CLCN6	-0.50	-0.57	-0.32
CNGA1	0.25	-0.34	-0.23
VDAC2	-0.82	0.24	-0.47
CUL5	0.86	0.21	0.80
FXYD2	-0.01	-0.32	-0.31

shRNA	Tumor shRNA enrichment		
	M214	M481	M491
FXYD3	-0.74	-1.07	-1.97
FXYD6	-0.42	-1.37	-1.37
GABRP	-1.31	-1.01	-1.66
GABRR2	0.42	-0.24	0.38
GAR1	-0.60	-0.24	-1.17
GRIK2	0.29	-0.15	0.40
GRIN2A	-2.53	-1.66	-2.63
HCN1	0.57	-0.19	-0.55
HCN1	-0.98	-0.74	-1.47
HCN2	-0.83	-1.42	-1.25
ITPR2	-0.11	0.76	-1.25
KCNB2	-0.32	-0.52	-0.52
KCNE3	0.27	-0.36	0.31
KCNG4	-1.65	-2.46	-3.69
KCNH5	0.13	-0.26	0.19
KCNIP2	-2.24	-2.16	-2.50
KCNJ11	-0.75	-0.89	-1.74
KCNJ3	0.48	0.27	0.34
KCNK18	0.22	0.16	0.32
KCNK3	-0.29	-0.38	0.12
KCNMB1	-0.98	-0.18	-1.51
KCNMB1	-2.04	-1.21	-2.57
KCNN2	-0.01	0.26	0.50
KCNQ1	-0.82	-0.35	-2.03
KCNQ5	-0.26	-0.53	-1.35
KCNT1	-0.75	0.06	-1.23
KCTD15	0.09	-0.33	-0.11
KCTD3	-0.56	-1.53	-0.83
KCTD6	-0.51	-1.55	-2.37
MS4A2	0.23	0.50	0.64
P2RX2	-0.17	-0.47	-0.72
PKD1L2	-1.45	-1.18	-1.84
PKD2L2	-0.09	-0.40	-0.32
PKD2L2	0.14	-0.03	0.01
SCN8A	-0.31	0.03	-1.31
SCNN1A	-0.60	-1.01	-0.86
TNFAIP1	-1.00	-0.35	-0.97
TPCN1	0.26	0.03	0.14
TRPA1	-0.03	-0.44	-0.26
TRPC1	-0.24	-0.60	-0.81
TRPC6	-0.40	0.29	0.18
TRPC6	-0.66	-0.60	-1.13
TRPC7	-1.05	-1.24	-1.84
TRPM2	-1.72	-1.74	-2.75
TRPM3	-0.82	-0.48	-1.40
TRPM7	-0.98	-1.53	-2.05
TRPM8	-0.11	-0.35	-0.79
TSPO	-0.48	-0.33	-0.64
TTYH1	-1.01	-1.23	-1.23
ATP13A4	0.09	0.07	0.26
ATP13A4	0.29	0.29	0.00
ATP1A1	0.72	-0.10	0.32
ATP1A4	0.15	0.06	0.06
ATP1A4	-1.16	-0.65	-1.29
ATP1A4	-0.57	-0.27	-0.76
ATP1B2	-0.81	-0.06	-0.81
ATP2A1	0.59	0.07	0.14
ATP2A1	-0.79	0.01	-0.03
ATP2A2	-0.25	-0.36	-0.47
ATP2A2	0.07	-0.56	-0.76
ATP2A2	0.92	-0.03	0.27
ATP2A2	0.87	-0.06	0.85
ATP2B1	-0.71	0.10	0.09
ATP2B4	-1.14	-0.44	-0.80
ATP2C2	0.91	0.02	0.15
ATP2C2	0.35	0.23	0.60

shRNA	Tumor shRNA enrichment		
	M214	M481	M491
ATP2C2	-0.70	-0.47	-0.39
ATP4A	0.00	0.01	0.25
ATP4A	-0.43	-0.17	-0.54
ATP4A	-1.64	-1.03	-2.61
ATP4A	-1.01	-1.21	-1.27
ATP5C1	-0.48	-0.92	-1.03
ATP5G3	-0.02	0.42	0.12
ATP5G3	0.73	0.12	0.33
ATP6V0D1	-2.12	-1.39	-3.89
ATP6V0D1	-1.98	-2.76	-2.20
ATP6V0E1	-0.28	-0.05	-0.12
ATP6V1C2	0.51	0.49	-0.02
ATP6V1C2	-0.46	0.00	-0.09
ATP6V1G1	-0.94	-0.05	-1.05
ATP7A	-0.51	-0.46	-1.11
ATP7A	-0.44	-0.28	-0.86
SLC10A1	-0.76	-0.88	-1.13
SLC10A1	-2.14	-2.23	-1.65
SLC10A1	-0.30	0.10	-0.34
SLC10A2	0.11	0.30	0.46
SLC11A2	-1.48	-0.94	-1.08
SLC12A6	-0.34	0.00	-0.91
SLC13A1	0.66	0.02	0.31
SLC13A4	-1.39	-3.59	-2.21
SLC13A5	-1.44	-1.53	-2.32
SLC13A5	-0.15	-0.57	-1.20
SLC17A3	-0.14	0.29	0.46
SLC20A1	-0.27	-0.40	-0.78
SLC20A1	-0.08	0.28	-0.05
SLC22A12	-2.09	-2.59	-1.93
SLC22A12	-2.15	-0.52	-2.40
SLC22A2	-0.70	0.20	-0.58
SLC22A4	0.17	0.23	0.18
SLC22A8	-0.34	-0.25	-0.38
SLC24A2	0.03	-0.17	0.03
SLC24A2	-0.03	0.12	0.23
SLC24A2	-1.40	-0.64	-1.00
SLC24A2	0.28	-0.12	-0.50
SLC26A10	0.01	0.03	0.21
SLC26A10	-2.79	-2.82	-1.58
SLC26A3	0.88	0.39	0.01
SLC26A3	-1.41	-0.64	-0.30
SLC26A4	-0.43	-0.60	-1.09
SLC26A5	-1.44	-0.87	-0.60
SLC26A5	0.50	0.64	0.26
SLC26A5	-0.12	-0.35	-0.60
SLC26A9	-1.41	1.16	-2.68
SLC30A2	-1.41	-2.45	-2.88
SLC30A2	0.48	0.21	1.02
SLC30A2	-1.04	-0.25	-1.63
SLC31A1	-0.92	-0.68	-0.65
SLC36A1	0.26	-0.02	0.52
SLC36A1	-1.00	-0.53	-0.24
SLC36A2	-0.22	0.44	-0.17
SLC36A2	-2.39	-1.32	-3.03
SLC36A3	-1.16	-0.80	-0.38
SLC39A1	-0.37	-0.87	0.09
SLC41A1	-1.44	-0.82	-1.12
SLC4A10	-2.13	-0.80	-1.31
SLC4A3	-1.17	-0.84	-1.23
SLC4A3	-2.66	-1.08	-1.78
SLC4A3	-1.37	-1.90	-1.87
SLC4A4	0.07	-0.04	0.19
SLC4A5	0.31	0.36	0.22
SLC4A5	-0.77	-0.15	-0.35
SLC5A10	-0.54	0.19	-0.12

shRNA	Tumor shRNA enrichment		
	M214	M481	M491
SLC5A12	-1.08	-0.77	-1.31
SLC5A4	0.58	0.06	0.23
SLC5A7	-0.14	-0.51	-0.12
SLC8A1	-0.08	0.12	0.22
SLC8A3	0.09	-0.42	-0.09
SLC8A3	-1.57	-0.66	-1.64
SLC8A3	0.09	0.19	0.11
SLC9A6	0.24	0.01	0.00
SLCO1C1	-0.50	0.30	-0.03
SLCO2B1	-1.03	-0.25	-1.17
TCIRG1	-1.34	-2.80	-1.93
UCP2	-0.53	-0.41	0.17
UCP2	-0.44	-0.13	-1.09
ATP13A1	-1.25	-1.04	-1.72
ATP13A2	-1.63	-2.73	-2.00
ATP13A2	0.04	-0.19	0.66
ATP13A3	0.04	-0.32	0.11
ATP13A3	-0.27	-0.41	0.07
ATP13A3	-0.58	-0.42	-0.05
ATP1A2	-1.63	-0.64	-1.41
ATP1A3	0.05	0.30	-0.07
ATP1B1	0.46	0.45	0.50
ATP1B4	0.11	0.12	0.33
ATP2B1	0.45	-0.02	-0.44
ATP2B1	0.13	-0.39	-0.45
ATP2B2	-1.23	-1.09	-1.55
ATP2B2	-0.15	-0.89	-1.09
ATP2B2	-1.79	-0.83	-0.26
ATP2B2	-0.77	-0.83	-1.91
ATP2B2	-0.23	-0.29	-0.80
ATP2B3	-0.16	-0.18	-0.59
ATP2B3	-0.33	-0.40	-0.34
ATP2B3	0.48	0.18	0.04
ATP2C1	-0.40	-0.34	-0.96
ATP2C1	-0.71	-0.72	0.03
ATP2C1	-0.52	-0.85	-0.09
ATP2C1	0.20	-0.67	-0.45
ATP4B	-0.51	-0.57	-1.12
ATP4B	-0.30	-0.20	-0.45
ATP5A1	-0.26	-0.84	-0.89
ATP5E	-0.28	-1.48	-0.57
ATP5G2	-0.63	-2.57	-2.55
ATP5O	-0.47	-0.17	-1.38
ATP6V0A1	-0.30	-0.60	-0.65
ATP6V0D2	0.44	0.26	-0.11
ATP6V1B1	-1.28	-1.22	-1.66
ATP6V1B1	-1.09	-0.83	-1.06
ATP6V1B2	0.12	0.15	0.08
ATP6V1E1	0.20	-0.48	0.95
ATP6V1G2	-2.89	-2.08	-2.93
ATP6V1H	-0.99	-1.03	-0.69
SLC11A1	-0.82	-0.13	-0.53
SLC11A1	-1.03	-0.99	-1.60
SLC12A3	-0.67	-1.14	-1.07
SLC12A5	-1.06	-4.54	-2.23
SLC12A9	-1.40	-1.51	-0.82
SLC17A3	0.10	-0.36	0.24
SLC20A2	-1.46	-1.55	-2.76
SLC22A11	0.15	0.08	-0.26
SLC22A18	-1.51	-1.33	-1.61
SLC22A18	-0.29	-0.54	-1.30
SLC22A18	-0.08	-0.03	0.07
SLC22A25	-0.52	-0.82	-0.83
SLC22A5	0.25	0.27	-0.15
SLC22A5	-0.96	-1.21	-1.24
SLC22A6	-0.34	-0.44	-0.71

shRNA	Tumor shRNA enrichment		
	M214	M481	M491
SLC22A6	-1.02	-1.34	-1.49
SLC22A7	-0.19	-0.53	0.21
SLC22A7	-0.38	-1.82	-1.12
SLC22A8	-0.54	-0.92	-0.14
SLC22A9	0.09	0.16	0.02
SLC22A9	0.23	-0.34	-0.09
SLC24A1	-0.10	-0.39	0.28
SLC24A1	0.46	-0.12	0.40
SLC30A3	-2.29	-2.34	-2.10
SLC30A3	-0.76	-1.03	0.17
SLC30A7	0.42	0.12	-0.04
SLC31A1	-0.29	-0.22	-0.04
SLC31A2	-0.57	-0.18	0.22
SLC34A1	-0.19	-0.09	0.14
SLC34A1	-1.22	-2.14	-3.94
SLC34A2	-0.26	0.40	-0.35
SLC34A2	0.21	-0.48	0.35
SLC34A3	-0.96	-0.84	-0.80
SLC39A2	0.12	-0.58	-0.07
SLC39A3	-0.91	-2.14	-1.60
SLC39A4	-1.65	-2.93	-2.91
SLC39A4	-0.66	-1.93	-1.38
SLC39A4	-1.09	-1.92	-1.20
SLC41A3	-0.69	-1.40	-0.94
SLC41A3	0.46	0.56	0.30
SLC4A2	-1.31	-1.89	-1.94
SLC4A2	-0.37	-0.81	-0.96
SLC4A2	-0.73	-0.13	0.03
SLC4A9	-1.42	-1.13	-1.59
SLC5A2	-0.91	-1.20	-0.04
SLC5A2	-2.08	-3.51	-2.45
SLC5A6	-0.89	-0.19	-0.53
SLC8A2	-0.09	-0.36	0.36
SLC8A2	-0.41	-1.42	-0.31
SLC8A2	-4.61	-2.20	-2.78
SLC9A5	-1.04	-0.39	-0.94
SLCO1B1	0.78	0.47	0.42
SLCO2A1	-0.73	0.34	-1.71
SLCO5A1	-1.14	-1.36	-0.01
SLCO6A1	-0.28	-0.35	-0.21
UCP1	-0.01	-0.53	0.59
UCP1	0.16	0.22	-0.03
UCP1	-1.86	-1.45	-1.55
ATP13A1	-0.01	-0.06	-0.30
ATP1B1	0.47	0.02	0.20
ATP1B1	0.21	0.35	0.42
ATP1B4	-0.74	-2.92	-3.02
ATP1B4	-0.11	-0.06	0.39
ATP2A2	0.65	0.11	-0.05
ATP2C2	-0.58	-1.32	-0.46
ATP4B	-0.55	-2.27	-1.44
ATP5D	-1.88	-1.23	-3.87
ATP5D	0.09	-0.64	-1.00
ATP5D	-0.61	-1.08	-2.29
ATP5E	0.11	0.03	-0.08
ATP5F1	-0.13	0.07	-0.05
ATP5H	-0.56	-0.48	-0.83
ATP5J2	-0.06	-0.12	-0.21
ATP5J2	0.05	-0.40	0.42
ATP5L	-0.53	-0.64	-0.86
ATP5L	0.61	0.27	-0.66
ATP5L	-1.13	-0.19	-3.06
ATP6V0B	-0.19	-0.19	-0.89
ATP6V0B	0.60	0.14	0.40
ATP6V0B	-0.75	0.19	-0.16
ATP6V0C	-0.83	-0.87	-1.17

shRNA	Tumor shRNA enrichment		
	M214	M481	M491
ATP6V0C	-1.40	-0.24	-0.89
ATP6V0C	-1.99	-1.82	-2.57
ATP6V0D2	0.12	0.08	0.46
ATP6V0E2	-0.98	-1.78	-1.93
ATP6V0E2	0.06	0.17	0.29
ATP6V0E2	-0.01	-0.18	0.04
SLC10A3	-0.82	-0.27	0.38
SLC10A3	-0.50	-0.50	-0.63
SLC10A5	-0.12	0.13	0.32
SLC10A6	-0.06	-0.27	1.06
SLC10A6	-0.17	-0.70	-0.83
SLC12A3	0.01	0.23	-0.27
SLC12A8	-0.10	-0.63	-0.72
SLC12A8	-0.49	-0.79	-1.20
SLC17A2	-0.54	-0.84	-1.05
SLC20A2	-0.76	-0.29	-0.35
SLC22A14	-1.57	-1.36	-1.94
SLC22A16	-0.16	0.05	-0.03
SLC22A2	-0.35	0.11	-0.37
SLC22A20	-0.03	-0.68	-0.48
SLC22A20	-1.08	-1.58	-1.95
SLC22A20	-0.62	-0.81	-2.51
SLC22A6	-0.20	-1.56	-1.50
SLC24A5	0.21	-0.27	0.02
SLC25A28	-0.25	-0.68	-1.34
SLC26A1	-1.03	-1.22	-1.45
SLC26A1	-1.77	-2.53	-1.59
SLC26A1	-0.49	-0.26	0.09
SLC26A6	-0.45	-1.53	-0.78
SLC26A9	-0.07	-0.04	0.35
SLC30A3	-1.05	-1.30	-2.15
SLC30A7	-0.55	-0.64	-0.18
SLC39A1	-0.30	-0.82	-0.52
Slc39a10	-0.14	-0.46	-0.13
SLC39A11	0.39	0.04	0.14
SLC39A11	-0.64	-0.96	-1.10
SLC39A13	-0.22	-0.44	-1.70
SLC39A13	-0.54	-1.95	-1.19
SLC39A13	0.04	0.35	-0.43
SLC39A14	-0.05	0.05	-1.09
SLC39A14	-0.74	-2.02	-2.54
SLC39A3	-1.24	-2.31	-2.42
SLC39A5	-1.63	-4.55	-1.49
SLC39A5	-1.19	-2.13	-2.73
SLC39A5	-1.79	-1.29	-1.01
SLC39A6	0.19	-0.03	0.27
SLC39A6	0.32	0.26	0.11
SLC4A11	-0.63	-2.11	-2.08
SLC5A2	-0.74	-0.42	-0.74
SLC5A3	0.03	-0.50	-0.36
SLC5A3	-0.73	-1.05	-1.68
SLC5A4	-0.08	-0.48	-0.21
SLC5A8	0.31	0.24	0.36
SLC5A9	-0.82	-2.12	-3.13
SLC5A9	0.10	-0.03	0.28
SLC8B1	-1.74	-1.49	-2.67
SLC8B1	-0.18	-0.80	-1.35
SLC9A4	-0.13	-0.24	0.07
SLC9A4	0.18	0.23	0.07
SLC9A7	-1.59	-0.55	-1.90
SLC9A8	-1.04	-0.85	-1.76
SLC9B1	0.08	0.26	0.45
SLC9B2	-0.13	-0.31	-0.10
SLC9B2	-0.44	-0.42	-0.86
SLC9B2	-0.21	-0.11	-0.60
SLC9C1	-0.55	-0.75	-0.76

shRNA	Tumor shRNA enrichment		
	M214	M481	M491
SLC9C1	0.28	0.29	0.19
SLC9C2	0.38	0.31	0.59
SLCO1B7	-0.27	0.15	0.52
SLCO1B7	0.16	0.11	-0.04
SLCO1B7	-0.07	-0.23	-0.12
SLCO1C1	-0.23	-0.17	-0.47
ATP5J2	-0.62	-1.53	-1.61
SLC17A2	-0.45	0.15	-0.58
SLC4A11	-0.46	-2.26	-1.36
SLC8B1	-0.72	-0.65	0.31
SLC9B1	-0.38	-0.06	-0.80
SLC9B1	-0.89	0.24	-0.46
SLC9C1	0.15	-0.50	-0.51
SLC9C2	0.02	-0.65	-0.03
SLC9C2	0.10	-1.73	-2.54
ATP12A	0.18	-0.57	0.34
ATP12A	-0.17	0.15	0.39
ATP13A2	0.12	-0.64	-1.23
ATP1A1	0.47	0.37	0.34
ATP1A3	0.14	-0.22	-0.43
ATP1B3	-0.27	-1.68	-0.39
ATP1B3	-0.11	-1.80	-1.41
ATP2A2	-0.35	-1.04	-0.98
ATP2A3	-0.58	-2.90	-0.93
ATP2B1	-0.33	-0.76	-0.42
ATP2C1	-0.22	-1.38	-1.12
ATP4B	-1.79	-2.75	-3.89
ATP5C1	0.73	-0.10	-0.66
ATP5H	-0.24	-0.48	-0.76
ATP5J	-0.40	-0.34	-0.44
ATP5O	0.22	-0.09	-0.24
ATP6V1C1	0.11	-0.01	-0.05
ATP6V1C1	0.10	0.05	-0.23
ATP6V1C1	0.11	0.64	-0.20
ATP6V1C2	0.23	0.02	0.00
ATP6V1D	0.25	0.07	0.30
ATP6V1E1	-0.23	-0.18	-0.32
ATP6V1F	-0.54	0.04	-0.03
ATP6V1G1	0.24	-0.46	-1.00
ATP6V1G2	0.38	-0.05	0.13
ATP6V1G2	0.17	0.16	0.02
ATP6V1H	0.12	0.14	0.16
ATP7B	-0.36	-1.19	-0.92
ATP7B	0.34	-0.48	-0.24
SLC10A3	0.62	0.50	0.15
SLC10A5	0.17	0.42	0.29
SLC10A7	0.55	-0.99	-0.90
SLC10A7	-0.45	0.09	0.36
SLC12A2	-0.07	-0.72	0.18
SLC12A2	0.16	-1.50	-1.03
SLC12A4	0.09	-0.11	-0.05
SLC12A5	0.18	-0.16	-0.12
SLC13A3	0.19	-1.35	-1.87
SLC13A3	0.19	-1.09	-1.20
SLC22A10	0.11	-0.43	-0.29
SLC22A10	0.13	-0.01	-0.34
SLC22A13	0.15	0.10	-0.51
SLC22A14	-0.34	-0.25	-0.50
SLC22A15	-0.04	0.43	0.22
SLC22A17	0.14	-0.01	0.08
SLC22A24	-1.30	-2.30	-2.53
SLC22A3	-0.26	0.12	-0.20
SLC22A4	-0.14	-1.11	-1.23
SLC22A9	-0.85	-1.34	-1.21
SLC24A2	-1.80	-1.42	-1.02
SLC24A3	0.44	-0.09	-0.08

shRNA	Tumor shRNA enrichment		
	M214	M481	M491
SLC24A4	-0.45	0.09	0.45
SLC24A5	-0.16	-0.06	0.23
SLC26A10	0.07	0.19	0.21
SLC26A11	-0.14	-0.62	-0.10
SLC26A4	0.07	0.14	0.52
SLC30A1	-0.16	-0.29	0.80
SLC30A4	-0.20	0.18	0.26
SLC30A4	-0.18	-0.10	-0.51
SLC30A5	-1.52	-2.02	-1.28
SLC30A8	-0.03	-1.27	-1.94
SLC31A2	-0.71	-2.09	-1.51
SLC34A3	0.30	-0.92	-1.21
SLC36A2	-1.37	-0.61	-0.38
SLC36A4	0.00	-0.05	-0.25
SLC36A4	-0.04	-0.70	-0.27
SLC39A10	-0.83	-1.85	0.51
SLC39A12	-0.02	-0.04	0.04
SLC39A7	-0.65	-1.71	-2.40
SLC41A3	0.51	0.10	0.26
SLC4A5	0.03	-0.50	-0.66
SLC4A7	-0.53	-2.38	-2.52
SLC5A10	-0.21	-0.27	-0.87
SLC5A10	-0.21	-1.80	-1.19
SLC5A11	-0.27	-0.71	-1.60
SLC5A12	0.35	-0.30	-0.44
SLC5A1	0.13	-0.58	-0.59
SLC5A1	-0.38	-1.66	-0.85
SLC5A5	-0.19	-0.45	-1.28
SLC5A6	-0.02	-1.06	-1.29
SLC8A1	0.08	-0.21	-1.42
SLC9A2	-0.34	-1.31	-0.80
SLC9A6	0.04	-0.10	-0.07
SLC9A6	0.09	0.12	0.36
SLC9A7	-0.10	-0.58	-0.84
SLCO3A1	-0.01	0.39	0.39
SLCO4A1	-0.09	-0.62	-0.54
SLCO4A1	-0.08	-0.20	-0.18
SLCO4A1	-0.74	-2.63	-1.48
SLCO6A1	-0.28	0.29	0.12
SLCO6A1	0.23	-0.23	-0.35
TCIRG1	0.25	-1.41	-2.27
UCP2	-0.55	0.46	-0.26
ATP1B2	-0.10	-0.56	0.08
ATP1B2	-0.09	-0.82	-0.16
ATP2A3	-0.99	-1.52	-1.09
ATP2B3	-0.32	-0.48	-0.68
ATP2B4	-0.31	0.31	0.38
ATP2B4	-0.19	-0.36	-1.39
ATP4A	-0.63	-0.86	-0.21
ATP5A1	-1.14	-1.44	-1.30
ATP5A1	-0.13	-1.06	-3.23
ATP5B	0.50	0.18	0.14
ATP5G2	-0.59	-1.05	-1.56
ATP5H	-0.04	0.04	-0.02
ATP5I	-0.62	-0.71	-0.15
ATP5I	-0.28	-1.11	-1.15
ATP6V0A1	-0.58	-0.18	0.01
ATP6V0A2	-0.03	-0.21	0.24
ATP6V0A4	-0.80	-0.59	-1.15
ATP6V0D2	0.48	-0.49	-0.22
ATP6V0E1	-0.01	-0.39	-0.10
ATP6V1A	-0.14	-0.19	-0.06
ATP6V1B1	0.32	-1.18	-1.69
ATP6V1D	-0.71	-1.30	-0.54
ATP6V1D	-0.56	-0.95	-0.46
ATP6V1E2	0.37	-0.40	-0.32

shRNA	Tumor shRNA enrichment		
	M214	M481	M491
ATP6V1E2	0.13	-1.31	-0.65
ATP6V1F	-0.30	-0.42	-0.20
SLC10A4	-0.55	-0.59	-0.71
SLC10A5	-0.23	0.44	0.29
SLC10A7	-0.31	-0.83	-0.68
SLC12A1	-0.31	0.23	0.28
SLC12A5	-0.07	-1.13	-0.62
SLC12A7	-0.13	0.30	0.03
SLC12A7	-0.09	-0.07	-1.10
SLC12A8	-1.24	-1.97	-1.34
SLC12A9	-1.23	-1.56	-1.66
SLC13A1	-0.21	-0.64	-1.08
SLC13A1	0.23	0.37	0.37
SLC13A2	0.12	0.01	0.36
SLC13A3	0.01	0.25	0.50
SLC13A4	-0.62	-1.26	-0.88
SLC20A1	-0.63	-1.05	-1.47
SLC22A1	0.44	0.03	-1.04
SLC22A14	0.11	-1.25	-3.28
SLC22A15	-0.35	0.36	-1.21
SLC22A16	-0.60	-0.73	0.33
SLC22A17	-0.04	-0.67	0.24
SLC22A23	0.18	-0.84	-0.92
SLC22A25	-0.49	-0.27	0.25
SLC22A5	-0.94	-3.00	-2.49
SLC24A3	-0.66	-1.24	-0.55
SLC24A5	-0.76	-0.45	-0.51
SLC26A11	-0.03	-0.39	-0.73
SLC26A2	-0.73	-0.27	0.40
SLC26A2	-0.82	-0.11	-0.93
SLC30A5	-0.45	-1.09	-0.98
SLC30A6	0.11	0.22	0.54
SLC30A7	0.20	0.22	0.31
SLC30A8	-0.06	-0.24	-0.65
SLC30A9	0.19	0.14	0.31
SLC30A9	-0.24	-0.97	-0.73
SLC31A1	-0.38	-0.96	-0.93
SLC34A1	0.59	-0.83	-1.22
SLC36A4	-0.13	-0.79	-0.38
SLC39A1	0.26	0.21	0.19
SLC39A12	-0.47	0.31	-0.21
SLC39A3	0.62	-0.46	0.61
SLC39A8	-0.23	0.41	0.11
SLC39A8	-0.11	0.06	0.08
SLC39A8	-0.51	-0.47	-0.80
SLC39A9	-0.11	-1.46	-2.76
SLC41A1	-1.51	-0.76	-1.59
SLC41A1	-0.19	-0.21	0.16
SLC41A2	-0.17	0.36	0.20
SLC4A1	-0.12	-0.18	0.16
SLC4A10	0.23	-0.28	-0.49
SLC4A4	-0.21	-0.16	0.02
SLC4A7	-0.71	-0.75	-0.08
SLC4A8	-0.02	0.23	0.22
SLC4A8	-0.59	-0.31	-0.22
SLC4A9	0.70	0.06	-0.01
SLC5A11	-0.52	-0.15	-0.23
SLC5A11	-0.69	-0.91	-0.85
SLC5A3	0.16	0.14	0.08
SLC5A9	-0.15	-0.50	-0.51
SLC8A1	0.10	0.19	0.12
SLC8A2	-0.09	0.01	0.33
SLC9A1	0.94	-0.16	0.07
SLC9A3	-0.08	-0.53	0.00
SLC9A5	-1.47	-2.53	-1.93
SLC9A7	0.54	-0.13	-0.47

shRNA	Tumor shRNA enrichment		
	M214	M481	M491
SLC9A8	-0.32	0.09	-0.06
SLC9A9	0.40	-0.32	-0.30
SLCO1B1	-0.15	0.31	0.23
SLCO1B3	0.07	-0.49	-0.01
SLCO5A1	-0.11	-0.58	-0.36
UCP3	0.26	-0.24	-0.55
ATP12A	0.06	-0.13	-0.31
ATP13A4	-0.13	-1.63	-1.29
ATP13A5	0.38	-0.07	-0.19
ATP13A5	-0.87	-0.40	-0.91
ATP1A2	-0.35	0.03	0.00
ATP2B1	-0.59	-0.99	-0.55
ATP2B2	-0.77	-0.07	-0.42
ATP2B2	-0.73	-1.34	-1.03
ATP2B3	-0.04	-0.20	-0.07
ATP2C1	-0.21	-0.05	-0.69
ATP5B	-0.53	-0.52	-0.45
ATP5E	0.26	0.16	-0.01
ATP5G1	-1.50	-0.26	-1.52
ATP5G1	-0.17	-0.07	0.01
ATP5G3	-0.30	-0.03	0.04
ATP5J	0.14	-0.16	-0.21
ATP5J	-0.07	0.28	0.12
ATP6V0A2	0.52	0.01	-0.09
ATP6V0A2	-0.15	0.14	0.01
ATP6V0A4	-0.01	-0.41	0.37
ATP6V0A4	-0.27	0.05	-0.23
ATP6V1B2	-0.38	-0.25	-0.27
ATP6V1E2	0.03	-0.80	-0.48
ATP6V1G3	0.17	-0.17	-0.06
ATP6V1G3	-0.42	-0.31	-0.08
ATP6V1G3	-0.02	-0.03	-0.29
ATP6V1H	-1.03	-1.59	-1.29
ATP7B	-0.12	-1.33	-1.63
SLC10A2	0.44	0.14	0.06
SLC11A2	-0.56	-0.59	-0.51
SLC12A1	-0.40	-0.50	0.23
SLC12A1	-0.12	-0.04	0.04
SLC12A2	-0.19	0.23	0.03
SLC12A3	-1.67	-1.77	-1.68
SLC12A4	-0.02	-0.10	-0.26
SLC12A6	-1.02	-0.32	-1.19
SLC12A9	-0.35	-0.76	-1.35
SLC13A2	-0.55	-2.00	-1.75
SLC13A2	-0.20	-0.17	-0.40
SLC13A5	0.07	0.20	-1.80
SLC17A1	0.35	-0.13	0.12
SLC17A1	-0.25	-0.38	-0.51
SLC17A1	0.05	-0.38	-0.71
SLC17A3	0.23	0.18	-0.28
SLC22A11	-0.16	-1.67	-3.18
SLC22A17	0.52	0.10	0.42
SLC22A1	0.19	0.32	0.36
SLC22A23	0.42	-0.08	-0.09
SLC22A23	0.03	-0.49	-0.87
SLC22A24	-0.27	-0.34	-1.15
SLC22A3	-0.62	-0.05	-0.23
SLC22A7	-0.19	-0.18	-0.06
SLC24A4	0.29	0.21	-0.09
SLC26A11	-0.79	-2.50	-0.67
SLC26A3	-0.52	-0.44	-1.76
SLC26A8	0.14	-0.06	-0.30
SLC26A8	-0.02	-0.07	-0.09
SLC30A10	0.00	0.22	0.16
SLC30A10	0.22	0.42	0.59
SLC30A1	0.38	0.38	0.56

shRNA	Tumor shRNA enrichment		
	M214	M481	M491
SLC30A1	0.23	0.14	0.21
SLC30A4	-0.46	-0.46	-0.49
SLC36A3	-0.33	-0.49	-0.12
SLC39A11	0.00	-0.47	-0.95
SLC39A12	0.22	-0.05	-0.15
SLC39A2	-0.74	0.01	-0.50
SLC39A2	-0.10	-0.28	-0.54
SLC39A7	-0.49	-0.49	-0.02
SLC39A9	-0.66	-0.57	-1.00
SLC39A9	0.32	0.26	0.28
SLC40A1	-0.12	0.29	0.25
SLC41A2	-0.19	0.15	0.26
SLC4A10	-0.86	-1.36	-0.99
SLC4A11	-2.23	-2.33	-0.98
SLC4A1	-1.14	-1.40	-0.91
SLC4A8	-0.61	-0.91	-0.83
SLC5A12	-0.80	-0.48	-0.79
SLC5A1	-0.34	-0.46	-0.48
SLC5A5	-0.59	-0.52	-0.36
SLC5A6	0.13	-1.30	-0.65
SLC5A7	-1.33	-1.23	-0.60
SLC9A4	0.38	0.05	-0.15
SLC9A5	0.13	-0.05	0.06
SLC9A9	-0.57	-0.24	-0.20
SLC9A9	0.05	0.01	-0.11
SLCO1B1	0.50	-0.39	-0.21
SLCO1B3	-0.45	-0.49	-0.21
SLCO1C1	-0.70	-0.10	-0.70
SLCO2B1	-0.45	-0.05	-0.27
SLCO3A1	0.13	0.17	0.34
SLCO4C1	0.12	-0.25	0.11
SLCO4C1	-0.10	-0.51	0.39
SLCO4C1	-0.78	-0.01	-0.60
UCP3	-2.77	-1.63	-2.99
ATP13A1	-1.90	-2.35	-1.82
ATP13A5	-1.14	-0.08	-0.11
ATP1A1	-2.11	-2.12	-2.44
ATP1A2	-0.61	0.22	-0.76
ATP1A3	-0.90	-0.77	-1.50
ATP1B3	-0.22	-0.87	-0.64
ATP2A1	-2.15	-1.43	-0.96
ATP2A2	0.60	0.20	-0.04
ATP2A3	-0.60	-0.56	-0.32
ATP2B2	-1.15	-1.26	-3.00
ATP2B3	-2.21	-2.94	-2.68
ATP2B4	-2.18	-0.42	-0.43
ATP2C1	-0.47	0.18	-0.51
ATP4A	-1.11	-1.23	-1.15
ATP5B	-0.81	-0.92	-2.90
ATP5C1	0.17	0.76	0.67
ATP5F1	-0.87	-1.26	-1.28
ATP5F1	0.20	0.21	-0.21
ATP5G1	-0.60	0.06	0.33
ATP5G2	-0.05	0.48	0.93
ATP5I	-0.67	-0.30	-0.77
ATP5O	-3.06	-1.94	-1.49
ATP6V0A1	-0.66	-0.75	-1.34
ATP6V0D1	-1.56	-1.96	-1.23
ATP6V0E1	0.64	0.00	0.72
ATP6V1A	-0.73	-0.46	-1.04
ATP6V1A	0.20	-0.37	0.19
ATP6V1B2	-0.22	0.03	0.24
ATP6V1E1	-0.60	-0.37	-0.11
ATP6V1F	-0.58	-0.12	0.34
ATP6V1G1	0.37	0.06	0.22
ATP7A	-0.14	0.15	0.19

shRNA	Tumor shRNA enrichment		
	M214	M481	M491
SLC10A2	-0.04	-0.28	-0.68
SLC10A4	-1.05	-1.21	-0.96
SLC10A4	-0.81	-0.88	-0.91
SLC10A6	-0.12	-0.27	-0.23
SLC11A1	-0.71	-3.25	-2.09
SLC11A2	-1.55	-0.13	-1.11
SLC12A4	-0.23	-0.33	-0.02
SLC12A6	-0.47	-1.35	-0.93
SLC12A7	-0.94	0.19	-0.35
SLC13A4	0.06	0.17	0.52
SLC17A2	0.80	0.38	-0.09
SLC20A2	-0.75	-0.62	-0.10
SLC22A10	0.37	-0.73	-0.17
SLC22A11	-0.83	-0.94	-0.33
SLC22A12	-1.89	0.01	-1.73
SLC22A13	-0.56	-0.10	-0.41
SLC22A13	-1.33	-0.27	-0.29
SLC22A15	0.10	-0.47	-0.34
SLC22A16	-0.91	-0.59	-0.36
SLC22A24	-0.26	-0.26	0.48
SLC22A25	-1.13	-1.18	-0.52
SLC22A3	-1.65	-1.58	-1.87
SLC22A8	-0.03	0.19	0.62
SLC24A1	-0.04	-0.51	0.13
SLC24A2	-0.37	-0.24	0.26
SLC24A2	0.01	0.09	0.08
SLC24A3	0.38	0.12	0.07
SLC24A4	0.16	-0.14	-0.26
SLC25A28	0.27	-0.51	-0.51
SLC25A28	0.36	-0.40	-0.54
SLC26A4	-0.17	-3.07	-2.44
SLC26A6	-0.98	-1.12	-1.39
SLC26A6	-0.72	-1.83	-1.45
SLC26A8	-0.62	-1.46	-0.88

shRNA	Tumor shRNA enrichment		
	M214	M481	M491
SLC30A5	-0.77	-0.39	-0.68
SLC30A6	-0.58	-0.12	0.45
SLC30A6	0.07	-0.07	0.08
SLC30A8	-0.62	-0.65	-0.20
SLC30A9	0.14	0.75	-0.26
SLC31A1	0.68	0.38	0.37
SLC31A2	-0.14	-0.51	0.22
SLC34A2	-0.09	-0.66	-0.97
SLC34A3	-0.63	0.27	-0.08
SLC36A1	-0.58	0.20	0.43
SLC36A3	0.24	-0.42	0.30
SLC39A10	0.23	0.00	0.18
SLC40A1	0.08	0.22	0.15
SLC4A1	0.14	-0.35	-0.98
SLC4A7	-0.37	-0.60	0.13
SLC4A9	-2.09	-1.39	-1.27
SLC5A4	-0.92	-2.88	-1.18
SLC5A8	-0.31	-0.23	0.05
SLC8A2	0.13	0.33	0.62
SLC9A2	-2.25	-0.32	-0.89
SLC9A3	0.53	0.11	0.48
SLC9A8	0.69	0.24	0.20
SLCO1B3	0.19	0.09	-0.09
SLCO2A1	-0.38	-0.09	-0.13
SLCO2A1	-0.48	0.27	0.13
SLCO2B1	-0.02	0.37	-0.02
SLCO3A1	-0.67	-0.40	-0.24
TCIRG1	-1.94	-3.84	-2.57
UCP3	-0.61	-0.94	-1.33
SLC22A24	-0.32	-0.24	-0.62
SLC22A4	-0.18	-0.25	0.18
SLC26A2	0.21	-0.03	0.10
SLC4A4	0.07	-0.63	-1.17
SLC5A7	-0.05	0.25	-0.14

APPENDIX B

Log₂-transformed tumor shRNA enrichment values in the secondary shRNA screen

shRNA	Tumor shRNA enrichment			shRNA	Tumor shRNA enrichment		
	M214	M481	M491		M214	M481	M491
MCOLN1	-1.66	-2.38	-2.15	KCNA5	0.40	-1.36	-1.03
MCOLN1	-2.59	-1.65	-2.15	KCNA5	-1.60	-0.32	-0.75
MCOLN1	-2.12	-2.62	-3.66	KCNA5	-0.02	0.65	0.34
MCOLN1	-1.85	-1.47	-1.19	KCNC4	0.53	-0.18	-0.21
ATP13A1	-0.61	-0.40	-0.89	KCNC4	-1.71	-1.74	-1.85
ATP13A1	0.57	-1.05	0.38	KCNC4	-0.66	0.24	0.01
ATP13A1	-0.06	-0.31	-0.33	KCNC4	-2.66	-0.71	-1.17
ATP5D	0.42	-0.58	-1.25	KCNC4	-0.27	-0.58	-1.00
ATP5D	-0.53	-1.40	-1.80	KCNG1	0.01	-0.97	-2.97
ATP5D	0.73	0.19	-0.36	KCNG1	-1.49	-1.74	-1.72
ATP6V0D1	-1.04	-0.31	-1.41	KCNG1	0.79	-0.88	-0.53
ATP6V0D1	-0.26	-1.18	-1.79	KCNG1	0.57	-1.10	-1.85
ATP6V0D1	-0.58	-0.64	-0.46	KCNG1	0.24	0.26	0.04
CACNB1	0.05	-0.25	-1.12	KCNG1	-1.36	-2.53	-3.57
CACNB1	0.46	0.25	0.47	KCNH2	-0.36	-0.96	-1.47
CACNB1	-0.85	-0.75	0.06	KCNH2	-2.53	-0.37	-0.85
CACNB1	-0.42	-1.25	-1.14	KCNH2	-0.17	-1.18	-1.66
CACNB1	1.52	-0.67	-2.51	KCNH2	-0.09	-0.11	0.57
CACNB1	-0.31	0.36	0.39	KCNH2	-0.36	0.33	-1.07
CLCN4	-0.15	-0.92	-1.70	KCNH2	-0.18	0.20	0.23
CLCN4	-0.63	-0.70	-1.17	KCNJ12	0.17	0.02	0.37
CLCN4	0.24	0.33	1.03	KCNJ12	-1.07	-0.39	-2.94
CLCN4	0.40	0.67	1.17	KCNJ12	-0.29	-2.00	-2.71
CLCN4	-1.18	-0.37	-0.90	KCNK15	1.43	-1.96	-1.84
CLCN4	-1.85	0.28	0.35	KCNK15	-0.43	-1.35	-3.64
FXYD1	0.12	0.03	-1.38	KCNK15	-1.53	-0.61	0.57
FXYD1	-0.03	-1.36	-1.60	KCNK15	-0.74	-2.50	-2.56
FXYD1	-0.17	-0.79	-1.18	KCNK15	-1.32	-2.04	-2.69
FXYD1	0.40	-0.07	0.36	KCNK15	-2.98	-0.93	-1.78
FXYD3	-0.01	-0.67	-1.09	KCNK5	-0.30	-0.07	0.64
FXYD3	0.39	-0.13	-0.93	KCNK5	-0.20	0.19	-0.15
FXYD3	-1.74	-1.35	-2.47	KCNK5	-0.31	-1.28	-1.62
FXYD3	-1.89	-0.68	-0.62	KCNK5	-0.45	0.38	0.64
FXYD3	-0.53	0.36	0.45	KCNK5	-0.04	-0.72	-1.04
FXYD3	-1.43	-0.86	-1.03	KCTD12	-0.08	0.33	-0.63
FXYD4	-0.37	-0.72	-0.37	KCTD12	-0.88	-0.90	-1.55
FXYD7	0.81	-0.84	-1.56	KCTD12	-0.13	-1.22	-1.23
FXYD7	-0.52	0.29	0.60	KCTD12	0.07	0.33	0.39
FXYD7	-0.99	-0.73	-1.11	KCTD12	0.23	0.02	-0.03
FXYD7	-0.36	-1.97	-1.62	KCTD12	0.08	-0.50	-0.09
FXYD7	-0.82	0.27	0.36	KCTD14	-0.63	-0.95	-0.16
HCN1	-0.45	0.08	-0.28	KCTD14	-0.75	0.31	0.40
HCN1	-1.09	-0.16	-0.06	KCTD14	-0.56	0.89	-2.40
HCN1	0.42	0.09	-0.07	KCTD14	-2.94	-0.62	-1.82
HCN1	-0.20	0.32	0.00	KCTD14	-0.05	0.21	-0.22
HCN1	-0.05	-0.78	-1.76	KCTD14	-2.19	0.13	0.29
HCN1	0.29	0.62	0.03	KCTD15	-1.57	0.44	0.83
HCN1	-0.15	-0.49	-0.58	KCTD15	-5.19	-1.58	-0.09
HCN1	-0.19	-1.21	-0.74	KCTD15	0.66	0.26	0.04
ITPR3	2.06	-0.99	-1.64	KCTD15	-0.31	-1.06	-3.54
ITPR3	0.33	-0.86	-2.41	KCTD15	-0.08	-0.43	-0.16
ITPR3	-0.90	-0.78	-0.82	KCTD7	0.67	0.04	-0.63
ITPR3	-0.76	-0.17	-0.57	KCTD7	-0.48	0.24	0.12
ITPR3	-0.29	-0.68	-1.19	KCTD7	0.49	-0.41	-1.98
ITPR3	0.28	-0.66	-0.92	KCTD7	-0.76	-0.53	-1.05
KCNA5	0.22	-0.28	-1.68	KCTD7	-3.09	-2.15	-3.66
KCNA5	-0.08	0.12	-0.45	KCTD7	0.45	0.14	-0.15
KCNA5	0.37	0.68	0.60	KCTD7	-0.57	-1.66	-1.10
KCNA5	-0.82	-1.56	-2.39	KCTD7	-0.82	-0.81	-1.09

shRNA	Tumor shRNA enrichment		
	M214	M481	M491
KCTD7	-0.49	-0.50	-0.48
MLC1	-0.75	-0.46	-0.16
MLC1	-0.11	-1.47	-2.08
MLC1	-0.65	0.13	-1.04
MLC1	-0.07	0.29	0.18
MLC1	-0.75	-1.14	-2.59
MLC1	-0.06	-0.02	0.09
P2RX4	0.47	-0.47	-0.60
P2RX4	-0.22	-0.70	-2.35
P2RX4	0.60	-0.51	-2.18
P2RX4	-0.73	-0.30	-0.50
P2RX4	0.98	-1.09	-1.58
PKD1	-0.17	-0.04	0.28
PKD1	-0.54	-1.03	0.44
PKD1	-0.47	1.41	3.49
PKD2	0.04	0.11	-0.45
PKD2	0.27	0.42	0.71
PKD2	-0.75	-0.34	-0.30
PKD2	-0.01	0.05	0.05
PKD2	-0.85	-2.87	-1.76
PKD2	0.51	0.27	0.77
RYR1	-0.20	0.50	0.36
RYR1	-0.36	-0.60	-0.57
RYR1	-2.42	-1.42	-1.53
RYR1	0.22	0.02	0.74
RYR1	-0.52	-0.87	-1.11
RYR1	-0.90	-1.44	-1.59
SCN9A	-0.48	0.01	0.20
SCN9A	-0.94	-0.75	0.13
SCN9A	-0.06	0.04	-0.12
SCN9A	-1.08	-1.10	-0.85
SCN9A	-0.34	-0.39	-0.20
SCN9A	0.99	-0.15	0.69
SCN9A	-2.41	-1.86	-2.57
SLC12A9	-1.31	-1.32	-1.33
SLC12A9	0.01	-0.35	-1.13
SLC12A9	-0.32	-1.13	-0.25
SLC22A5	-1.64	-1.06	-0.86
SLC22A5	0.28	0.27	0.57
SLC22A5	-1.54	-1.86	-2.52
SLC39A3	0.34	-0.03	-0.42
SLC39A3	-0.22	-1.86	-0.78
SLC39A3	0.25	-0.34	-0.45
SLC39A4	-1.63	-1.20	-0.33
SLC39A4	-0.19	-0.04	-0.45

shRNA	Tumor shRNA enrichment		
	M214	M481	M491
SLC41A1	0.27	-0.38	0.30
SLC41A1	0.73	-0.97	0.08
SLC41A1	-0.62	0.09	-0.08
SLC9A1	1.32	2.67	3.07
SLC9A1	2.14	2.50	2.38
SLC9A1	-0.47	1.41	3.49
SLC9A1	0.33	1.49	2.41
SLC9A1	-2.83	2.01	1.88
SLC9A1	0.15	-1.19	-0.36
TOMM40	-0.30	0.10	0.49
TOMM40	-0.23	-1.53	-1.95
TOMM40	-0.05	-1.76	-2.61
TOMM40	-0.97	0.02	-3.30
TOMM40	-0.36	0.05	-2.03
TPCN1	-0.42	-0.79	-1.29
TPCN1	0.34	0.18	0.83
TPCN1	-0.53	0.77	-0.28
TPCN1	0.20	0.40	0.43
TPCN1	0.32	-0.17	0.26
TPCN1	0.04	0.31	0.22
TPCN1	-1.89	0.07	-0.51
TPCN1	0.11	0.53	0.27
TPCN1	-1.18	-1.76	-0.09
TPCN2	0.68	-0.29	-0.18
TPCN2	-1.37	-1.09	-0.73
TPCN2	0.20	-0.37	0.69
TPCN2	-0.32	-0.35	-0.11
TPCN2	0.64	-0.21	-0.50
TPCN2	-2.53	-1.26	-0.81
TPCN2	-0.52	-0.95	-0.70
TRPM2	-0.34	-0.15	-0.17
TRPM2	-0.68	-1.80	-2.95
TRPM2	-0.28	-0.21	0.83
TRPM2	-2.08	-0.49	-1.60
TRPM2	-1.47	-1.07	-0.71
TRPM2	-0.62	-0.94	-1.18
TRPM2	-0.55	-0.84	-0.49
TSPO	-1.14	-1.37	-3.82
TSPO	-2.00	0.19	-0.29
TSPO	-1.04	-1.91	-3.50
TSPO	-0.08	-0.73	0.09
TTYH1	0.97	-1.79	-2.21
TTYH1	2.01	-0.61	-1.30
TTYH1	-0.34	-0.21	0.02
TTYH1	-0.64	-0.51	-0.17

APPENDIX C

Significantly changed metabolites in metabolomics of parental versus *MCOLN1*-deficient tumors with and without rapamycin treatment

Metabolite	Normalized Peak Areas								
	A375			M214			M481		
	WT	MCOLN1 ^{KO}	MCOLN1 ^{KO} + rapamycin	WT	MCOLN1 ^{KO}	MCOLN1 ^{KO} + rapamycin	WT	MCOLN1 ^{KO}	MCOLN1 ^{KO} + rapamycin
Platelet-activating factor	1369965	1162527	1495418	0	0	0	0	0	0
L-alpha-lysophosphatidylcholine	49625	52626	73754	0	0	0	0	0	0
Nicotinamide	2143505	1948724	2123880	0	0	0	0	0	0
1-oleoyl-sn-glycero-3-phosphoethanolamine	85579	134204	202581	0	0	0	90975	181691	91050
D-pantothenic acid	4130067	3362756	4790664	3534983	1941350	2259977	1722937	2440295	1125590
Proline	13069372	17734501	24103054	218065	139093	164498	2033585	2207419	1281538
Prolylleucine	109320	92034	139482	0	0	0	0	0	0
Bethanidine	7591	560778	188840	0	0	0	0	0	0
Acetyl-beta-methylcholine	270922	268592	340879	134530	71925	84978	104855	119640	81642
Acetylcholine	1065534	1402666	1635634	580865	357999	416903	428920	493171	269984
Methionine sulfoxide	207356	214273	336145	0	0	0	0	0	0
Choline	98276229	85973240	116046745	1122069	16088622	16413226	0	0	0
Dihydrothymine	1744153	1545434	1509029	0	0	0	680980	657478	452369
Threonine	21326291	18654249	20080766	18572232	14281352	15439872	12578362	16617404	11631219
Nicotinamide adenine dinucleotide (NAD+)	252542	401954	544372	218065	139093	164498	68059	83115	41969
Nicotinamide	415344	631657	775255	0	0	0	0	0	0
L-Glutathione (reduced)	14267535	10603614	15996532	8701183	5248610	6986349	3213266	2593599	1595440
L-Serine	35288838	3026050	37173577	25044009	1366058	17419723	17890234	1803202	15217375
L-(+)-Citrulline	1123101	885825	1020096	372512	220759	237084	0	0	0
Carnosine	460960	321776	433417	0	0	0	253548	174453	216724
4-Methylene-L-glutamine	731173	578341	729584	0	0	0	0	0	0
L-Glutamic acid	47006934	53139145	63433284	25383224	21495834	24285396	12573593	21000692	10438484
L-Aspartic acid	1017525	896856	1006993	1527943	378367	487060	447994	656348	291150
N-Acetyl-L-glutamic acid	62514	47073	64246	0	0	0	0	0	0
L-Cystine	522372	438147	373711	0	0	0	0	0	0
Phosphocreatine	2489260	1586851	1904773	0	0	0	935315	557848	268521
UDP-N-acetylglucosamine	218140	302840	388947	174589	116986	148793	17381	20268	8809
S-Adenosylmethionine	721699	609625	870709	0	0	0	31914	44000	15425
Diethanolamine	14155501	520350	517577	0	0	0	0	0	0
Cystathionine	139413	75485	110812	69451	35807	44291	0	0	0
uridine 5'-diphosphate	259393	212513	294286	250251	133268	162604	0	0	0
Adenosine triphosphate (ATP)	1373958	1815634	2325829	1222821	729194	1012007	462235	581551	286776
N-Acetyl-1-aspartylglutamic acid	152363	89589	132117	0	0	0	0	0	0
N-6-,N-6--Dimethyllysine	155775	126435	154490	0	0	0	0	0	0
N3,N4-Dimethyl-L-arginine	902720	809009	843959	510989	287981	295898	0	0	0
6-Methylnicotinamide	19957661	15753357	24344663	0	0	0	0	0	0
L-(+)-Lactic acid	46788833	42652695	55883305	0	0	0	0	0	0
Cytidine	987295	1474420	1746493	0	0	0	0	0	0
L-Histidine	3287783	3548671	4081231	20935201	15709621	16774784	17396649	19586627	15458949
N-Acetylneuraminic acid	393890	324846	624459	0	0	0	0	0	0
Taurine	2403947	3631504	4053403	1283176	1760113	1735859	1235890	1807077	775115
Cyclic ADP-ribose	84322	130502	189648	0	0	0	0	0	0
Glycine	1083148	626284	1359486	0	0	0	0	0	0
Inositol	10000391	7975878	9321490	0	0	0	0	0	0

N-Acetylaspartic acid	7650390	3780529	5541209	784595	575319	784828	526889	509337	285505
N-Acetylalanine	317070	168836	229394	0	0	0	0	0	0
Succinic Acid	1792357	1609450	1815410	960900	538934	544577	0	0	0
alpha-Ketoglutaric acid	398359	440577	507230	0	0	0	0	0	0
D-(+)-Malic acid	9728148	8652008	9446914	9780984	6002637	7030840	3146380	2863360	2065756
Uridine 5'-diphosphogalactose	174303	122856	202998	154470	65164	79832	0	0	0
Citric acid	947730	1210246	1959680	438554	104026	91771	293991	301941	172644
1-Linoleoyl-sn-glycero-3-phosphocholine	0	0	0	126162	51005	72815	0	0	0
3,4,5,6-Tetrahydrohippurate	0	0	0	12329359	7495484	8380078	0	0	0
3-Methylhistidine	0	0	0	504938	199708	219963	407743	429318	287982
Acetohydroxamic acid	0	0	0	695900	403442	484746	572392	666440	396966
Acetyl-L-carnitine	0	0	0	792546	1100192	1337640	837029	1053447	711928
Creatinine	0	0	0	2978707	1618667	1719179	0	0	0
D-(-)-Glutamine	0	0	0	128902785	82361970	76217143	90658318	114210215	87326502
DL-Arginine	0	0	0	13195662	5996067	6036477	0	0	0
DL-Carnitine	0	0	0	5935522	2117659	2541442	3626149	3799016	2350117
DL-Lysine	0	0	0	3879590	1387982	1484293	0	0	0
DL-Tryptophan	0	0	0	878297	531892	556616	0	0	0
Glycerolphosphatidylethanolamine	0	0	0	374142	81478	84578	0	0	0
Leucine/Isoleucine	0	0	0	41743911	26473803	29236690	34929816	40375335	29185990
L-Phenylalanine	0	0	0	12367278	7532655	8408619	0	0	0
L-Pyroglutamic acid	0	0	0	125115231	80450857	74309595	0	0	0
L-Tyrosine	0	0	0	3530467	2154633	2355850	2820727	3187272	2283278
Methionine	0	0	0	3005654	1895388	1831264	2359376	2786459	1934588
N6,N6,N6-Trimethyl-L-lysine	0	0	0	505873	304200	389581	0	0	0
N-Acetyl-DL-histidine	0	0	0	490946	170392	173804	0	0	0
N-acetyl-L-2-aminoadipic acid	0	0	0	332905	150766	177956	72917	95217	40405
N-Acetylmethionine	0	0	0	167195	48686	62938	105840	91347	52348
Palmitoyl sphingomyelin	0	0	0	1685704	562798	664304	0	0	0
1-(sn-glycero-3-phospho)-1D-myo-inositol	0	0	0	363401	68839	93066	0	0	0
2-Hydroxyphenylalanine	0	0	0	1606198	983319	1067924	0	0	0
3-Hydroxy-3-methylglutaric acid	0	0	0	830534	356486	418552	0	0	0
4-Oxoproline	0	0	0	8486285	4783444	4975369	7867644	11347401	6912331
5-Aminovaleric acid	0	0	0	5551554	3346441	3839273	0	0	0
D-(+)-Galactose	0	0	0	9963610	3375153	4087762	0	0	0
D-(+)-Mannose	0	0	0	1009114	606074	602501	0	0	0
Uric acid	0	0	0	495204	390270	445058	0	0	0
DL-Dipalmitoylphosphatidylcholine	0	0	0	0	0	0	545754	786668	357269
Lyso-palmitoylphosphatidylcholine	0	0	0	0	0	0	1599655	2413071	1556851
Butyrylcarnitine	0	0	0	0	0	0	80979	125966	78253
Trigonelline	0	0	0	0	0	0	296100	39531	23894
2-Aminoadipic acid	0	0	0	0	0	0	200637	408332	202500
Creatine	0	0	0	0	0	0	38169315	36816222	22011827
2-Amino-4-methylpyrimidine	0	0	0	0	0	0	3912600	4368685	3444388
Hypotaurine	0	0	0	0	0	0	185816	323192	134489
Phosphoserine	0	0	0	0	0	0	147029	166092	124023
Adenosine diphosphate (ADP)	0	0	0	0	0	0	67568	86529	52057
Adenosine triphosphate (ATP)	0	0	0	0	0	0	462235	581551	286776
Uridine 5'-triphosphate	0	0	0	0	0	0	79188	106362	38146
DL-3-Aminoisobutyric acid	0	0	0	0	0	0	543029	689168	433592
Oxalic acid	0	0	0	0	0	0	2296379	2334311	1956233

REFERENCES

Agrawal, N., Frederick, M. J., Pickering, C. R., Bettgowda, C., Chang, K., Li, R. J., Fakhry, C., Xie, T. X., Zhang, J., Wang, J., *et al.* (2011). Exome sequencing of head and neck squamous cell carcinoma reveals inactivating mutations in NOTCH1. *Science* 333, 1154-1157.

Alberts, B. (2002). *Molecular biology of the cell*, 4th edn (New York: Garland Science).

Almanzar, G., Olkhanud, P. B., Bodogai, M., Dell'agnola, C., Baatar, D., Hewitt, S. M., Ghimenton, C., Tummala, M. K., Weeraratna, A. T., Hoek, K. S., *et al.* (2009). Sperm-derived SPANX-B is a clinically relevant tumor antigen that is expressed in human tumors and readily recognized by human CD4+ and CD8+ T cells. *Clin Cancer Res* 15, 1954-1963.

Amir, N., Zlotogora, J., and Bach, G. (1987). Mucopolidosis type IV: clinical spectrum and natural history. *Pediatrics* 79, 953-959.

Aronson, P. S. (1985). Kinetic properties of the plasma membrane Na⁺-H⁺ exchanger. *Annu Rev Physiol* 47, 545-560.

Ashcroft, F. M., Harrison, D. E., and Ashcroft, S. J. (1984). Glucose induces closure of single potassium channels in isolated rat pancreatic beta-cells. *Nature* 312, 446-448.

Ashcroft, F. M., and Rorsman, P. (1989). Electrophysiology of the pancreatic beta-cell. *Prog Biophys Mol Biol* 54, 87-143.

Bar-Peled, L., Schweitzer, L. D., Zoncu, R., and Sabatini, D. M. (2012). Ragulator is a GEF for the rag GTPases that signal amino acid levels to mTORC1. *Cell* 150, 1196-1208.

Bar-Sagi, D., and Feramisco, J. R. (1986). Induction of membrane ruffling and fluid-phase pinocytosis in quiescent fibroblasts by ras proteins. *Science* 233, 1061-1068.

Barbieri, C. E., Baca, S. C., Lawrence, M. S., Demichelis, F., Blattner, M., Theurillat, J. P., White, T. A., Stojanov, P., Van Allen, E., Stransky, N., *et al.* (2012). Exome sequencing identifies recurrent SPOP, FOXA1 and MED12 mutations in prostate cancer. *Nat Genet* 44, 685-689.

Bargal, R., Avidan, N., Ben-Asher, E., Olender, Z., Zeigler, M., Frumkin, A., Raas-Rothschild, A., Glusman, G., Lancet, D., and Bach, G. (2000). Identification of the gene causing mucopolidosis type IV. *Nat Genet* 26, 118-123.

Bartkova, J., Rezaei, N., Liontos, M., Karakaidos, P., Kletsas, D., Issaeva, N., Vassiliou, L. V., Kolettas, E., Niforou, K., Zoumpourlis, V. C., *et al.* (2006). Oncogene-induced senescence is part of the tumorigenesis barrier imposed by DNA damage checkpoints. *Nature* 444, 633-637.

Bartolomeo, R., Cinque, L., De Leonibus, C., Forrester, A., Salzano, A. C., Monfregola, J., De Gennaro, E., Nusco, E., Azario, I., Lanzara, C., *et al.* (2017). mTORC1 hyperactivation arrests bone growth in lysosomal storage disorders by suppressing autophagy. *J Clin Invest* 127, 3717-3729.

Bates, E. (2015). Ion channels in development and cancer. *Annu Rev Cell Dev Biol* 31, 231-247.

Berger, M. F., Hodis, E., Heffernan, T. P., Deribe, Y. L., Lawrence, M. S., Protopopov, A., Ivanova, E., Watson, I. R., Nickerson, E., Ghosh, P., *et al.* (2012). Melanoma genome sequencing reveals frequent PREX2 mutations. *Nature* 485, 502-506.

Berridge, M. J. (1995). Calcium signalling and cell proliferation. *Bioessays* 17, 491-500.

Berridge, M. J., Bootman, M. D., and Lipp, P. (1998). Calcium--a life and death signal. *Nature* 395, 645-648.

Berridge, M. J., Bootman, M. D., and Roderick, H. L. (2003). Calcium signalling: dynamics, homeostasis and remodelling. *Nat Rev Mol Cell Biol* 4, 517-529.

Berridge, M. J., Lipp, P., and Bootman, M. D. (2000). The versatility and universality of calcium signalling. *Nat Rev Mol Cell Biol* 1, 11-21.

Beuschlein, F., Boulkroun, S., Osswald, A., Wieland, T., Nielsen, H. N., Lichtenauer, U. D., Penton, D., Schack, V. R., Amar, L., Fischer, E., *et al.* (2013). Somatic mutations in ATP1A1 and ATP2B3 lead to aldosterone-producing adenomas and secondary hypertension. *Nat Genet* 45, 440-444.

Blair, H. C., Teitelbaum, S. L., Ghiselli, R., and Gluck, S. (1989). Osteoclastic bone resorption by a polarized vacuolar proton pump. *Science* 245, 855-857.

Blaustein, M. P., and Lederer, W. J. (1999). Sodium/calcium exchange: its physiological implications. *Physiol Rev* 79, 763-854.

Blomen, V. A., Majek, P., Jae, L. T., Bigenzahn, J. W., Nieuwenhuis, J., Staring, J., Sacco, R., van Diemen, F. R., Olk, N., Stukalov, A., *et al.* (2015). Gene essentiality and synthetic lethality in haploid human cells. *Science* 350, 1092-1096.

Bolanz, K. A., Hediger, M. A., and Landowski, C. P. (2008). The role of TRPV6 in breast carcinogenesis. *Mol Cancer Ther* 7, 271-279.

Boron, W. F. (1986). Intracellular pH regulation in epithelial cells. *Annu Rev Physiol* 48, 377-388.

Brackenbury, W. J., Yuan, Y., O'Malley, H. A., Parent, J. M., and Isom, L. L. (2013). Abnormal neuronal patterning occurs during early postnatal brain development of *Scn1b*-null mice and precedes hyperexcitability. *Proc Natl Acad Sci U S A* 110, 1089-1094.

Braig, M., Lee, S., Loddenkemper, C., Rudolph, C., Peters, A. H., Schlegelberger, B., Stein, H., Dorken, B., Jenuwein, T., and Schmitt, C. A. (2005). Oncogene-induced senescence as an initial barrier in lymphoma development. *Nature* 436, 660-665.

Bric, A., Miething, C., Bialucha, C. U., Scuoppo, C., Zender, L., Krasnitz, A., Xuan, Z., Zuber, J., Wigler, M., Hicks, J., *et al.* (2009). Functional identification of tumor-suppressor genes through an in vivo RNA interference screen in a mouse lymphoma model. *Cancer Cell* 16, 324-335.

Brummelkamp, T. R., Bernards, R., and Agami, R. (2002). A system for stable expression of short interfering RNAs in mammalian cells. *Science* 296, 550-553.

Brundage, R. A., Fogarty, K. E., Tuft, R. A., and Fay, F. S. (1991). Calcium gradients underlying polarization and chemotaxis of eosinophils. *Science* 254, 703-706.

Cahalan, M. D., Chandy, K. G., DeCoursey, T. E., and Gupta, S. (1985). A voltage-gated potassium channel in human T lymphocytes. *J Physiol* 358, 197-237.

Calcraft, P. J., Ruas, M., Pan, Z., Cheng, X., Arredouani, A., Hao, X., Tang, J., Rietdorf, K., Teboul, L., Chuang, K. T., *et al.* (2009). NAADP mobilizes calcium from acidic organelles through two-pore channels. *Nature* 459, 596-600.

Callies, C., Fels, J., Liashkovich, I., Kliche, K., Jeggle, P., Kusche-Vihrog, K., and Oberleithner, H. (2011). Membrane potential depolarization decreases the stiffness of vascular endothelial cells. *J Cell Sci* 124, 1936-1942.

Camacho, J. (2006). Ether a go-go potassium channels and cancer. *Cancer Lett* 233, 1-9.

Campbell, T. M., Main, M. J., and Fitzgerald, E. M. (2013). Functional expression of the voltage-gated Na⁽⁺⁾-channel Nav1.7 is necessary for EGF-mediated invasion in human non-small cell lung cancer cells. *J Cell Sci* 126, 4939-4949.

Cang, C., Zhou, Y., Navarro, B., Seo, Y. J., Aranda, K., Shi, L., Battaglia-Hsu, S., Nissim, I., Clapham, D. E., and Ren, D. (2013). mTOR regulates lysosomal ATP-sensitive two-pore Na⁽⁺⁾ channels to adapt to metabolic state. *Cell* 152, 778-790.

Carafoli, E., Santella, L., Branca, D., and Brini, M. (2001). Generation, control, and processing of cellular calcium signals. *Crit Rev Biochem Mol Biol* 36, 107-260.

Cardone, R. A., Casavola, V., and Reshkin, S. J. (2005). The role of disturbed pH dynamics and the Na⁺/H⁺ exchanger in metastasis. *Nat Rev Cancer* 5, 786-795.

Casey, J. R., Grinstein, S., and Orlowski, J. (2010). Sensors and regulators of intracellular pH. *Nat Rev Mol Cell Biol* 11, 50-61.

Caterina, M. J., Schumacher, M. A., Tominaga, M., Rosen, T. A., Levine, J. D., and Julius, D. (1997). The capsaicin receptor: a heat-activated ion channel in the pain pathway. *Nature* 389, 816-824.

Catterall, W. A., Perez-Reyes, E., Snutch, T. P., and Striessnig, J. (2005). International Union of Pharmacology. XLVIII. Nomenclature and structure-function relationships of voltage-gated calcium channels. *Pharmacol Rev* 57, 411-425.

Chan, H. C., and Nelson, D. J. (1992). Chloride-dependent cation conductance activated during cellular shrinkage. *Science* 257, 669-671.

Chen, C. F., Corbley, M. J., Roberts, T. M., and Hess, P. (1988). Voltage-sensitive calcium channels in normal and transformed 3T3 fibroblasts. *Science* 239, 1024-1026.

Chen, C. S., Bach, G., and Pagano, R. E. (1998). Abnormal transport along the lysosomal pathway in mucopolipidosis, type IV disease. *Proc Natl Acad Sci U S A* 95, 6373-6378.

Chen, Z., Trotman, L. C., Shaffer, D., Lin, H. K., Dotan, Z. A., Niki, M., Koutcher, J. A., Scher, H. I., Ludwig, T., Gerald, W., *et al.* (2005). Crucial role of p53-dependent cellular senescence in suppression of Pten-deficient tumorigenesis. *Nature* 436, 725-730.

Cheng, X., Shen, D., Samie, M., and Xu, H. (2010). Mucolipins: Intracellular TRPML1-3 channels. *FEBS Lett* 584, 2013-2021.

Chilton, L., Ohya, S., Freed, D., George, E., Drobic, V., Shibukawa, Y., Maccannell, K. A., Imaizumi, Y., Clark, R. B., Dixon, I. M., and Giles, W. R. (2005). K⁺ currents regulate the resting membrane potential, proliferation, and contractile responses in ventricular fibroblasts and myofibroblasts. *Am J Physiol Heart Circ Physiol* 288, H2931-2939.

Chin, L. (2003). The genetics of malignant melanoma: lessons from mouse and man. *Nat Rev Cancer* 3, 559-570.

Chittajallu, R., Chen, Y., Wang, H., Yuan, X., Ghiani, C. A., Heckman, T., McBain, C. J., and Gallo, V. (2002). Regulation of Kv1 subunit expression in oligodendrocyte progenitor cells and their role in G1/S phase progression of the cell cycle. *Proc Natl Acad Sci U S A* 99, 2350-2355.

Choi, M., Scholl, U. I., Yue, P., Bjorklund, P., Zhao, B., Nelson-Williams, C., Ji, W., Cho, Y., Patel, A., Men, C. J., *et al.* (2011). K⁺ channel mutations in adrenal aldosterone-producing adenomas and hereditary hypertension. *Science* 331, 768-772.

Citri, A., and Yarden, Y. (2006). EGF-ERBB signalling: towards the systems level. *Nat Rev Mol Cell Biol* 7, 505-516.

Clapham, D. E. (2003). TRP channels as cellular sensors. *Nature* 426, 517-524.

Clapham, D. E. (2007). Calcium signaling. *Cell* 131, 1047-1058.

Colatsky, T. J., Follmer, C. H., and Starmer, C. F. (1990). Channel specificity in antiarrhythmic drug action. Mechanism of potassium channel block and its role in suppressing and aggravating cardiac arrhythmias. *Circulation* 82, 2235-2242.

Commisso, C., Davidson, S. M., Soydaner-Azeloglu, R. G., Parker, S. J., Kamphorst, J. J., Hackett, S., Grabocka, E., Nofal, M., Drebin, J. A., Thompson, C. B., *et al.* (2013). Macropinocytosis of protein is an amino acid supply route in Ras-transformed cells. *Nature* 497, 633-637.

Cone, C. D., Jr. (1971). Unified theory on the basic mechanism of normal mitotic control and oncogenesis. *J Theor Biol* 30, 151-181.

Cone, C. D., Jr., and Cone, C. M. (1976). Induction of mitosis in mature neurons in central nervous system by sustained depolarization. *Science* 192, 155-158.

Cong, L., Ran, F. A., Cox, D., Lin, S., Barretto, R., Habib, N., Hsu, P. D., Wu, X., Jiang, W., Marraffini, L. A., and Zhang, F. (2013). Multiplex genome engineering using CRISPR/Cas systems. *Science* 339, 819-823.

Cook, D. L., and Hales, C. N. (1984). Intracellular ATP directly blocks K⁺ channels in pancreatic B-cells. *Nature* 311, 271-273.

Cordat, E., and Casey, J. R. (2009). Bicarbonate transport in cell physiology and disease. *Biochem J* 417, 423-439.

Crane, R. K. (1960). Intestinal absorption of sugars. *Physiol Rev* 40, 789-825.

Cullen, P. J., and Steinberg, F. (2018). To degrade or not to degrade: mechanisms and significance of endocytic recycling. *Nat Rev Mol Cell Biol* 19, 679-696.

D'Mello S, A., Joseph, W. R., Green, T. N., Leung, E. Y., During, M. J., Finlay, G. J., Baguley, B. C., and Kalev-Zylinska, M. L. (2016). Selected GRIN2A mutations in melanoma cause oncogenic effects that can be modulated by extracellular glutamate. *Cell Calcium* 60, 384-395.

Dancey, J. (2010). mTOR signaling and drug development in cancer. *Nat Rev Clin Oncol* 7, 209-219.

- Dartsch, P. C., Ritter, M., Gschwentner, M., Lang, H. J., and Lang, F. (1995). Effects of calcium channel blockers on NIH 3T3 fibroblasts expressing the Ha-ras oncogene. *Eur J Cell Biol* 67, 372-378.
- Dayam, R. M., Saric, A., Shilliday, R. E., and Botelho, R. J. (2015). The Phosphoinositide-Gated Lysosomal Ca(2+) Channel, TRPML1, Is Required for Phagosome Maturation. *Traffic* 16, 1010-1026.
- DeCoursey, T. E., Chandy, K. G., Gupta, S., and Cahalan, M. D. (1984). Voltage-gated K⁺ channels in human T lymphocytes: a role in mitogenesis? *Nature* 307, 465-468.
- Demaurex, N., and Grinstein, S. (1994). Na⁺/H⁺ antiport: modulation by ATP and role in cell volume regulation. *J Exp Biol* 196, 389-404.
- DeNicola, G. M., Chen, P. H., Mullarky, E., Sudderth, J. A., Hu, Z., Wu, D., Tang, H., Xie, Y., Asara, J. M., Huffman, K. E., *et al.* (2015). NRF2 regulates serine biosynthesis in non-small cell lung cancer. *Nat Genet* 47, 1475-1481.
- Deutsch, C., and Chen, L. Q. (1993). Heterologous expression of specific K⁺ channels in T lymphocytes: functional consequences for volume regulation. *Proc Natl Acad Sci U S A* 90, 10036-10040.
- Di Fiore, P. P., and De Camilli, P. (2001). Endocytosis and signaling. an inseparable partnership. *Cell* 106, 1-4.
- Dong, X. P., Shen, D., Wang, X., Dawson, T., Li, X., Zhang, Q., Cheng, X., Zhang, Y., Weisman, L. S., Delling, M., and Xu, H. (2010). PI(3,5)P(2) controls membrane trafficking by direct activation of mucolipin Ca(2+) release channels in the endolysosome. *Nat Commun* 1, 38.

Dong, Z., and Zhang, J. T. (2006). Initiation factor eIF3 and regulation of mRNA translation, cell growth, and cancer. *Crit Rev Oncol Hematol* 59, 169-180.

Douglas, W. W., and Rubin, R. P. (1961). The role of calcium in the secretory response of the adrenal medulla to acetylcholine. *J Physiol* 159, 40-57.

Downie, B. R., Sanchez, A., Knotgen, H., Contreras-Jurado, C., Gymnopoulos, M., Weber, C., Stuhmer, W., and Pardo, L. A. (2008). Eag1 expression interferes with hypoxia homeostasis and induces angiogenesis in tumors. *J Biol Chem* 283, 36234-36240.

Dunham, P. B., Jessen, F., and Hoffmann, E. K. (1990). Inhibition of Na-K-Cl cotransport in Ehrlich ascites cells by antiserum against purified proteins of the cotransporter. *Proc Natl Acad Sci U S A* 87, 6828-6832.

Dunn, K. W., Kamocka, M. M., and McDonald, J. H. (2011). A practical guide to evaluating colocalization in biological microscopy. *Am J Physiol Cell Physiol* 300, C723-742.

Eskiocak, U., Ramesh, V., Gill, J. G., Zhao, Z., Yuan, S. W., Wang, M., Vandergriff, T., Shackleton, M., Quintana, E., Johnson, T. M., *et al.* (2016). Synergistic effects of ion transporter and MAP kinase pathway inhibitors in melanoma. *Nat Commun* 7, 12336.

Evan, G. I., Wyllie, A. H., Gilbert, C. S., Littlewood, T. D., Land, H., Brooks, M., Waters, C. M., Penn, L. Z., and Hancock, D. C. (1992). Induction of apoptosis in fibroblasts by c-myc protein. *Cell* 69, 119-128.

Falchook, G. S., Lewis, K. D., Infante, J. R., Gordon, M. S., Vogelzang, N. J., DeMarini, D. J., Sun, P., Moy, C., Szabo, S. A., Roadcap, L. T., *et al.* (2012). Activity of the oral

MEK inhibitor trametinib in patients with advanced melanoma: a phase 1 dose-escalation trial. *Lancet Oncol* 13, 782-789.

Farias, L. M., Ocana, D. B., Diaz, L., Larrea, F., Avila-Chavez, E., Cadena, A., Hinojosa, L. M., Lara, G., Villanueva, L. A., Vargas, C., *et al.* (2004). Ether a go-go potassium channels as human cervical cancer markers. *Cancer Res* 64, 6996-7001.

Felipe, A., Snyders, D. J., Deal, K. K., and Tamkun, M. M. (1993). Influence of cloned voltage-gated K⁺ channel expression on alanine transport, Rb⁺ uptake, and cell volume. *Am J Physiol* 265, C1230-1238.

Feron, O. (2009). Pyruvate into lactate and back: from the Warburg effect to symbiotic energy fuel exchange in cancer cells. *Radiother Oncol* 92, 329-333.

Fidelman, M. L., Seeholzer, S. H., Walsh, K. B., and Moore, R. D. (1982). Intracellular pH mediates action of insulin on glycolysis in frog skeletal muscle. *Am J Physiol* 242, C87-93.

Findlay, I., Ashcroft, F. M., Kelly, R. P., Rorsman, P., Petersen, O. H., and Trube, G. (1989). Calcium currents in insulin-secreting beta-cells. *Ann N Y Acad Sci* 560, 403-409.

Fixemer, T., Wissenbach, U., Flockerzi, V., and Bonkhoff, H. (2003). Expression of the Ca²⁺-selective cation channel TRPV6 in human prostate cancer: a novel prognostic marker for tumor progression. *Oncogene* 22, 7858-7861.

Frankel, A. E., Eskiocak, U., Gill, J. G., Yuan, S., Ramesh, V., Froehlich, T. W., Ahn, C., and Morrison, S. J. (2017). Digoxin Plus Trametinib Therapy Achieves Disease Control in BRAF Wild-Type Metastatic Melanoma Patients. *Neoplasia* 19, 255-260.

Fraser, S. P., and Pardo, L. A. (2008). Ion channels: functional expression and therapeutic potential in cancer. *Colloquium on Ion Channels and Cancer. EMBO Rep* 9, 512-515.

Gadsby, D. C. (2009). Ion channels versus ion pumps: the principal difference, in principle. *Nat Rev Mol Cell Biol* 10, 344-352.

Gargiulo, G., Serresi, M., Cesaroni, M., Hulsman, D., and van Lohuizen, M. (2014). In vivo shRNA screens in solid tumors. *Nat Protoc* 9, 2880-2902.

Geck, P., and Pfeiffer, B. (1985). Na⁺K⁺2Cl⁻ cotransport in animal cells--its role in volume regulation. *Ann N Y Acad Sci* 456, 166-182.

Ghiani, C. A., Yuan, X., Eisen, A. M., Knutson, P. L., DePinho, R. A., McBain, C. J., and Gallo, V. (1999). Voltage-activated K⁺ channels and membrane depolarization regulate accumulation of the cyclin-dependent kinase inhibitors p27(Kip1) and p21(CIP1) in glial progenitor cells. *J Neurosci* 19, 5380-5392.

Gomez, T. M., Snow, D. M., and Letourneau, P. C. (1995). Characterization of spontaneous calcium transients in nerve growth cones and their effect on growth cone migration. *Neuron* 14, 1233-1246.

Gomez-Varela, D., Zwick-Wallasch, E., Knotgen, H., Sanchez, A., Hettmann, T., Ossipov, D., Weseloh, R., Contreras-Jurado, C., Rothe, M., Stuhmer, W., and Pardo, L. A. (2007). Monoclonal antibody blockade of the human Eag1 potassium channel function exerts antitumor activity. *Cancer Res* 67, 7343-7349.

Grinstein, S., Clarke, C. A., and Rothstein, A. (1983). Activation of Na⁺/H⁺ exchange in lymphocytes by osmotically induced volume changes and by cytoplasmic acidification. *J Gen Physiol* 82, 619-638.

Gross, E., and Hopfer, U. (1999). Effects of pH on kinetic parameters of the Na-HCO₃ cotransporter in renal proximal tubule. *Biophys J* 76, 3066-3075.

Grunder, S., Thiemann, A., Pusch, M., and Jentsch, T. J. (1992). Regions involved in the opening of ClC-2 chloride channel by voltage and cell volume. *Nature* 360, 759-762.

Guertin, D. A., and Sabatini, D. M. (2007). Defining the role of mTOR in cancer. *Cancer Cell* 12, 9-22.

Guilbert, A., Gautier, M., Dhennin-Duthille, I., Haren, N., Sevestre, H., and Ouadid-Ahidouch, H. (2009). Evidence that TRPM7 is required for breast cancer cell proliferation. *Am J Physiol Cell Physiol* 297, C493-502.

Halestrap, A. P. (2013). Monocarboxylic acid transport. *Compr Physiol* 3, 1611-1643.

Halestrap, A. P., and Meredith, D. (2004). The SLC16 gene family—from monocarboxylate transporters (MCTs) to aromatic amino acid transporters and beyond. *Pflugers Arch* 447, 619-628.

Hanahan, D., and Weinberg, R. A. (2000). The hallmarks of cancer. *Cell* 100, 57-70.

Hanahan, D., and Weinberg, R. A. (2011). Hallmarks of cancer: the next generation. *Cell* 144, 646-674.

Hartness, M. E., Lewis, A., Searle, G. J., O'Kelly, I., Peers, C., and Kemp, P. J. (2001). Combined antisense and pharmacological approaches implicate hTASK as an airway O₂ sensing K(+) channel. *J Biol Chem* 276, 26499-26508.

Haussinger, D. (1996). The role of cellular hydration in the regulation of cell function. *Biochem J* 313 (Pt 3), 697-710.

Henquin, J. C., and Meissner, H. P. (1984). Significance of ionic fluxes and changes in membrane potential for stimulus-secretion coupling in pancreatic B-cells. *Experientia* 40, 1043-1052.

Hodi, F. S., Chiarion-Sileni, V., Gonzalez, R., Grob, J. J., Rutkowski, P., Cowey, C. L., Lao, C. D., Schadendorf, D., Wagstaff, J., Dummer, R., *et al.* (2018). Nivolumab plus ipilimumab or nivolumab alone versus ipilimumab alone in advanced melanoma (CheckMate 067): 4-year outcomes of a multicentre, randomised, phase 3 trial. *Lancet Oncol* 19, 1480-1492.

Hodis, E., Watson, I. R., Kryukov, G. V., Arold, S. T., Imielinski, M., Theurillat, J. P., Nickerson, E., Auclair, D., Li, L., Place, C., *et al.* (2012). A landscape of driver mutations in melanoma. *Cell* 150, 251-263.

Hoeflich, K. P., and Ikura, M. (2002). Calmodulin in action: diversity in target recognition and activation mechanisms. *Cell* 108, 739-742.

Inamura, N., Kito, M., Go, S., Kishi, S., Hosokawa, M., Asai, K., Takakura, N., Takebayashi, H., Matsuda, J., and Enokido, Y. (2018). Developmental defects and aberrant accumulation of endogenous psychosine in oligodendrocytes in a murine model of Krabbe disease. *Neurobiol Dis* 120, 51-62.

Jahn, R., and Scheller, R. H. (2006). SNAREs--engines for membrane fusion. *Nat Rev Mol Cell Biol* 7, 631-643.

Jan, L. Y., and Jan, Y. N. (1989). Voltage-sensitive ion channels. *Cell* 56, 13-25.

Johannessen, C. M., Reczek, E. E., James, M. F., Brems, H., Legius, E., and Cichowski, K. (2005). The NF1 tumor suppressor critically regulates TSC2 and mTOR. *Proc Natl Acad Sci U S A* 102, 8573-8578.

Jorgensen, P. L., Hakansson, K. O., and Karlish, S. J. (2003). Structure and mechanism of Na,K-ATPase: functional sites and their interactions. *Annu Rev Physiol* 65, 817-849.

Jung, J., Cho, K.-J., Naji, A. K., Clemons, K. N., Wong, C. O., Villanueva, M., Gregory, S., Karagas, N. E., Tan, L., Liang, H., *et al.* (2019). HRAS-driven cancer cells are vulnerable to TRPML1 inhibition. *EMBO Rep* 20, e46685.

Kamphorst, J. J., Nofal, M., Commisso, C., Hackett, S. R., Lu, W., Grabocka, E., Vander Heiden, M. G., Miller, G., Drebin, J. A., Bar-Sagi, D., *et al.* (2015). Human pancreatic cancer tumors are nutrient poor and tumor cells actively scavenge extracellular protein. *Cancer Res* 75, 544-553.

Kaplan, J. H. (2002). Biochemistry of Na,K-ATPase. *Annu Rev Biochem* 71, 511-535.

Katzmann, D. J., Odorizzi, G., and Emr, S. D. (2002). Receptor downregulation and multivesicular-body sorting. *Nat Rev Mol Cell Biol* 3, 893-905.

Kawashima, N., Tsuji, D., Okuda, T., Itoh, K., and Nakayama, K. (2009). Mechanism of abnormal growth in astrocytes derived from a mouse model of GM2 gangliosidosis. *J Neurochem* 111, 1031-1041.

Kerem, B., Rommens, J. M., Buchanan, J. A., Markiewicz, D., Cox, T. K., Chakravarti, A., Buchwald, M., and Tsui, L. C. (1989). Identification of the cystic fibrosis gene: genetic analysis. *Science* 245, 1073-1080.

Kew, J. N. C., and Davies, C. H. (2010). *Ion channels : from structure to function*, 2nd edn (Oxford ; New York: Oxford University Press).

Kirk, K., Ellory, J. C., and Young, J. D. (1992). Transport of organic substrates via a volume-activated channel. *J Biol Chem* 267, 23475-23478.

Komuro, H., and Rakic, P. (1992). Selective role of N-type calcium channels in neuronal migration. *Science* 257, 806-809.

Kong, S. K., Suen, Y. K., Choy, Y. M., Fung, K. P., and Lee, C. Y. (1991). Membrane depolarization was required to induce DNA synthesis in murine macrophage cell line PU5-1.8. *Immunopharmacol Immunotoxicol* 13, 329-339.

Krapivinsky, G., Gordon, E. A., Wickman, K., Velimirovic, B., Krapivinsky, L., and Clapham, D. E. (1995). The G-protein-gated atrial K⁺ channel IKACH is a heteromultimer of two inwardly rectifying K(+) channel proteins. *Nature* 374, 135-141.

Krauthammer, M., Kong, Y., Ha, B. H., Evans, P., Bacchiocchi, A., McCusker, J. P., Cheng, E., Davis, M. J., Goh, G., Choi, M., *et al.* (2012). Exome sequencing identifies recurrent somatic RAC1 mutations in melanoma. *Nat Genet* 44, 1006-1014.

Kurkdjian, A., and Guern, J. (1989). Intracellular Ph - Measurement and Importance in Cell-Activity. *Annu Rev Plant Phys* 40, 271-303.

Lang, F., Busch, G. L., Ritter, M., Volkl, H., Waldegger, S., Gulbins, E., and Haussinger, D. (1998a). Functional significance of cell volume regulatory mechanisms. *Physiol Rev* 78, 247-306.

Lang, F., Busch, G. L., and Volkl, H. (1998b). The diversity of volume regulatory mechanisms. *Cell Physiol Biochem* 8, 1-45.

Lang, F., Foller, M., Lang, K., Lang, P., Ritter, M., Vereninov, A., Szabo, I., Huber, S. M., and Gulbins, E. (2007). Cell volume regulatory ion channels in cell proliferation and cell death. *Methods Enzymol* 428, 209-225.

Lang, F., Stehle, T., and Haussinger, D. (1989). Water, K⁺, H⁺, lactate and glucose fluxes during cell volume regulation in perfused rat liver. *Pflugers Arch* 413, 209-216.

Langmead, B., and Salzberg, S. L. (2012). Fast gapped-read alignment with Bowtie 2. *Nat Methods* 9, 357-359.

Lawrence, R. E., and Zoncu, R. (2019). The lysosome as a cellular centre for signalling, metabolism and quality control. *Nat Cell Biol* 21, 133-142.

Lee, J., Ishihara, A., Oxford, G., Johnson, B., and Jacobson, K. (1999). Regulation of cell movement is mediated by stretch-activated calcium channels. *Nature* 400, 382-386.

Leestemaker, Y., de Jong, A., Witting, K. F., Penning, R., Schuurman, K., Rodenko, B., Zaal, E. A., van de Kooij, B., Laufer, S., Heck, A. J. R., *et al.* (2017). Proteasome Activation by Small Molecules. *Cell Chem Biol* 24, 725-736 e727.

Levitan, I. B. (1988). Modulation of ion channels in neurons and other cells. *Annu Rev Neurosci* 11, 119-136.

Lewis, R. S., and Cahalan, M. D. (1995). Potassium and calcium channels in lymphocytes. *Annu Rev Immunol* 13, 623-653.

Li, M., Zhang, Y., Liu, Z., Bharadwaj, U., Wang, H., Wang, X., Zhang, S., Liuzzi, J. P., Chang, S. M., Cousins, R. J., *et al.* (2007). Aberrant expression of zinc transporter ZIP4 (SLC39A4) significantly contributes to human pancreatic cancer pathogenesis and progression. *Proc Natl Acad Sci U S A* 104, 18636-18641.

Li, R. J., Xu, J., Fu, C., Zhang, J., Zheng, Y. G., Jia, H., and Liu, J. O. (2016a). Regulation of mTORC1 by lysosomal calcium and calmodulin. *Elife* 5.

Li, X., Rydzewski, N., Hider, A., Zhang, X., Yang, J., Wang, W., Gao, Q., Cheng, X., and Xu, H. (2016b). A molecular mechanism to regulate lysosome motility for lysosome positioning and tubulation. *Nat Cell Biol* 18, 404-417.

Liao, J., Li, H., Zeng, W., Sauer, D. B., Belmares, R., and Jiang, Y. (2012). Structural insight into the ion-exchange mechanism of the sodium/calcium exchanger. *Science* 335, 686-690.

Liu, J., Xu, Y., Stoleru, D., and Salic, A. (2012). Imaging protein synthesis in cells and tissues with an alkyne analog of puromycin. *Proc Natl Acad Sci U S A* 109, 413-418.

Locasale, J. W. (2013). Serine, glycine and one-carbon units: cancer metabolism in full circle. *Nat Rev Cancer* 13, 572-583.

Ma, L., Chen, Z., Erdjument-Bromage, H., Tempst, P., and Pandolfi, P. P. (2005). Phosphorylation and functional inactivation of TSC2 by Erk implications for tuberous sclerosis and cancer pathogenesis. *Cell* 121, 179-193.

Ma, X. M., and Blenis, J. (2009). Molecular mechanisms of mTOR-mediated translational control. *Nat Rev Mol Cell Biol* 10, 307-318.

MacFarlane, S. N., and Sontheimer, H. (2000). Changes in ion channel expression accompany cell cycle progression of spinal cord astrocytes. *Glia* 30, 39-48.

Madshus, I. H. (1988). Regulation of intracellular pH in eukaryotic cells. *Biochem J* 250, 1-8.

Mamelak, A. N., and Jacoby, D. B. (2007). Targeted delivery of antitumoral therapy to glioma and other malignancies with synthetic chlorotoxin (TM-601). *Expert Opin Drug Deliv* 4, 175-186.

Manders, E. M. M., Verbeek, F. J., and Aten, J. A. (1993). Measurement of co-localization of objects in dual-colour confocal images. *J Microsc* 169, 375-382.

Margolin, K., Longmate, J., Baratta, T., Synold, T., Christensen, S., Weber, J., Gajewski, T., Quirt, I., and Doroshow, J. H. (2005). CCI-779 in metastatic melanoma: a phase II trial of the California Cancer Consortium. *Cancer* 104, 1045-1048.

Martin, M. (2011). Cutadapt removes adapter sequences from high-throughput sequencing reads. *EMBnetjournal* 17, 10-12.

Matsui, H., Grubb, B. R., Tarran, R., Randell, S. H., Gatzky, J. T., Davis, C. W., and Boucher, R. C. (1998). Evidence for periciliary liquid layer depletion, not abnormal ion composition, in the pathogenesis of cystic fibrosis airways disease. *Cell* 95, 1005-1015.

McEwan, P. E., Lindop, G. B., and Kenyon, C. J. (1996). Control of cell proliferation in the rat adrenal gland in vivo by the renin-angiotensin system. *Am J Physiol* 271, E192-198.

McFerrin, M. B., and Sontheimer, H. (2006). A role for ion channels in glioma cell invasion. *Neuron Glia Biol* 2, 39-49.

Medina, D. L., Di Paola, S., Peluso, I., Armani, A., De Stefani, D., Venditti, R., Montefusco, S., Scotto-Rosato, A., Prezioso, C., Forrester, A., *et al.* (2015). Lysosomal calcium signalling regulates autophagy through calcineurin and TFEB. *Nat Cell Biol* 17, 288-299.

Meeth, K., Wang, J. X., Micevic, G., Damsky, W., and Bosenberg, M. W. (2016). The YUMM lines: a series of congenic mouse melanoma cell lines with defined genetic alterations. *Pigment Cell Melanoma Res* 29, 590-597.

Minke, B. (1977). *Drosophila* mutant with a transducer defect. *Biophys Struct Mech* 3, 59-64.

Mody, I., and MacDonald, J. F. (1995). NMDA receptor-dependent excitotoxicity: the role of intracellular Ca²⁺ release. *Trends Pharmacol Sci* 16, 356-359.

Monteith, G. R., McAndrew, D., Faddy, H. M., and Roberts-Thomson, S. J. (2007). Calcium and cancer: targeting Ca²⁺ transport. *Nat Rev Cancer* 7, 519-530.

Mu, D., Chen, L., Zhang, X., See, L. H., Koch, C. M., Yen, C., Tong, J. J., Spiegel, L., Nguyen, K. C., Servoss, A., *et al.* (2003). Genomic amplification and oncogenic properties of the KCNK9 potassium channel gene. *Cancer Cell* 3, 297-302.

Muller, M. R., and Rao, A. (2010). NFAT, immunity and cancer: a transcription factor comes of age. *Nat Rev Immunol* 10, 645-656.

Nazarian, R., Shi, H., Wang, Q., Kong, X., Koya, R. C., Lee, H., Chen, Z., Lee, M. K., Attar, N., Sazegar, H., *et al.* (2010). Melanomas acquire resistance to B-RAF(V600E) inhibition by RTK or N-RAS upregulation. *Nature* 468, 973-977.

Nelson, M., Millican-Slater, R., Forrest, L. C., and Brackenbury, W. J. (2014). The sodium channel beta1 subunit mediates outgrowth of neurite-like processes on breast cancer cells and promotes tumour growth and metastasis. *Int J Cancer* 135, 2338-2351.

O'Sullivan, B. P., and Freedman, S. D. (2009). Cystic fibrosis. *Lancet* 373, 1891-1904.

Paddison, P. J., Caudy, A. A., Bernstein, E., Hannon, G. J., and Conklin, D. S. (2002). Short hairpin RNAs (shRNAs) induce sequence-specific silencing in mammalian cells. *Genes Dev* 16, 948-958.

Palm, W., Park, Y., Wright, K., Pavlova, N. N., Tuveson, D. A., and Thompson, C. B. (2015). The Utilization of Extracellular Proteins as Nutrients Is Suppressed by mTORC1. *Cell* 162, 259-270.

Pappas, C. A., and Ritchie, J. M. (1998). Effect of specific ion channel blockers on cultured Schwann cell proliferation. *Glia* 22, 113-120.

Pardo, L. A., del Camino, D., Sanchez, A., Alves, F., Bruggemann, A., Beckh, S., and Stuhmer, W. (1999). Oncogenic potential of EAG K(+) channels. *EMBO J* 18, 5540-5547.

Pardo, L. A., and Stuhmer, W. (2014). The roles of K(+) channels in cancer. *Nat Rev Cancer* 14, 39-48.

Pawlikowski, M., Gruszka, A., Mucha, S., and Melen-Mucha, G. (2001). Angiotensins II and IV stimulate the rat adrenocortical cell proliferation acting via different receptors. *Endocr Regul* 35, 139-142.

Pedersen, S. F., and Stock, C. (2013). Ion channels and transporters in cancer: pathophysiology, regulation, and clinical potential. *Cancer Res* 73, 1658-1661.

Pei, L., Wiser, O., Slavin, A., Mu, D., Powers, S., Jan, L. Y., and Hoey, T. (2003). Oncogenic potential of TASK3 (Kcnk9) depends on K+ channel function. *Proc Natl Acad Sci U S A* 100, 7803-7807.

Peier, A. M., Moqrich, A., Hergarden, A. C., Reeve, A. J., Andersson, D. A., Story, G. M., Earley, T. J., Dragoni, I., McIntyre, P., Bevan, S., and Patapoutian, A. (2002). A TRP channel that senses cold stimuli and menthol. *Cell* 108, 705-715.

Perera, R. M., and Zoncu, R. (2016). The Lysosome as a Regulatory Hub. *Annu Rev Cell Dev Biol* 32, 223-253.

Peretz, L., Besser, E., Hajbi, R., Casden, N., Ziv, D., Kronenberg, N., Gigi, L. B., Sweetat, S., Khawaled, S., Aqeilan, R., and Behar, O. (2018). Combined shRNA over CRISPR/cas9 as a methodology to detect off-target effects and a potential compensatory mechanism. *Sci Rep* 8, 93.

Perry, P. B., and O'Neill, W. C. (1993). Swelling-activated K fluxes in vascular endothelial cells: volume regulation via K-Cl cotransport and K channels. *Am J Physiol* 265, C763-769.

Petersen, O. H., and Findlay, I. (1987). Electrophysiology of the pancreas. *Physiol Rev* 67, 1054-1116.

Peterson, T. R., Laplante, M., Thoreen, C. C., Sancak, Y., Kang, S. A., Kuehl, W. M., Gray, N. S., and Sabatini, D. M. (2009). DEPTOR is an mTOR inhibitor frequently overexpressed in multiple myeloma cells and required for their survival. *Cell* 137, 873-886.

Piskounova, E., Agathocleous, M., Murphy, M. M., Hu, Z., Huddleston, S. E., Zhao, Z., Leitch, A. M., Johnson, T. M., DeBerardinis, R. J., and Morrison, S. J. (2015). Oxidative stress inhibits distant metastasis by human melanoma cells. *Nature* 527, 186-191.

Plasschaert, L. W., Zilionis, R., Choo-Wing, R., Savova, V., Knehr, J., Roma, G., Klein, A. M., and Jaffe, A. B. (2018). A single-cell atlas of the airway epithelium reveals the CFTR-rich pulmonary ionocyte. *Nature* 560, 377-381.

Pouyssegur, J., Franchi, A., L'Allemain, G., and Paris, S. (1985). Cytoplasmic pH, a key determinant of growth factor-induced DNA synthesis in quiescent fibroblasts. *FEBS Lett* 190, 115-119.

Prevarskaya, N., Skryma, R., and Shuba, Y. (2010). Ion channels and the hallmarks of cancer. *Trends Mol Med* 16, 107-121.

Prickett, T. D., Zerlanko, B. J., Hill, V. K., Gartner, J. J., Qutob, N., Jiang, J., Simaan, M., Wunderlich, J., Gutkind, J. S., Rosenberg, S. A., and Samuels, Y. (2014). Somatic mutation of GRIN2A in malignant melanoma results in loss of tumor suppressor activity via aberrant NMDAR complex formation. *J Invest Dermatol* 134, 2390-2398.

Purves, D. (2004). *Neuroscience*, 3rd edn (Sunderland, Mass.: Sinauer Associates, Publishers).

Quintana, E., Shackleton, M., Sabel, M. S., Fullen, D. R., Johnson, T. M., and Morrison, S. J. (2008). Efficient tumour formation by single human melanoma cells. *Nature* 456, 593-598.

Ramsey, I. S., Delling, M., and Clapham, D. E. (2006). An introduction to TRP channels. *Annu Rev Physiol* 68, 619-647.

Ran, F. A., Hsu, P. D., Wright, J., Agarwala, V., Scott, D. A., and Zhang, F. (2013). Genome engineering using the CRISPR-Cas9 system. *Nat Protoc* 8, 2281-2308.

Rink, J., Ghigo, E., Kalaidzidis, Y., and Zerial, M. (2005). Rab conversion as a mechanism of progression from early to late endosomes. *Cell* 122, 735-749.

Roger, S., Gillet, L., Le Guennec, J. Y., and Besson, P. (2015). Voltage-gated sodium channels and cancer: is excitability their primary role? *Front Pharmacol* 6, 152.

Roos, A., and Boron, W. F. (1981). Intracellular pH. *Physiol Rev* 61, 296-434.

Rorsman, P., and Trube, G. (1985). Glucose dependent K⁺-channels in pancreatic beta-cells are regulated by intracellular ATP. *Pflugers Arch* 405, 305-309.

Sabatini, D. M. (2006). mTOR and cancer: insights into a complex relationship. *Nat Rev Cancer* 6, 729-734.

Sachs, G., Shin, J. M., Briving, C., Wallmark, B., and Hersey, S. (1995). The pharmacology of the gastric acid pump: the H⁺,K⁺ ATPase. *Annu Rev Pharmacol Toxicol* 35, 277-305.

Samie, M., Wang, X., Zhang, X., Goschka, A., Li, X., Cheng, X., Gregg, E., Azar, M., Zhuo, Y., Garrity, A. G., *et al.* (2013). A TRP channel in the lysosome regulates large particle phagocytosis via focal exocytosis. *Dev Cell* 26, 511-524.

Sancak, Y., Bar-Peled, L., Zoncu, R., Markhard, A. L., Nada, S., and Sabatini, D. M. (2010). Ragulator-Rag complex targets mTORC1 to the lysosomal surface and is necessary for its activation by amino acids. *Cell* 141, 290-303.

Sardiello, M., Palmieri, M., di Ronza, A., Medina, D. L., Valenza, M., Gennarino, V. A., Di Malta, C., Donaudy, F., Embrione, V., Polishchuk, R. S., *et al.* (2009). A gene network regulating lysosomal biogenesis and function. *Science* 325, 473-477.

Saxton, R. A., and Sabatini, D. M. (2017). mTOR Signaling in Growth, Metabolism, and Disease. *Cell* 169, 361-371.

Schneider, S. W., Pagel, P., Rotsch, C., Danker, T., Oberleithner, H., Radmacher, M., and Schwab, A. (2000). Volume dynamics in migrating epithelial cells measured with atomic force microscopy. *Pflugers Arch* 439, 297-303.

Scholl, U. I., Goh, G., Stolting, G., de Oliveira, R. C., Choi, M., Overton, J. D., Fonseca, A. L., Korah, R., Starker, L. F., Kunstman, J. W., *et al.* (2013). Somatic and germline CACNA1D calcium channel mutations in aldosterone-producing adenomas and primary aldosteronism. *Nat Genet* 45, 1050-1054.

Schulla, V., Renstrom, E., Feil, R., Feil, S., Franklin, I., Gjinovci, A., Jing, X. J., Laux, D., Lundquist, I., Magnuson, M. A., *et al.* (2003). Impaired insulin secretion and glucose tolerance in beta cell-selective Ca(v)1.2 Ca²⁺ channel null mice. *EMBO J* 22, 3844-3854.

Schultz, S. G., and Curran, P. F. (1970). Coupled transport of sodium and organic solutes. *Physiol Rev* 50, 637-718.

Schwab, A., Fabian, A., Hanley, P. J., and Stock, C. (2012). Role of ion channels and transporters in cell migration. *Physiol Rev* 92, 1865-1913.

Seki, A., and Rutz, S. (2018). Optimized RNP transfection for highly efficient CRISPR/Cas9-mediated gene knockout in primary T cells. *J Exp Med* 215, 985-997.

Settembre, C., Di Malta, C., Polito, V. A., Garcia Arencibia, M., Vetrini, F., Erdin, S., Erdin, S. U., Huynh, T., Medina, D., Colella, P., *et al.* (2011). TFEB links autophagy to lysosomal biogenesis. *Science* 332, 1429-1433.

Settembre, C., Fraldi, A., Medina, D. L., and Ballabio, A. (2013). Signals from the lysosome: a control centre for cellular clearance and energy metabolism. *Nat Rev Mol Cell Biol* 14, 283-296.

Shalem, O., Sanjana, N. E., Hartenian, E., Shi, X., Scott, D. A., Mikkelsen, T., Heckl, D., Ebert, B. L., Root, D. E., Doench, J. G., and Zhang, F. (2014). Genome-scale CRISPR-Cas9 knockout screening in human cells. *Science* 343, 84-87.

Shaw, R. J., and Cantley, L. C. (2006). Ras, PI(3)K and mTOR signalling controls tumour cell growth. *Nature* 441, 424-430.

Shen, D., Coleman, J., Chan, E., Nicholson, T. P., Dai, L., Sheppard, P. W., and Patton, W. F. (2011). Novel cell- and tissue-based assays for detecting misfolded and aggregated protein accumulation within aggresomes and inclusion bodies. *Cell Biochem Biophys* 60, 173-185.

Shen, D., Wang, X., Li, X., Zhang, X., Yao, Z., Dibble, S., Dong, X. P., Yu, T., Lieberman, A. P., Showalter, H. D., and Xu, H. (2012). Lipid storage disorders block lysosomal trafficking by inhibiting a TRP channel and lysosomal calcium release. *Nat Commun* 3, 731.

Shifrut, E., Carnevale, J., Tobin, V., Roth, T. L., Woo, J. M., Bui, C. T., Li, P. J., Diolaiti, M. E., Ashworth, A., and Marson, A. (2018). Genome-wide CRISPR Screens in Primary Human T Cells Reveal Key Regulators of Immune Function. *Cell* 175, 1958-1971 e1915.

Signer, R. A., Magee, J. A., Salic, A., and Morrison, S. J. (2014). Haematopoietic stem cells require a highly regulated protein synthesis rate. *Nature* 509, 49-54.

Smits, P. (1996). Role of potassium channels in the modulation of insulin release. *Diabetologia* 39, 865-867.

Soleimani, M., Lesoine, G. A., Bergman, J. A., and McKinney, T. D. (1991). A pH modifier site regulates activity of the Na⁺:HCO₃⁻ cotransporter in basolateral membranes of kidney proximal tubules. *J Clin Invest* 88, 1135-1140.

Song, Z., He, C. D., Liu, J., Sun, C., Lu, P., Li, L., Gao, L., Zhang, Y., Xu, Y., Shan, L., *et al.* (2012). Blocking glutamate-mediated signalling inhibits human melanoma growth and migration. *Exp Dermatol* 21, 926-931.

- Sontheimer, H. (2008). An unexpected role for ion channels in brain tumor metastasis. *Exp Biol Med (Maywood)* 233, 779-791.
- Soroceanu, L., Manning, T. J., Jr., and Sontheimer, H. (1999). Modulation of glioma cell migration and invasion using Cl(-) and K(+) ion channel blockers. *J Neurosci* 19, 5942-5954.
- Spat, A., and Hunyady, L. (2004). Control of aldosterone secretion: a model for convergence in cellular signaling pathways. *Physiol Rev* 84, 489-539.
- Stringer, B. K., Cooper, A. G., and Shepard, S. B. (2001). Overexpression of the G-protein inwardly rectifying potassium channel 1 (GIRK1) in primary breast carcinomas correlates with axillary lymph node metastasis. *Cancer Res* 61, 582-588.
- Sudhof, T. C. (2004). The synaptic vesicle cycle. *Annu Rev Neurosci* 27, 509-547.
- Sun, H., Luo, L., Lal, B., Ma, X., Chen, L., Hann, C. L., Fulton, A. M., Leahy, D. J., Laterra, J., and Li, M. (2016). A monoclonal antibody against KCNK9 K(+) channel extracellular domain inhibits tumour growth and metastasis. *Nat Commun* 7, 10339.
- Sun, M., Goldin, E., Stahl, S., Falardeau, J. L., Kennedy, J. C., Acierno, J. S., Jr., Bove, C., Kaneski, C. R., Nagle, J., Bromley, M. C., *et al.* (2000). Mucopolipidosis type IV is caused by mutations in a gene encoding a novel transient receptor potential channel. *Hum Mol Genet* 9, 2471-2478.
- Sundelacruz, S., Levin, M., and Kaplan, D. L. (2009). Role of membrane potential in the regulation of cell proliferation and differentiation. *Stem Cell Rev* 5, 231-246.

Takahashi, N., Chen, H. Y., Harris, I. S., Stover, D. G., Selfors, L. M., Bronson, R. T., Deraedt, T., Cichowski, K., Welm, A. L., Mori, Y., *et al.* (2018). Cancer Cells Co-opt the Neuronal Redox-Sensing Channel TRPA1 to Promote Oxidative-Stress Tolerance. *Cancer Cell* 33, 985-1003 e1007.

Tanabe, A., Naruse, M., Arai, K., Naruse, K., Yoshimoto, T., Seki, T., Imaki, T., Kobayashi, M., Miyazaki, H., and Demura, H. (1998). Angiotensin II stimulates both aldosterone secretion and DNA synthesis via type 1 but not type 2 receptors in bovine adrenocortical cells. *J Endocrinol Invest* 21, 668-672.

Tang, Y. B., Liu, Y. J., Zhou, J. G., Wang, G. L., Qiu, Q. Y., and Guan, Y. Y. (2008). Silence of CIC-3 chloride channel inhibits cell proliferation and the cell cycle via G/S phase arrest in rat basilar arterial smooth muscle cells. *Cell Prolif* 41, 775-785.

Teitelbaum, S. L. (2000). Bone resorption by osteoclasts. *Science* 289, 1504-1508.

Thiemann, A., Grunder, S., Pusch, M., and Jentsch, T. J. (1992). A chloride channel widely expressed in epithelial and non-epithelial cells. *Nature* 356, 57-60.

Thoreen, C. C., Kang, S. A., Chang, J. W., Liu, Q., Zhang, J., Gao, Y., Reichling, L. J., Sim, T., Sabatini, D. M., and Gray, N. S. (2009). An ATP-competitive mammalian target of rapamycin inhibitor reveals rapamycin-resistant functions of mTORC1. *J Biol Chem* 284, 8023-8032.

Traynelis, S. F., Wollmuth, L. P., McBain, C. J., Menniti, F. S., Vance, K. M., Ogden, K. K., Hansen, K. B., Yuan, H., Myers, S. J., and Dingledine, R. (2010). Glutamate receptor ion channels: structure, regulation, and function. *Pharmacol Rev* 62, 405-496.

Trusolino, L., Bertotti, A., and Comoglio, P. M. (2010). MET signalling: principles and functions in development, organ regeneration and cancer. *Nat Rev Mol Cell Biol* 11, 834-848.

Turner, K. L., and Sontheimer, H. (2014). KCa3.1 modulates neuroblast migration along the rostral migratory stream (RMS) in vivo. *Cereb Cortex* 24, 2388-2400.

Ueno, Y., Sakurai, H., Tsunoda, S., Choo, M. K., Matsuo, M., Koizumi, K., and Saiki, I. (2008). Heregulin-induced activation of ErbB3 by EGFR tyrosine kinase activity promotes tumor growth and metastasis in melanoma cells. *Int J Cancer* 123, 340-347.

Ui, M. (1966). A role of phosphofructokinase in pH-dependent regulation of glycolysis. *Biochim Biophys Acta* 124, 310-322.

Valvezan, A. J., and Manning, B. D. (2019). Molecular logic of mTORC1 signalling as a metabolic rheostat. *Nature Metabolism* 1, 321-333.

Venkatachalam, K., Wong, C. O., and Zhu, M. X. (2015). The role of TRPMLs in endolysosomal trafficking and function. *Cell Calcium* 58, 48-56.

Verbalis, J. G., and Gullans, S. R. (1991). Hyponatremia causes large sustained reductions in brain content of multiple organic osmolytes in rats. *Brain Res* 567, 274-282.

Volk, T., Fromter, E., and Korbmacher, C. (1995). Hypertonicity activates nonselective cation channels in mouse cortical collecting duct cells. *Proc Natl Acad Sci U S A* 92, 8478-8482.

Volkl, H., and Lang, F. (1988). Ionic requirement for regulatory cell volume decrease in renal straight proximal tubules. *Pflugers Arch* 412, 1-6.

Walter, P., and Ron, D. (2011). The unfolded protein response: from stress pathway to homeostatic regulation. *Science* 334, 1081-1086.

Wang, E., Yin, Y., Zhao, M., Forrester, J. V., and McCaig, C. D. (2003). Physiological electric fields control the G1/S phase cell cycle checkpoint to inhibit endothelial cell proliferation. *FASEB J* 17, 458-460.

Wang, G. L., Wang, X. R., Lin, M. J., He, H., Lan, X. J., and Guan, Y. Y. (2002). Deficiency in CIC-3 chloride channels prevents rat aortic smooth muscle cell proliferation. *Circ Res* 91, E28-32.

Wang, T., Birsoy, K., Hughes, N. W., Krupczak, K. M., Post, Y., Wei, J. J., Lander, E. S., and Sabatini, D. M. (2015). Identification and characterization of essential genes in the human genome. *Science* 350, 1096-1101.

Wang, Z. (2004). Roles of K⁺ channels in regulating tumour cell proliferation and apoptosis. *Pflugers Arch* 448, 274-286.

Watkins, S., and Sontheimer, H. (2011). Hydrodynamic cellular volume changes enable glioma cell invasion. *J Neurosci* 31, 17250-17259.

Webb, B. A., Chimenti, M., Jacobson, M. P., and Barber, D. L. (2011). Dysregulated pH: a perfect storm for cancer progression. *Nat Rev Cancer* 11, 671-677.

Wehner, F., Olsen, H., Tinel, H., Kinne-Saffran, E., and Kinne, R. K. (2003). Cell volume regulation: osmolytes, osmolyte transport, and signal transduction. *Rev Physiol Biochem Pharmacol* 148, 1-80.

Wehner, F., Sauer, H., and Kinne, R. K. (1995). Hypertonic stress increases the Na⁺ conductance of rat hepatocytes in primary culture. *J Gen Physiol* 105, 507-535.

Wei, C., Wang, X., Chen, M., Ouyang, K., Song, L. S., and Cheng, H. (2009). Calcium flickers steer cell migration. *Nature* 457, 901-905.

Wei, X., Walia, V., Lin, J. C., Teer, J. K., Prickett, T. D., Gartner, J., Davis, S., Program, N. C. S., Stemke-Hale, K., Davies, M. A., *et al.* (2011). Exome sequencing identifies GRIN2A as frequently mutated in melanoma. *Nat Genet* 43, 442-446.

Weinstock, L., Furness, A. M., Herron, S., Smith, S. S., Sankar, S., DeRosa, S. G., Gao, D., Mepyans, M. E., Scotto Rosato, A., Medina, D. L., *et al.* (2018). Fingolimod Phosphate Inhibits Astrocyte Inflammatory Activity in Mucopolidosis IV. *Hum Mol Genet* 27, 2725-2738.

Weiss, H., and Lang, F. (1992). Ion channels activated by swelling of Madin Darby canine kidney (MDCK) cells. *J Membr Biol* 126, 109-114.

White, M. B., Amos, J., Hsu, J. M., Gerrard, B., Finn, P., and Dean, M. (1990). A frame-shift mutation in the cystic fibrosis gene. *Nature* 344, 665-667.

Wollheim, C. B., and Sharp, G. W. (1981). Regulation of insulin release by calcium. *Physiol Rev* 61, 914-973.

Wonderlin, W. F., and Strobl, J. S. (1996). Potassium channels, proliferation and G1 progression. *J Membr Biol* 154, 91-107.

Wong, C.-O., Li, R., Montell, C., and Venkatachalam, K. (2012). *Drosophila* TRPML is required for TORC1 activation. *Current biology : CB* 22, 1616-1621.

Wright, E. M., Loo, D. D., and Hirayama, B. A. (2011). Biology of human sodium glucose transporters. *Physiol Rev* 91, 733-794.

Yang, M., Kozminski, D. J., Wold, L. A., Modak, R., Calhoun, J. D., Isom, L. L., and Brackenbury, W. J. (2012). Therapeutic potential for phenytoin: targeting Na(v)1.5 sodium channels to reduce migration and invasion in metastatic breast cancer. *Breast Cancer Res Treat* 134, 603-615.

Yang, S., Zhang, J. J., and Huang, X. Y. (2009). Orai1 and STIM1 are critical for breast tumor cell migration and metastasis. *Cancer Cell* 15, 124-134.

Zender, L., Xue, W., Zuber, J., Semighini, C. P., Krasnitz, A., Ma, B., Zender, P., Kubicka, S., Luk, J. M., Schirmacher, P., *et al.* (2008). An oncogenomics-based in vivo RNAi screen identifies tumor suppressors in liver cancer. *Cell* 135, 852-864.

Zhang, X., Cheng, X., Yu, L., Yang, J., Calvo, R., Patnaik, S., Hu, X., Gao, Q., Yang, M., Lawas, M., *et al.* (2016). MCOLN1 is a ROS sensor in lysosomes that regulates autophagy. *Nat Commun* 7, 12109.

Zhang, X., Hu, M., Yang, Y., and Xu, H. (2018). Organellar TRP channels. *Nat Struct Mol Biol* 25, 1009-1018.

Zhang, Y., Hoon, M. A., Chandrashekar, J., Mueller, K. L., Cook, B., Wu, D., Zuker, C. S., and Ryba, N. J. (2003). Coding of sweet, bitter, and umami tastes: different receptor cells sharing similar signaling pathways. *Cell* 112, 293-301.